FZJ-IKP(TH)-1999-37, FTUV-IFIC-99-1215

Chiral Unitary approach to meson-meson and meson-baryon interactions and nuclear applications

J. A. OLLER

Forschungzentrum Jülich, Institut für Kernphysik (Theorie)

D-52425 Jülich, Germany

E. OSET

Departamento de Física Teórica and IFIC, Centro Mixto Universidad de Valencia-CSIC,

46100 Burjassot (Valencia), Spain

and

A. RAMOS

Departament d'Estructura i Constituents de la Matèria, Universitat de Barcelona,

08028-Barcelona, Spain

Abstract

We report on recent nonperturbative techniques that combine the information of chiral Lagrangians (with and without resonances) with unitarity in coupled channels and other requirements of the S-matrix theory of the strong interactions. As a result, the region of applicability of such techniques is much larger than the one of Chiral Perturbation Theory allowing one to study also resonance physics. Applications to meson-meson and meson-baryon scattering, as well as to problems where pairs of mesons or a meson and a baryon appear in the initial or final state are shown. Implications in several nuclear problems are also discussed.

PACS: 11.15.Tk, 11.80.Gw, 12.38.Lg, 12.39.Fe, 13.25.Jx, 13.40.Hq, 13.60.Le, 13.60.Rj, 13.75.Gx, 13.75.Jz, 13.75.Lb, 25.80.Hp, 25.80.Nv

Keywords: Chiral symmetry, coupled channels, unitarity, nonperturbative methods, meson-meson scattering, meson-baryon scattering, final state interactions

Contents

Chapter 1

Introduction

Nowadays it is believed that QCD is the theory for the strong interactions. However, while in the high energy regime, due to the asymptotic freedom, the theory has been successfully tested by the experiment, this is not the case for low energies. In this case, one is in the confinement regime of QCD and perturbative methods cannot be applied.

On the other hand, in the low energy region the spectrum of QCD presents an interesting fact which is the appearance of the isospin pion triplet with a mass much smaller than the rest of the QCD states. This can be extended to SU(3) by considering the lowest octet of pseudoscalar states (π, K, η). This fact can be understood by the presence in the QCD Lagrangian of a chiral symmetry for the light quark sector (u, d, s) which spontaneously breaks down giving rise, by the Goldstone theorem, to the aforementioned states. The presence of this symmetry pattern constrains also tremendously the interactions between these Goldstone bosons. As a consequence, a successful theory has emerged, Chiral Perturbation Theory (χPT), which exploits these facts giving rise to a series of Lagrangians in a power momentum expansion treating the quark masses in a perturbative way. This power series is valid up to some high energy scale, $\Lambda_{\chi PT}$, which is of the order of 1 GeV. Hence, the χPT expansion is valid for momenta $p << \Lambda_{\chi PT} \approx 1$ GeV.

Although χPT is a powerful tool for the low energy region, its convergence is limited to a narrow interval (for example, for energies below 0.5 GeV in meson-meson scattering or close to the threshold region in meson-baryon scattering). As a consequence, one of the most representative and interesting facts of strong interacting phenomena, resonances and their properties, cannot be studied. Furthermore, when one tries to increase the energy region of applicability of χPT just by including higher orders, the predictive power of the theory is rapidly lost since the number of free parameters increases tremendously with the order. For instance, the leading order χPT Lagrangian has essentially no free parameters, in the next-to-leading one there are 12 and in the next-next-to-leading order there are more than 100.

Hence, the development of nonperturbative techniques which can extend the energy region of applicability of the theory, without loosing predictive power, is an important issue. This is the topic to which this report is devoted. We shall indeed see that this can be done successfully and that a good description of the meson-meson and meson-baryon interactions, even for energies above 1 GeV, arises from χPT, supplied with exact unitarity

with or without explicit resonance exchanges.

The manuscript is organized as follows. In *chapter 2* an overall introduction to the emerging chiral Lagrangians is given. *Chapter 3* is devoted to deducing the various nonperturbative methods reported here, as well as to discussing their applications to strong meson-meson and meson-baryon scattering processes. In *chapters 4* and *5* it is discussed how the previous strong amplitudes are implemented to account for final and initial state interactions, which turn out to be crucial to understand the physics of many reactions. Applications of the former nonperturbative methods in nuclear physics are reported in *chapter 6*. Finally, conclusions and remarks are collected in the last section. Every chapter has its own introduction where one can find a more detailed, although still general, overview of its contents.

Chapter 2

Effective chiral Lagrangians

In this chapter we want to review the chiral Lagrangians that are going to be used in the following. After giving a brief account of chiral symmetry from the QCD Lagrangian we will report on the lowest and next to leading order χPT Lagrangians without baryons. We will also discuss the inclusion of explicit meson resonance fields. Then, we will consider the meson-baryon system where the lowest order χPT Lagrangian will be given. There are many good reviews about Chiral Perturbation Theory [1–3] to which the interested reader is referred for further details.

2.1 Chiral symmetry

The QCD Lagrangian with massless u, d and s quarks coupled to several external sources reads:

$$\mathcal{L}_{QCD} = \mathcal{L}^0_{QCD} + i\bar{q}D^\mu\gamma_\mu q + \bar{q}\gamma^\mu(v_\mu + \gamma_5 a_\mu)q - \bar{q}(s - i\gamma_5 p)q \tag{2.1}$$

where $\mathcal{L}^0_{QCD}$ is the part of the QCD Lagrangian for the heavier quarks c, b and t and gluons, v_μ, a_μ, s and p are the vector, axial, scalar and pseudoscalar external sources, D_μ is the covariant derivative for the $SU(3)$-colour gauge symmetry and

$$q = \begin{pmatrix} u \\ d \\ s \end{pmatrix} \tag{2.2}$$

is a vector in the three dimensional flavour space.

The Lagrangian eq. (2.1) exhibits a local $SU(3)_L \otimes SU(3)_R$ flavour symmetry under the following transformation rules

$$\begin{aligned} q &\rightarrow g_R\frac{1}{2}(1+\gamma_5)q + g_L\frac{1}{2}(1-\gamma_5)q \\ v_\mu \pm a_\mu &\rightarrow g_{R,L}(v_\mu \pm a_\mu)g^\dagger_{R,L} + i\, g_{R,L}\partial_\mu\, g^\dagger_{R,L} \\ s + ip &\rightarrow g_R(s+ip)g^\dagger_L \\ g_{R,L} &\in SU(3)_{R,L} \end{aligned} \tag{2.3}$$

This chiral symmetry, which should be rather good in the light quark sector, is not seen in the hadronic spectrum. Although hadrons can be classified in $SU(3)_V \equiv SU(3)_{R+L}$ representations, degenerate multiplets with opposite parity are not observed. Moreover, the octet of the lightest pseudoscalar mesons (π, K, η) can be understood if the chiral $SU(3)_L \otimes SU(3)_R$ symmetry spontaneously breaks down to $SU(3)_V$. Then, according

to the Goldstone theorem [4], an octet of pseudoscalar massless bosons appears in the theory, and these mesons will have the same quantum numbers as the broken generators of $SU(3)_A \equiv SU(3)_{R-L}$. One thus expects that (π, K, η) are to be identified with this octet of Goldstone bosons.

Furthermore, Chiral Symmetry is also explicitly broken by a mass term in eq. (2.1)

$$-\bar{q} M_q q \tag{2.4}$$

when fixing the scalar source $s(x) = M = diag(m_u, m_d, m_s)$, where m_u, m_d and m_s are the masses of the respective quarks. Because of this term, the Goldstone bosons acquire a small mass giving rise to the masses of the (π, K, η). On the other hand $SU(3)_V$ in the hadronic spectrum is only an approximate symmetry because m_s is much larger than m_u or m_d.

2.2 Chiral Perturbation Theory

Taking advantage of the mass gap separating the lightest pseudoscalar octet from the rest of the hadronic spectrum one can build an effective field theory containing only the Goldstone modes. These Goldstone fields, $\vec{\phi}$, can be collected in a traceless $SU(3)$ matrix

$$\Phi = \frac{\vec{\lambda}}{\sqrt{2}}\,\vec{\phi} = \begin{pmatrix} \frac{1}{\sqrt{2}}\pi^0 + \frac{1}{\sqrt{6}}\eta_8 & \pi^+ & K^+ \\ \pi^- & -\frac{1}{\sqrt{2}}\pi^0 + \frac{1}{\sqrt{6}}\eta_8 & K^0 \\ K^- & \bar{K}^0 & -\frac{2}{\sqrt{6}}\eta_8 \end{pmatrix} \tag{2.5}$$

where λ_i are the Gell-Mann's matrices with $\mathrm{Tr}(\lambda_i \lambda_j) = 2\delta_{ij}$. From the field Φ one builds the matrix $U(\phi) = e^{i\sqrt{2}\Phi/f}$, with f a constant. This matrix transforms linearly under $SU(3)_L \otimes SU(3)_R$ as:

$$U(\phi) \to g_R U(\phi) g_L^\dagger \tag{2.6}$$

and, hence, the Goldstone boson fields $\vec{\phi}$ transform in a non-linear form.

The effective Lagrangian will be constructed as a power expansion series in terms of the external Goldstone momenta and the quark mass matrix.

2.3 Lowest and next to leading order χPT Lagrangian

The lowest order chiral Lagrangian invariant under Lorentz transformations, parity and charge conjugation with only two derivatives and linear in the quark masses is [5]

$$\mathcal{L}_2 = \frac{f^2}{4} < D_\mu U^\dagger\, D^\mu U + U^\dagger\, \mathcal{M} + \mathcal{M}^\dagger\, U > \,, \tag{2.7}$$

where $<>$ means $SU(3)$-flavour trace and

$$\mathcal{M} = 2B_0(s + ip) \,, \tag{2.8}$$

with B_0 a constant and the covariant derivative is defined as

$$D_\mu U = \partial_\mu U - i r_\mu U + i U \ell_\mu \,, \tag{2.9}$$

where $r_\mu(\ell_\mu) = v_\mu + (-)a_\mu$.

The external sources can also be used to incorporate the electromagnetic and semileptonic weak interactions through the following relations:

$$
\begin{aligned}
r_\mu &= e\mathcal{Q}A_\mu + ... \\
\ell_\mu &= e\mathcal{Q}A_\mu + \frac{e}{\sqrt{2}\sin\theta_W}(W_\mu^\dagger T_+ + HC) + ...
\end{aligned}
\tag{2.10}
$$

where $\mathcal{Q} = \frac{1}{3}diag(2,-1,-1)$ is the quark-charge matrix and T_+ is a 3×3 matrix containg the relevant Cabibbo-Kobayashi-Maskawa factors

$$
T_+ = \begin{pmatrix} 0 & V_{ud} & V_{us} \\ 0 & 0 & 0 \\ 0 & 0 & 0 \end{pmatrix} \ . \tag{2.11}
$$

On the other hand, the former Lagrangian given in eq. (2.7) is quoted as $\mathcal{O}(p^2)$ because it contains at most masses squared, see eq. (2.12), and two derivatives. In general, when no baryons are present, the Lagrangian will have an even number of power of masses and derivatives. In this way, we will have $\mathcal{L} = \mathcal{L}_2 + \mathcal{L}_4 + \mathcal{L}_6 + ...$, where the subindex indicates the power in the momenta.

Fixing $s(x) = M$ and $p(x) = 0$, the $\mathcal{M}$ term in eq. (2.7) gives rise to a quadratic pseudoscalar mass term plus additional interactions proportional to the quark masses. This is the reason why in χPT the quark masses are considered as $\mathcal{O}(p^2)$.

In the isospin limit ($m_u = m_d$) with $\hat{m} = \dfrac{m_u + m_d}{2}$, the following relations arise from the lowest order χPT Lagrangian, $\mathcal{L}_2$:

$$
\begin{aligned}
m_\pi^2 &= 2\hat{m}B_0 \\
m_K^2 &= (\hat{m} + m_s)B_0 \\
m_{\eta_8}^2 &= \frac{2}{3}(\hat{m} + 2m_s)B_0
\end{aligned}
\tag{2.12}
$$

satisfying the Gell-Mann [6]-Okubo [7] mass relation.

$$
3\,m_{\eta_8}^2 = 4\,m_K^2 - m_\pi^2 \ . \tag{2.13}
$$

From eqs. (2.12), valid in the isospin limit, we can write the mass matrix $\mathcal{M}$ ($s(x) = M$ and $p = 0$) present in the lowest order Lagrangian, $\mathcal{L}_2$, as:

$$
\begin{pmatrix} m_\pi^2 & 0 & 0 \\ 0 & m_\pi^2 & 0 \\ 0 & 0 & 2m_K^2 - m_\pi^2 \end{pmatrix} \ . \tag{2.14}
$$

The meaning of the constant f can be appreciated when calculating from the lowest order Lagrangian, eq. (2.7), the axial current. Then f becomes the pion decay constant in the chiral limit, that is,

$$
f = f_\pi + \mathcal{O}(m_q) \ . \tag{2.15}
$$

The next to leading order Lagrangian, $\mathcal{L}_4$, is constructed with the same building blocks than $\mathcal{L}_2$, namely, eqs. (2.3), (2.5), (2.6) and (2.9). Preserving Lorentz invariance, parity and charge conjugation one has [5]:

$$
\begin{aligned}
\mathcal{L}_4 &= L_1 \left\langle D_\mu U^\dagger D^\mu U \right\rangle^2 + L_2 \left\langle D_\mu U^\dagger D_\nu U \right\rangle \left\langle D^\mu U^\dagger D^\nu U \right\rangle \\
&+ L_3 \left\langle D_\mu U^\dagger D^\mu U D_\nu U^\dagger D^\nu U \right\rangle + L_4 \left\langle D_\mu U^\dagger D^\mu U \right\rangle \left\langle U^\dagger \mathcal{M} + \mathcal{M}^\dagger U \right\rangle
\end{aligned}
$$

$$
\begin{aligned}
&+ \quad L_5 \left\langle D_\mu U^\dagger D^\mu U \left(U^\dagger \mathcal{M} + \mathcal{M}^\dagger U\right)\right\rangle + L_6 \left\langle U^\dagger \mathcal{M} + \mathcal{M}^\dagger U\right\rangle^2 \\
&+ \quad L_7 \left\langle U^\dagger \mathcal{M} - \mathcal{M}^\dagger U\right\rangle^2 + L_8 \left\langle \mathcal{M}^\dagger U \mathcal{M}^\dagger U + U^\dagger \mathcal{M} U^\dagger \mathcal{M}\right\rangle \\
&- \quad i L_9 < F_R^{\mu\nu} D_\mu U D_\nu U^\dagger + F_L^{\mu\nu} D_\mu U^\dagger D_\nu U > + L_{10} < U^\dagger F_R^{\mu\nu} U F_{L,\,\mu\nu} > \\
&+ \quad H_1 \left\langle F_{R\,\mu\nu} F_R^{\mu\nu} + F_{L\,\mu\nu} F_L^{\mu\nu}\right\rangle + H_2 \left\langle \mathcal{M}^\dagger \mathcal{M}\right\rangle
\end{aligned}
\tag{2.16}
$$

In $\mathcal{L}_4$ there is also the anomalous term [8,9] although we will not consider it. In the former equation we have also included the strength tensor:

$$
\begin{aligned}
F_L^{\mu\,\nu} &= \partial^\mu \ell^\nu - \partial^\nu \ell^\mu - i[\ell^\mu, \ell^\nu] \\
F_R^{\mu\,\nu} &= \partial^\mu r^\nu - \partial^\nu r^\mu - i[r^\mu, r^\nu]
\end{aligned}
\tag{2.17}
$$

In the $\mathcal{L}_4$ Lagrangian the terms proportional to H_1 and H_2 do not contain the pseudoscalar fields and are therefore not directly measurable. Thus, at $\mathcal{O}(p^4)$ we need ten additional coupling constants L_i to determine the low-energy behaviour of the Green functions. These couplings have an infinite plus a finite part. The infinite part cancels with the infinites from loops, so that at the end only the finite parts, L_i^r, remain. In χPT the $\overline{MS}$-1 scheme is the usual renormalization scheme. At the present time these L_i^r constants have to be fitted to the phenomenology. In general, the number of free parameters increases drastically with the order of the chiral expansion so that for $\mathcal{L}_6$ there are more than one hundred free couplings. This implies that the predictive power of the theory is rapidly lost with higher orders.

On the other hand, the convergence of the χPT series is restricted to low energies, typically for $\sqrt{s} < 500$ MeV, although this upper limit depends strongly on the process. Note that the lightest well established resonance, the $\rho(770)$ has a mass of 770 MeV. This resonance introduces a pole in the T-matrix which cannot be reproduced by a power expansion. Thus, the masses of the heavier states not included in eq. (2.5), put a clear upper limit to the χPT series and also give us an upper limit of the scale $\Lambda_{\chi PT}$ over which χPT is constructed

$$
\frac{\mathcal{O}(p^4)}{\mathcal{O}(p^2)} \sim \frac{p^2}{\Lambda^2_{\chi PT}}
\tag{2.18}
$$

with $\Lambda_{\chi PT} \approx M_\rho \approx 1$ GeV.

One can also obtain an estimation of $\Lambda_{\chi PT}$ by taking into account those contributions coming from loops when allowing a change in the regularization scale by a factor of $\mathcal{O}(1)$ [10]. The result is that

$$
\Lambda_{\chi PT} \leq 4\pi f_\pi \approx 1.2 \text{ GeV}
\tag{2.19}
$$

which is of the same order of magnitude than M_ρ.

2.4 Chiral Lagrangians with meson resonances

Following ref. [11] we include hadron states heavier than the lightest pseudoscalar mesons (π, K, η). The former states will include vector (V), axial (A), scalar (S) and pseudoscalar (P) octets and scalar (S_1) and pseudoscalar (P_1) singlets. The exchange of these resonances between the Goldstone bosons contains the resonance propagators which for $p^2 << M_R^2$ can be expanded as

$$
\frac{1}{p^2 - M_R^2} = \frac{-1}{M_R^2}\left(1 + \frac{p^2}{M_R^2} + \left(\frac{p^2}{M_R^2}\right)^2 + ...\right)
\tag{2.20}
$$

giving rise to contributions which should be embodied in the χPT counterterms. However, from the equation above it is obvious that a resummation to all orders of such local contributions is obtained when including explicit resonance fields.

The lowest order Lagrangian with resonance fields, conserving parity and charge conjugation is given in ref. [11]. Its kinetic part, expressing the vector and axial vector octets in terms of antisymmetric tensor fields $V_{\mu\nu}$ and $A_{\mu\nu}$ (see below), is:

$$\begin{aligned}
\mathcal{L}_{Kin}(R=V,A) &= -\frac{1}{2} < \bigtriangledown^\lambda R_{\lambda\mu} \bigtriangledown_\nu R^{\nu\mu} - \frac{1}{2} M_R^2 R_{\mu\nu} R^{\mu\nu} > \\
&- \frac{1}{2}\partial^\lambda R_{1,\lambda\mu}\partial_\nu R_1^{\nu\mu} + \frac{1}{4} M_{R_1}^2 R_{1,\mu\nu} R_1^{\mu\nu} \\
\mathcal{L}_{Kin}(R=S,P) &= \frac{1}{2} < \bigtriangledown^\mu R \bigtriangledown_\mu R - M_R^2 R^2 > + \frac{1}{2}\partial^\mu R_1 \partial_\mu R_1 - \frac{1}{2} M_{R_1}^2 R_1^2
\end{aligned} \tag{2.21}$$

where the covariant derivative $\bigtriangledown_\mu R$ is defined as

$$\bigtriangledown_\mu R = \partial_\mu R + [\Gamma_\mu, R] \tag{2.22}$$

with

$$\Gamma_\mu = \frac{1}{2}\left\{u^\dagger(\partial_\mu - i r_\mu) u + u(\partial_\mu - i l_\mu) u^\dagger\right\} \tag{2.23}$$

with u such that $u^2 = U$.

The interaction Lagrangians of the octets and singlets of resonances with spin$\leq$1 to lowest order in the chiral expansion are given in ref. [11]:

Vector Octet, $\mathbf{J^{PC} = 1^{--}}$

$$\frac{F_V}{2\sqrt{2}} < V_{\mu\nu} f_+^{\mu\nu} > + \frac{iG_V}{\sqrt{2}} < V_{\mu\nu} u^\mu u^\nu > \tag{2.24}$$

Axial Octet, $\mathbf{J^{PC} = 1^{++}}$

$$\frac{F_A}{2\sqrt{2}} < A_{\mu\nu} f_-^{\mu\nu} > \tag{2.25}$$

Scalar Octet, $\mathbf{J^{PC} = 0^{++}}$

$$c_d \, < S \, u_\mu u^\mu > + c_m \, < S \, \chi_+ > \tag{2.26}$$

Scalar Singlet, $\mathbf{J^{PC} = 0^{++}}$

$$\widetilde{c}_d \, S_1 \, < u_\mu u^\mu > + \widetilde{c}_m \, S_1 \, < \chi_+ > \tag{2.27}$$

Pseudosalar Octet, $\mathbf{J^{PC} = 0^{-+}}$

$$i \, d_m \, < P \, \chi_- > \tag{2.28}$$

Pseudoscalar Singlet, $\mathbf{J^{PC} = 0^{-+}}$

$$i \, \widetilde{d}_m \, P_1 \, < \chi_- > \tag{2.29}$$

where $V_{\mu\nu}$ is

$$V_{\mu\nu} = \begin{pmatrix} \frac{1}{\sqrt{2}}\rho^0 + \frac{1}{\sqrt{6}} w_8 & \rho^+ & K^{*\,+} \\ \rho^- & -\frac{1}{\sqrt{2}}\rho^0 + \frac{1}{\sqrt{6}} w_8 & K^{*\,0} \\ K^{*\,-} & \bar{K}^{*\,0} & -\frac{2}{\sqrt{6}} w_8 \end{pmatrix}_{\mu\nu} \tag{2.30}$$

and similarly for the rest of the octets. From eq. (2.24) and (2.25) the V and A resonances only couple at lowest order as octets. In the former equations the vector and axial octets are included as antisymmetric tensor fields, such that if $|W,p>$ represents a vector or axial resonance with momentum p and mass M, then

$$< 0 | W_{\mu\nu} | W, p > = i \, M^{-1} \left[p_\mu \, \epsilon_\nu(p) - p_\nu \, \epsilon_\mu(p)\right] \tag{2.31}$$

with $\epsilon_\mu(p)$ the polarization (axial)vector of the resonance state. The propagator is given by:

$$\frac{M^{-2}}{M^2-p^2-i\epsilon}\left[g_{\mu\rho}\,g_{\nu\sigma}\,(M^2-p^2)+g_{\mu\rho}\,p_\nu\,p_\sigma-g_{\mu\sigma}\,p_\nu\,p_\rho-(\mu\leftrightarrow\nu)\right] \tag{2.32}$$

In the Lagrangians given above we have also used the following objects which transform as $SU(3)_V$ octets:

$$\begin{aligned} u_\mu &= iu^\dagger D_\mu U u^\dagger = u_\mu^\dagger \\ \chi_\pm &= u^\dagger \mathcal{M} u^\dagger \pm u \mathcal{M}^\dagger u \\ f_\pm^{\mu\nu} &= u F_L^{\mu\nu} u^\dagger \pm u^\dagger F_R^{\mu\nu} u \end{aligned} \tag{2.33}$$

In ref. [11] the $\mathcal{O}(p^4)$ contributions resulting from the exchange of the above resonances are also studied. Note that this is the first order to which resonance exchange contributes to the χPT series since their couplings to the Goldstone fields are $\mathcal{O}(p^2)$.

At $\mathcal{O}(p^4)$ the resonance exchange gives contribution to all the terms of $\mathcal{L}_4$ in eq. (2.16). In fact, it is seen in that reference that, under certain assumptions for the mass and couplings of the scalar resonances, the numerical values obtained for the couplings L_i present in $\mathcal{L}_4$ are saturated by the resonance contributions to them.

2.5 Chiral Lagrangians with baryons

The inclusion of baryons in the chiral formalism is done in a similar way than the one used for the meson resonances, that is, exploiting their well defined linear transformation laws under $SU(3)_V$. We consider here the octet of baryons

$$B=\begin{pmatrix} \frac{1}{\sqrt{2}}\Sigma^0+\frac{1}{\sqrt{6}}\Lambda^0 & \Sigma^+ & p \\ \Sigma^- & -\frac{1}{\sqrt{2}}\Sigma^0+\frac{1}{\sqrt{6}}\Lambda^0 & n \\ \Xi^- & \Xi^0 & -\frac{2}{\sqrt{6}}\Lambda^0 \end{pmatrix} \tag{2.34}$$

The lowest order baryon-meson Lagrangian with at most two baryons can be written as:

$$\begin{aligned} \mathcal{L}_1 =< \bar{B} i\gamma^\mu \bigtriangledown_\mu B > -M_B < \bar{B}B > &+ \frac{1}{2}D < \bar{B}\gamma^\mu\gamma_5 \{u_\mu, B\} > \\ &+ \frac{1}{2}F < \bar{B}\gamma^\mu\gamma_5 [u_\mu, B] > \end{aligned} \tag{2.35}$$

where

$$\bigtriangledown_\mu B = \partial_\mu B + [\Gamma_\mu, B]\ , \tag{2.36}$$

Γ_μ is already defined in Eq. (2.23) and $D+F=g_A=1.257$ and $D-F=0.33$ [1].

Note that, while in the Lagrangians without baryons the number of derivatives is always even, in the case with baryons an odd number of derivatives also appear, and in fact, the former Lagrangian is $\mathcal{O}(p)$. On the other hand in eq. (2.35) M_B is the baryon octet mass in the chiral limit. The baryon mass splitting begins to appear at $\mathcal{O}(p^2)$ satisfying the Gell-Mann [6]-Okubo [7] mass relation for baryons [1].

Finally, from eq. (2.35) one can easily derive the well known Goldberger-Treiman [12] relation and the Kroll-Ruderman term [13].

Chapter 3

Nonperturbative models from chiral symmetry for meson-meson and meson-baryon interactions

The effective chiral Lagrangian techniques have become a widespread tool to address the problem of the low energy interactions of Goldstone bosons [5, 14]. We have presented in *chapter 2*, the χPT formalism [5] which is the low energy effective theory of the strong interactions (QCD). Another example is the standard model strongly interacting symmetry breaking sector (SISBS) [15] or the effective chiral Lagrangians in solid-state physics for high-T_c superconductors [16]. In all the cases, the chiral symmetry constraints are a powerful tool to determine the low energy matrix elements in a systematic way.

These Lagrangians consist of an expansion on the powers of the external momenta of the Goldstone bosons over some typical scale Λ, which is smaller than the masses of the heavier particles. For instance in QCD, resonances typically appear for $\sqrt{s} \gtrsim 0.8$ GeV, so that $\Lambda_{\chi PT} \lesssim 1$ GeV. Of course, when a resonance appears, there is no way to reproduce it from the perturbative expansion since it is associated to a pole in the scattering amplitude. Furthermore, as explained in *section 2.3*, there are also higher order corrections, as chiral loops, which make that $\Lambda_{\chi PT} < 4\,\pi\,f_\pi \approx 1.2$ GeV [10]. As a result, the χPT expansion is typically valid up to energies around 500 MeV with $\Lambda_{\chi PT} \approx 1$ GeV. Nevertheless, the constraints imposed by chiral symmetry breaking are rather powerful and not restricted to the region where χPT is meant to converge [17].

Another drawback of the effective chiral theories, is the appearance of a fast increasing number of free parameters (not fixed by the symmetry) as one increases the order of the calculation. At $\mathcal{O}(p^2)$ the χPT Lagrangian without baryons only contains the masses of pions, kaons and etas and f_π. At $\mathcal{O}(p^4)$ several new free parameters appear: for instance in χPT [5] there are 12 parameters and in the SISBS [18] one needs 13. At $\mathcal{O}(p^6)$ in χPT there are more than 100 new parameters. That is, the predictive power of the theory is lost as we go higher in order.

Because of the former reasons, nonperturbative schemes become necessary in order to go to higher energies and maintain the predictive power of the theory.

3.1 The inverse amplitude method with coupled channels

An attempt to extend the constraints of chiral symmetry to higher energies, constructing a unitary T-matrix, is the Inverse Amplitude Method (IAM) [19]. This approach proved efficient in reproducing low energy data and produced poles in the amplitudes associated

to the ρ and K^* in the vector channel as well as the σ in the scalar one. It has also been applied to study the SISBS resonances that could appear at LHC [20]. Since only elastic unitarity was imposed in the IAM, multichannel problems could not be addressed. In fact, the treatment of coupled channels has proved to be crucial in order to reproduce the basic features of the f_0 and a_0 resonances [21–23] and in general for all the scalar sector with $I = 0, 1, 1/2$ [24,25]. As a consequence, neither the f_0 nor a_0 resonances could be obtained by the elastic IAM [19].

We now proceed to the extension of the IAM with coupled channels which was given for first time in ref. [26].

Let T_L^I be a meson-meson partial wave amplitude with definite isospin I and angular momentum L. If T is the scattering matrix, $S = I - i\,T$ with S the S-matrix, then

$$\begin{aligned} \frac{T^I}{\sqrt{2}^\alpha} &= \sum_{L=0}^{\infty}(2L+1)T_L^I(s)P_L(\cos\theta) \\ T_L^I(s) &= \frac{1}{2\,(\sqrt{2})^\alpha}\int_{-1}^{1} d\cos\theta\, P_L(\cos\theta)\, T^I(s,\cos\theta) \end{aligned} \tag{3.1}$$

where $(\sqrt{2})^\alpha$ is a symmetry factor to take care of the presence of identical particle states as $\eta\eta$ or $\pi\pi$ in the isospin limit. The index α can be 0,1 or 2 depending on the number of times these identical particle states appear in the corresponding partial wave amplitude. For instance, $\alpha = 2$ for $\pi\pi \to \pi\pi$, $\alpha = 1$ for $\eta\eta \to K\bar{K}$, $\alpha = 0$ for $K\pi \to K\pi$ and so on. $P_L(\cos\theta)$ is the Legendre polynomial of L_{th} degree. In the following we will omit the indexes L and I in a partial wave, although it should be kept in mind that we are considering partial wave amplitudes with definite L and I, unless the contrary is said.

In our normalization unitarity in coupled channels reads:

$$\mathrm{Im}\, T_{if} = -T_{in}\,\rho_{nn}\,T^*_{nf} \tag{3.2}$$

where ρ is a real diagonal matrix whose elements account for the phase space of the two meson intermediate states n which are physically accessible. With our normalization, ρ is given by

$$\rho_{nn}(s) = \frac{k_n}{8\pi\sqrt{s}}\theta(s - (m_{1n} + m_{2n})^2) \tag{3.3}$$

where k_n is the on shell center mass (CM) momentum of the meson in the intermediate state n and m_{1n}, m_{2n} are the masses of the two mesons in this state.

Isolating ρ from eq. (3.2) one has:

$$\begin{aligned} \rho &= -T^{-1}\cdot \mathrm{Im}\, T\cdot T^{*-1} \\ &= -\frac{1}{2i}T^{-1}\cdot(T - T^*)\cdot T^{*-1} \\ &= -\frac{1}{2i}(T^{-1*} - T^{-1}) = \mathrm{Im}\, T^{-1} \end{aligned} \tag{3.4}$$

The former result is in fact the basis for the K-matrix formalism [27]. From eq. (3.4) we can write:

$$T^{-1} = \mathrm{Re}\, T^{-1} + i\rho \equiv K^{-1} + i\rho \tag{3.5}$$

where K is the K-matrix which from the former equation is given by

$$K^{-1} = \mathrm{Re}\, T^{-1} \tag{3.6}$$

Once the K-matrix ($\mathrm{Re}\, T^{-1}$) is given, the T-matrix follows by inverting eq. (3.5):

$$T = [K^{-1} + i\rho]^{-1} = [\mathrm{Re}\, T^{-1} + i\,\rho]^{-1} \tag{3.7}$$

We will approach the K-matrix by expanding $\mathrm{Re}\, T^{-1}$ from the $\mathcal{O}(p^4)$ χPT expansion of the T-matrix. In this way, unitarity will be fulfilled to all orders since we know exactly the imaginary part of T^{-1} from eq. (3.4). Another advantage of considering the expansion of T^{-1} is clear when T has a pole. In this case, T^{-1} will have just a zero and hence its expansion will not be affected by this pole of T.

Thus, expanding T^{-1} in powers of p^2 from the expansion of T, one has:

$$T \simeq T_2 + T_4 + ...$$

where T_2 is the lowest order χPT amplitude and T_4 the $\mathcal{O}(p^4)$ contribution,

$$T^{-1} = T_2^{-1} \cdot [1 + T_4 \cdot T_2^{-1} + ...]^{-1} = T_2^{-1} \cdot [1 - T_4 \cdot T_2^{-1} + ...] = T_2^{-1} \cdot [T_2 - T_4 + ...] \cdot T_2^{-1} \tag{3.8}$$

Inverting the former equation we finally have:

$$T = T_2 \cdot [T_2 - T_4]^{-1} \cdot T_2 \tag{3.9}$$

Note that eq. (3.8) fulfills the unitarity requirements given in eq. (3.4) because $\mathrm{Im}\, T_4 = -T_2 \cdot \rho \cdot T_2$ above the physical thresholds. Taking into account eq. (3.6), the K-matrix resulting from eq. (3.8) is given by:

$$K = T_2 \cdot [T_2 - \mathrm{Re}\, T_4]^{-1} \cdot T_2 \tag{3.10}$$

Eq. (3.9) is the extension of the IAM to coupled channels. In the next two sections we describe the application of the former formalism to the study of the meson-meson interactions up to $\sqrt{s} \lesssim 1.2$ GeV. For higher energies more than two meson states are needed since multipion states become increasingly important.

3.1.1 $\pi\pi$ and $K\bar{K}$ amplitudes

In this section we are going to present the results of applying the IAM with coupled channels to the study of the $\pi\pi$ partial wave amplitudes with (I, L)=(0,0), (1,1) and (2,0). The pions couple with the $K\bar{K}$ channel in the waves (0,0) and (1,1), although, as we will see below, this coupling is negligible in the (1,1) case. This study was developed in ref. [28].

In order to apply eq. (3.9) we need the χPT amplitudes up to $\mathcal{O}(p^4)$. For $\pi\pi \to \pi\pi$ this calculation was done in ref. [5] for the $SU(2)$ case and extended to $SU(3)$ in ref. [29]. The $\pi\pi \to K\bar{K}$ amplitude can be obtained by crossing from the $K\pi \to K\pi$ one calculated in ref. [29]. The $K\bar{K} \to K\bar{K}$ was first calculated in ref. [28].

The amplitudes we are considering in this section depend on the L_i couplings of the $\mathcal{O}(p^4)$ χPT Lagrangian, eq. (2.16), that enter in their calculations. These constants are: L_1, L_2, L_3, L_4, L_5 and $2L_6 + L_8$. They are fitted to the elastic $\pi\pi$ phase shifts in the partial waves $(I, L) = (0, 0)$ and (1,1) as shown in Fig. 3.1 and 3.2. The fit was done using MINUIT. In the energy region $\sqrt{s} = 500$–950 MeV the data from different experiments for S-wave $\pi\pi$ phase shifts are incompatible. Given that situation, the central value for each energy is taken as the mean value between the different experimental results [30–34]. For $\sqrt{s} = 0.95$–1 GeV, the mean value comes from [31, 33]. In both cases the

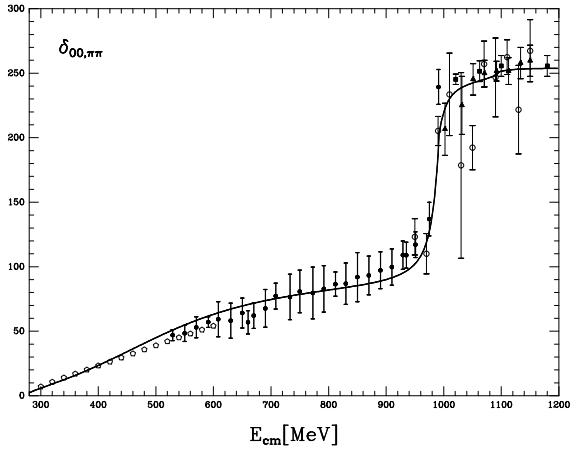

Figure 3.1: Phase shift for $\pi\pi \to \pi\pi$ in $I = L = 0$. Data: Empty pentagon [35]; empty circle [30]; full square [33]; full triangle [31]; full circle represents the average explained in the text.

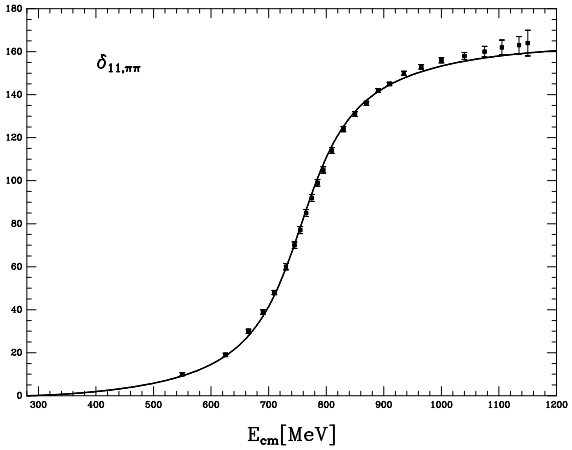

Figure 3.2: Phase shift for $\pi\pi \to \pi\pi$ in $I = L = 1$. Data: [34]

error is the maximum between the experimental errors and the largest distance between the experimental points and the average value. The fit is good with a $\chi^2 = 1.3$ per degree of freedom. The values of the L_i at the M_ρ scale are shown in Table 3.1. In the second column the values obtained from χPT fits at $\mathcal{O}(p^4)$ to the low energy data are also shown. We can see that the values obtained by applying the IAM [28], when the errors are taken into account, are compatible with those from χPT.

Table 3.1: $L_i\, 10^3$ coefficients.

	Fit	χPT
L_1	$0.72^{+0.03}_{-0.02}$	0.4 ± 0.3
L_2	$1.36^{+0.02}_{-0.05}$	1.4 ± 0.3
L_3	-3.24 ± 0.04	-3.5 ± 1.1
L_4	0.20 ± 0.10	-0.3 ± 0.5
L_5	$0.0^{+0.8}_{-0.4}$	1.4 ± 0.5
$2L_6 + L_8$	$0.00^{+0.26}_{-0.20}$	0.5 ± 0.7

With the former values for the L_i coefficients, the inelastic S-wave phase shifts for $K\bar{K} \to \pi\pi$, Fig. 3.3, $\dfrac{1-\eta_{00}^2}{4}$ where η_{00} is the inelasticity in the $I = L = 0$ channel, Fig. 3.4, and the elastic $\pi\pi$ S-wave phase shifts with $I = 2$, Fig. 3.5, are also calculated. In Fig. 3.3 one sees clearly the $\eta\eta$ threshold. Although this channel is not included in the unitarization process, it appears as an intermediate state in the loops of T_4. If we remove from T_4 the imaginary part coming from the intermediate $\eta\eta$ state above its threshold the dashed line results. It is clear then that the inclusion of the $\eta\eta$ channel in the unitarization procedure for the (0,0) channels is important. This point will be further considered in *section 3.2.3* and at the end of *section 3.3.1*.

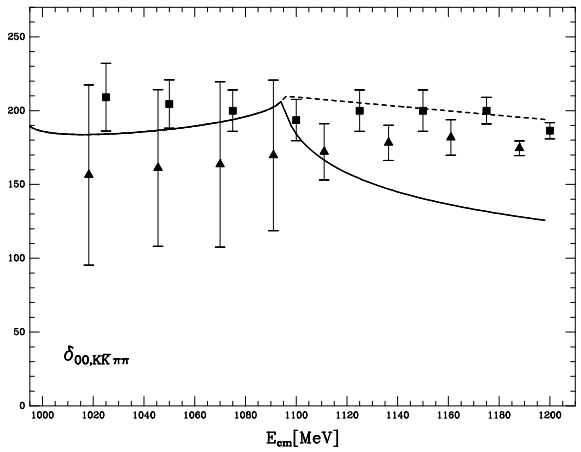

Figure 3.3: Phase shift for $\pi\pi \to K\bar{K}$ in $I = L = 0$. Data: full square [36], full triangle [37].

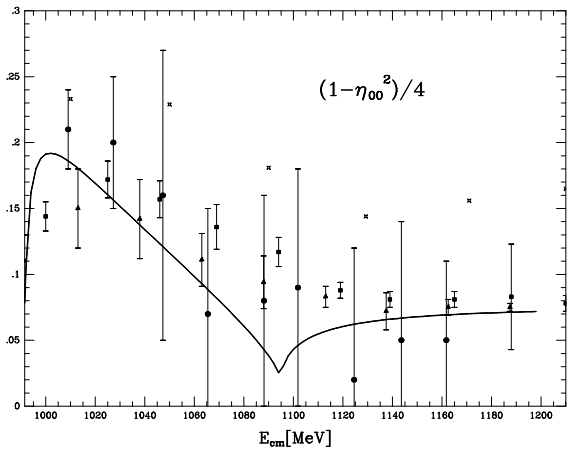

Figure 3.4: $(1-(\eta_{00})^2)/4$, where η_{00} is the inelasticity in $I = L = 0$. Data: starred square [35], full square [36], full triangle [37], full circle [38].

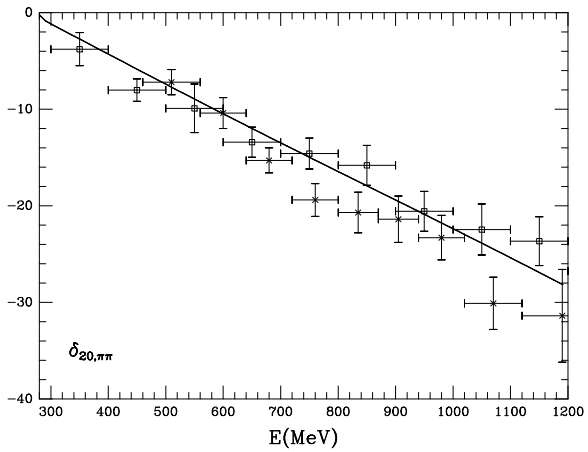

Figure 3.5: Phase shift for $\pi\pi \to \pi\pi$ in $I = 2, L = 0$. Data: cross [39], empty square [40].

The scattering lengths of the channels (I, L)=(0,0), (1,1) and (2,0) were also calculated in ref. [28]. These scattering lengths are denoted by a_L^I. In Table 3.2 we show the values obtained for a_L^I in ref. [28] together with the experimental ones and the χPT values up to $\mathcal{O}(p^4)$. We see in this table that a good agreement with experiment is accomplished. The values of ref. [28] are also close to the ones from χPT as one should expect because at low energies the IAM recovers the chiral expansion up to $\mathcal{O}(p^4)$.

Table 3.2: Comparison of scattering lengths in different channels.

a_L^I	χPT	Results from ref. [28]	Experiment
a_0^0	0.20 ± 0.01	0.210 ± 0.002	0.26 ± 0.05
a_1^1	0.037 ± 0.002	0.0356 ± 0.0008	0.038 ± 0.002
a_0^2	-0.041 ± 0.004	-0.040 ± 0.001	-0.028 ± 0.012

3.1.2 Two-meson scattering below 1.2 GeV

In the previous section the IAM with coupled channels was applied with the full $\mathcal{O}(p^4)$ χPT amplitudes. The calculation of the latter amplitudes is rather involved and it is not

done in all two-meson channels, for instance, in those channels with the η meson. In this section, following ref. [41], an approximation to calculate the $\mathcal{O}(p^4)$ amplitude, which turns out to be technically much simpler and rather accurate at the phenomenological level, is presented. Then, eq. (3.9) will be applied to study the partial waves (I, L)=(0,0), (1,0), (2,0), (1/2,0), (3/2,0), (1,1), (1/2,1) and (0,1). One considers the channels shown in Table 3.3, which are supposed to be the dominant ones up to $\sqrt{s} \lesssim 1.2$ GeV.

Table 3.3: Channels used in the different I, L channels

	$I=0$	$I=1/2$	$I=1$	$I=3/2$	$I=2$
L=0	$\pi\pi$ $K\bar{K}$	$K\pi$ $K\eta$	$\pi\eta$ $K\bar{K}$	$K\pi$	$\pi\pi$
L=1	$K\bar{K}$	$K\pi$ $K\eta$	$\pi\pi$ $K\bar{K}$		

The T_4 amplitudes are then approximated in ref. [41] by

$$T_4 \approx T_4^P + T_2 \cdot g(s) \cdot T_2 \tag{3.11}$$

where T_4^P represents the polynomial tree level amplitudes from the $\mathcal{O}(p^4)$ Lagrangian, eq. (2.16), and are given in the Appendix A of ref. [41]. On the other hand, $g(s)$ is a diagonal matrix corresponding to the loop integral with two meson propagators, given by:

$$g_{nn}(s) = i \int \frac{d^4q}{(2\pi)^4} \frac{1}{q^2 - m_{1n}^2 + i\epsilon} \frac{1}{(P-q)^2 - m_{2n}^2 + i\epsilon} \tag{3.12}$$

where P is the total initial four-momentum of the two meson system. This g matrix has the property

$$\text{Im } g_{nn}(s) = -\rho_{nn}(s) \tag{3.13}$$

as can be easily checked.

The real part of $g(s)$ is divergent and requires regularization. In ref. [41] it is evaluated by a cut off regularization with a maximum value, q_{max}, for the modulus of the three-momentum in the integral. Because the divergence in eq. (3.12) is only logarithmic its calculation making use of dimensional regularization is numerically equivalent when, depending on the considered renormalization scheme, the dimensional regularization scale μ is properly chosen as a function of q_{max}. For instance, in the $\overline{MS} - 1$ renormalization scheme, the one used in χPT, $\mu \approx 1.2\, q_{max}$ [41]. In *section 3.2.2* the expression of $g(s)$ in dimensional regularization is given.

When approximating T_4 by eq. (3.11) one is taking into account the close relationship between T_4^P and the vector mesons [11] and the dominant role that the unitarization with coupled channels of the lowest order χPT amplitudes has in the scalar sector [23, 42]. In fact, the approach of ref. [23] follows in the limit $T_4^P = 0$. With respect to a full $\mathcal{O}(p^4)$ χPT calculation, neither tadpoles nor loops in crossed channels are included. These are soft contributions which will be reabsorbed in the L_i coefficients, which are now denoted by $\hat{L}_i$ since differences begin to rise even at $\mathcal{O}(p^4)$ with respect to the L_i of χPT.

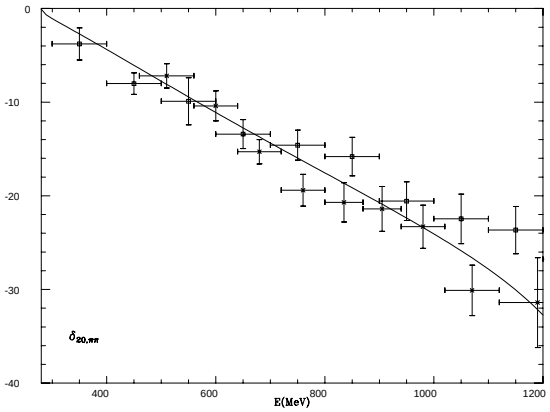

Figure 3.6: Phase shifts for $\pi\pi \to \pi\pi$ in the $I = 2$, $L = 0$ channel. Data: cross [39], empty square [40].

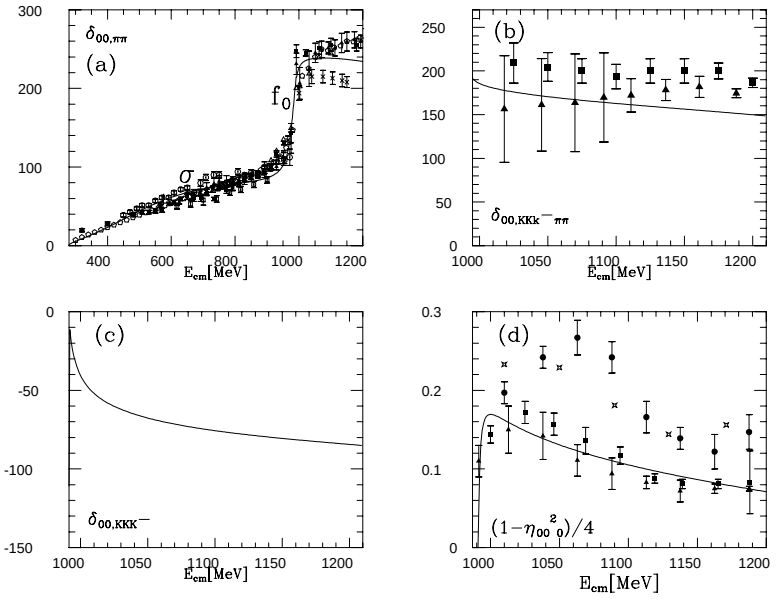

Figure 3.7: Results in the $I = L = 0$ channel. (a) phase shifts for $\pi\pi \to \pi\pi$ as a fraction of the c.m. energy of the meson pair: full triangle [31], open circle [32], full square [33], open triangle [43], open square [44] (all these are analysis of the same experiment [45]), cross [34], full circle [46], empty pentagon [35]. (b) phase shifts for $K\bar{K} \to \pi\pi$: full square [36] , full triangle [37]. (c) Phase shifts for $K\bar{K} \to K\bar{K}$. (d) Inelasticity: results and data for $(1 - \eta^2)/4$: starred square [35], full square [36] , full triangle [37], full circle [47].

From Fig. 3.6 to 3.13 we show the fit of ref. [55] to the meson-meson S and P-wave experimental data, phase shifts and inelasticities. In this reference an error was detected in the T_4^P amplitude $K^+K^- \to K^0\bar{K}^0$ calculated in ref. [41] (the corrected expression is given in the Appendix of ref. [55]). As a result, the fit presented in ref. [41] was redone making use of MINUIT and the results are the ones displayed in the former figures. In ref. [55] several sets of values of the $\hat{L}_i$ coefficients were found giving rise to fits of similar quality. The main difference between the different sets of values is in the value of $\hat{L}_7$ which can even change sign. We report here the fit with the $\hat{L}_i$ coefficients closer to the L_i of $\mathcal{O}(p^4)$ χPT.

In Table 3.4 the corresponding values of the couplings are given and compared with the ones of $\mathcal{O}(p^4)$ χPT. As we see from the figures, the results are in rather good agreement with a vast amount of experimental data. The resonances that appear are indicated with their corresponding names.

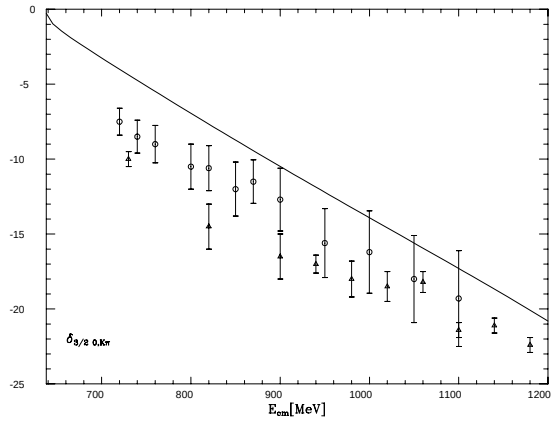

Figure 3.8: Phase shifts for $K\pi \to K\pi$ in the $I = 3/2$, $L = 0$ channel. Data: open triangle [48], open circle [49].

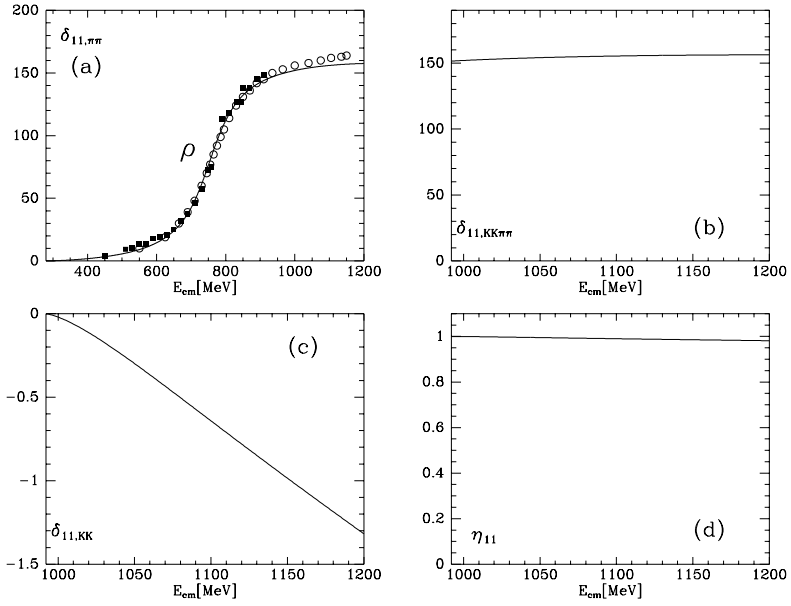

Figure 3.9: Results in the $I = L = 1$ channel. (a) phase shifts for $\pi\pi \to \pi\pi$. Data: open circle [34], black square [32]. (b), (c) same as in Fig. 3.7. (d) inelasticity.

Some comment is needed with respect to the (0,1) channel, Fig. 3.13. In this channel a pole appears with a mass around 910 MeV. Below 1.2 GeV there are two resonances with such quantum numbers. They are the ω and the ϕ, which fit well within the $q\bar{q}$ scheme, with practically ideal mixing, as $\frac{1}{\sqrt{2}}(u\bar{u} + d\bar{d})$ and $s\bar{s}$, respectively. In the limit of exact SU(3) symmetry these resonances manifest as one antisymmetric octet state and a symmetric singlet state. Since the spatial function of the $K\bar{K}$ state is antisymmetric its SU(3) wave function has to be also antisymmetric and therefore it only couples to the antisymmetric octet resonance. Of course, the amplitudes given by eq. (3.11), do contain some SU(3) breaking, but, in this channel only the $K\bar{K}$ state is considered, neglecting states with other mesons (like the three pion channel) and, hence, the formulae for this process do not contain any SU(3) symmetry breaking term. Thus, one just sees one pole,

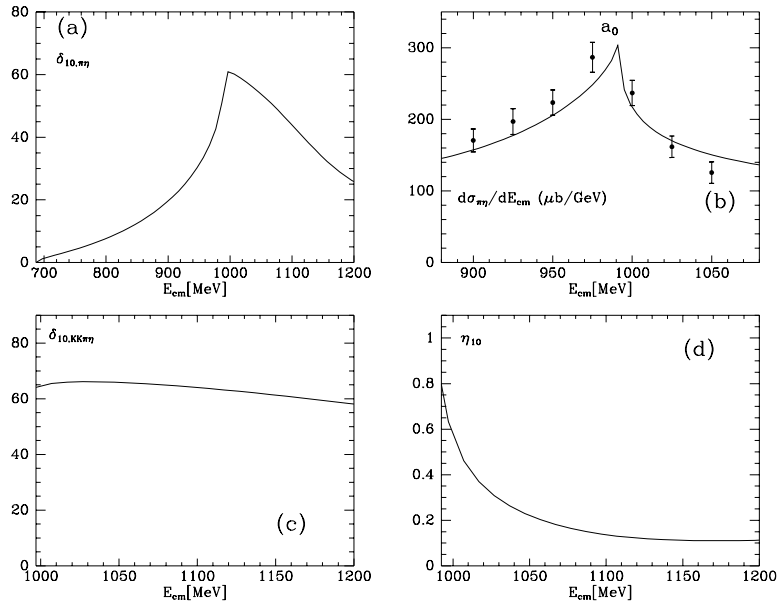

Figure 3.10: Results in the $I = 1$, $L = 0$ channel. (a) phase shifts for $\pi\eta \to \pi\eta$. (b) Invariant mass distribution for $\pi\eta$ data from [50]. (c) Phase shifts for $K\bar{K} \to \pi\eta$. (d) inelasticity.

ω_8, corresponding to the antisymmetric octet state of the exact SU(3) limit. The ω_8 meson will be studied in further detail in *section 4.2*, in connection with the ϕ resonance and its decays.

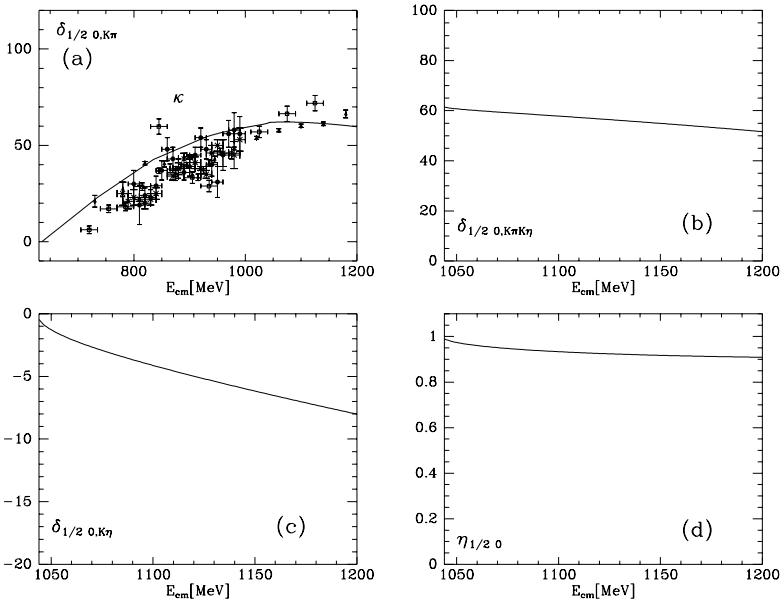

Figure 3.11: Results in the $I = 1/2$, $L = 0$ channel. (a) phase shifts for $K\pi \to K\pi$. Data: full circle [51], cross [52] , open square [53], full triangle [48], open circle [54]. (b) phase shifts for $K\pi \to K\eta$. (c) phase shifts for $K\eta \to K\eta$. (d) inelasticity.

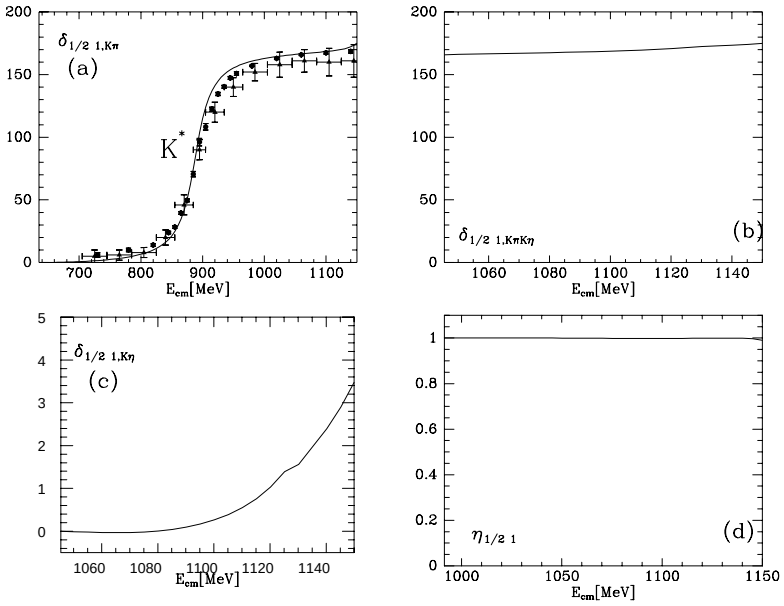

Figure 3.12: Results in the $I = 1/2$, $L = 1$ channel. (a) phase shifts for $K\pi \to K\pi$. Data: full triangle [51], open circle [48]. (b) phase shifts for $K\pi \to K\eta$. (c) phase shifts for $K\eta \to K\eta$. (d) inelasticity.

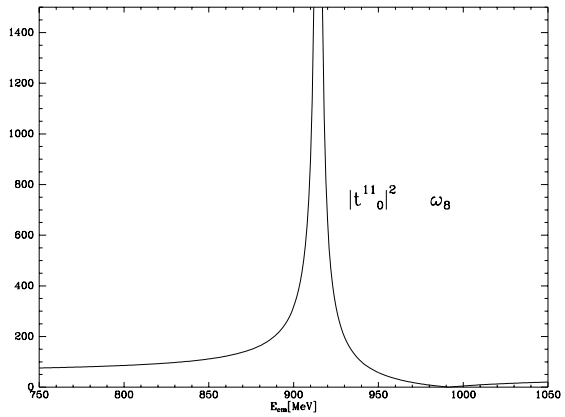

Figure 3.13: $|T_{IJ=01}|^2$ for $K\bar{K} \to K\bar{K}$ showing a singularity corresponding to a resonance belonging to the antisymmetric vector octet.

Table 3.4: Fit parameters $\hat{L}_i \cdot 10^3$ [55] and comparison with the $L_i^r \cdot 10^3$ of χPT

	q_{max} (MeV)	$\hat{L}_1$	$\hat{L}_2$	$\hat{L}_3$	$\hat{L}_4$	$\hat{L}_5$	$2\hat{L}_6 + \hat{L}_8$	$\hat{L}_7$
Fit	647	0.94	1.60	-3.74	-.019	0.94	0.67	-.051
χPT	DR Scale	L_1	L_2	L_3	L_4	L_5	$2L_6 + L_8$	L_7
	$\mu = M_\rho$	0.4 $\pm$0.3	1.4 $\pm$0.3	-3.5 $\pm$1.1	-0.3 $\pm$0.5	1.4 $\pm$0.5	0.5 $\pm$0.7	-0.4 $\pm$0.2

Pole positions, widths and partial decay widths

In ref. [41] the poles of the T-matrix in the complex plane, which appear in the unphysical Riemann sheets, are also studied and we refer to this reference for further details. These poles correspond to the $f_0(980)$, $a_0(980)$, σ, $\rho(770)$, $K^*(890)$, κ and the ω_8 resonance. The changes in the values of the masses, partial and total decay widths of the different

resonances [41], due to the error detected in ref. [55], are rather small except in the case of the $a_0(980)$ resonance. For the values of the $\hat{L}_i$ coefficients given in Table 3.4, the pole of the $a_0(980)$ in the second sheet ($k_{\pi^0\eta} < 0$, $k_{K\bar{K}} > 0$) appears at $(1195 - i\,350)$ MeV. However, a new one appears in the fourth sheet ($k_{\pi^0\eta} > 0$, $k_{K\bar{K}} < 0$) at: $(1111 - i\,118)$ MeV. When doing a fit, the $I = 1$, $L = 0$ channel has very little statistical weight due to the lack of experimental data so that an improvement of this experimental situation would be very welcome. For instance, we will see in the next section a good reproduction of the experimental scalar data showing an $a_0(980)$ resonance with just a pole also in the second sheet.

3.2 Inclusion of Explicit Resonance Fields

χPT [5] can be supplied with the exchange of explicit resonance fields [11]. In doing this, a resummation up to an infinite order in the chiral expansion can be achieved from the expansion of the bare propagator of a resonance, as we have already seen in eq. (2.20). However, the amplitudes that can be built directly from χPT at $\mathcal{O}(p^4)$ plus resonance exchanges as in ref. [56] need a unitarization procedure, in order to compare directly with experimental data (phase shifts, inelasticities...) for the different energy regions, in particular, around the resonance masses. This is one of the aims of the present section.

On the other hand, it is well known that the scalar sector is much more controversial than the vector one. In the latter case, the properties of the associated spectroscopy can be understood in terms of first principles coming directly from QCD as Chiral Symmetry and Large N_c plus unitarity, once we admit VMD as dictated by phenomenology [57, 58]. In ref. [25] the same basic principles than before, that is, Chiral Symmetry, Large N_c and unitarity in coupled channels, were applied in order to study the scalar resonant channels. We will also pay special attention to the issue of the nature of the scalar resonances that we will find in the amplitudes. As it is well known, the low energy scalar resonances have been ascribed [59] to different models as: conventional $q\bar{q}$ mesons [24, 60], $q^2\bar{q}^2$ states [61, 62], $K\bar{K}$ molecules [21–23], glueballs [63] and/or hybrids [64]. The question about the nature of the resonances is specially important in order to determine their contributions to the L_i counterterms. For instance, the resonances considered in ref. [11] are supposed to be preexisting ones (their masses are $\mathcal{O}(1)$ in Large N_c counting rules) and their contributions to the previous couplings arise dominantly from their bare propagators. However, as it is shown below, there are also resonances, like the σ or the $a_0(980)$, that are originated from the interactions between the pseudoscalars [25] and hence their contributions to the L_i come just from the loops of the pseudoscalars.

3.2.1 Formalism

We present here a formalism based on the N/D method [65] in order to provide physical amplitudes from χPT supplied with the exchange of explicit resonance fields as given in ref. [11]. This formalism was derived in ref. [25].

A $T(s)$ partial wave amplitude has two kinds of cuts. The right hand cut required by unitarity and the unphysical cuts from crossing symmetry. In our chosen normalization, the right hand cut leads to eq. (3.4):

$$\mathrm{Im}\, T^{-1} \;=\; \rho(s) \tag{3.14}$$

for $s > s_{threshold} \equiv s_{th}$. In the case of two particle scattering, the one we are concerned about, $s_{th} = (m_1 + m_2)^2$ and $\rho(s)$ is given in eq. (3.3).

The unphysical cuts comprise two types of cuts in the complex s-plane. For processes of the type $a+a \to a+a$ with $m_1 = m_2 = m_a$, there is only a left hand cut for $s < s_{Left}$. However for those of the type $a+b \to a+b$ with $m_1 = m_a$ and $m_2 = m_b$, apart from a left hand cut there is also a circular cut in the complex s-plane for $|s| = m_2^2 - m_1^2$, where we have taken $m_2 > m_1$. In the rest of this section, for simplicity in the formalism, we will just refer to the left hand cut as if it were the full set of unphysical cuts. This will be enough for our purposes in this section. In any case, if one works in the complex p^2-plane all the cuts will be linear cuts and then only the left hand cut will appear in this variable.

The left hand cut, for $s < s_{Left}$, reads:

$$T(s+i\epsilon) - T(s-i\epsilon) = 2i\mathrm{Im}\, T_{Left}(s) \tag{3.15}$$

The standard way of taking into account eqs. (3.14) and (3.15) is the N/D method [65]. In this method a $T(s)$ partial wave is expressed as a ratio of two functions,

$$T(s) = \frac{N(s)}{D(s)} \tag{3.16}$$

with the denominator function, $D(s)$, bearing the right hand cut and the numerator function, $N(s)$, the unphysical cuts.

In order to take explicitly into account the behavior of a partial wave amplitude near threshold, which vanishes as $p^{2L} \equiv \nu^L$, we consider the new quantity, T', given by:

$$T'(s) = \frac{T(s)}{\nu^L} \tag{3.17}$$

which also satisfies relations of the type of eqs. (3.14) and (3.15). Hence, we can write:

$$T'(s) = \frac{N'(s)}{D'(s)} \tag{3.18}$$

From eqs. (3.14), (3.15) and (3.17), $\mathrm{N}'(s)$ and $\mathrm{D}'(s)$ will obey the following equations:

$$\begin{array}{ll} \mathrm{Im}\, D' = \mathrm{Im}\, T'^{-1}\ N' = \rho(s) N' \nu^L, & s > s_{th} \\ \mathrm{Im}\, D' = 0, & s < s_{th} \end{array} \tag{3.19}$$

$$\begin{array}{ll} \mathrm{Im}\, N' = \mathrm{Im}\, T'_{Left}\ D', & s < s_{Left} \\ \mathrm{Im}\, N' = 0, & s > s_{Left} \end{array} \tag{3.20}$$

where $\mathrm{Im}\, T'_{Left} = \dfrac{\mathrm{Im}\, T_{left}}{\nu^L}$.

It is important to notice that N' and D' can be simultaneously multiplied by any arbitrary real analytic function without changing its ratio, T', nor eqs. (3.19) and (3.20). In this way, we can always consider N' free of poles.

Thus, using dispersion relations for $N'_L(s)$, we write from eq. (3.20):

$$N'(s) = \frac{(s-s_0)^{n+1}}{\pi} \int_{-\infty}^{s_{Left}} ds' \frac{\mathrm{Im}\, T'_{Left}(s') D'(s')}{\nu(s')^L (s'-s_0)^{n+1}(s'-s)} + \sum_{m=0}^{n} \overline{a}'_m s^m \tag{3.21}$$

with n such that

$$\lim_{s\to\infty} \frac{N'(s)}{s^{n+1}} = 0 \tag{3.22}$$

In the following, the unphysical cuts will be considered in a perturbative way. In fact, this was the case in the former section where we reported the IAM results from refs. [26, 28, 41, 55]. In this method the unphysical cuts are only considered up to $\mathcal{O}(p^4)$

as in the χPT calculations. That is, from the resummation done by the IAM one obtains fully unitarized partial wave amplitudes but satisfying crossing symmetry perturbatively up to $\mathcal{O}(p^4)$. As a matter of fact, we have seen that one can reproduce rather accurately the meson-meson interactions. Hence, the approach of considering the unphysical cuts in a perturbative way seems to be a realistic one for the physical region. First, we study the zeroth order approach, that is, no unphysical cuts at all, obtaining the most general structure that a partial wave amplitude has in such case. Note that any unitarization method without unphysical cuts must then implement this structure (as an example see the amplitudes of refs. [23,66]). Later on, we will also consider the inclusion of the unphysical cuts up to one loop calculated at $\mathcal{O}(p^4)$. In this case, the χPT expansion up to $\mathcal{O}(p^4)$ will be recovered for the low energy region and the IAM, eq. (3.9), will also appear as a special case.

No unphysical cuts

In this case, we have $\mathrm{Im}\, T_{Left} = 0$ and then from eq. (3.21):

$$N'(s) = \sum_{m=0}^{n} a'_m s^m \tag{3.23}$$

that is, N' is just a polynomial. Then, after dividing N' and D' by this polynomial, one has:

$$N' = 1 \tag{3.24}$$

and the dispersion relation for D' will read from eq. (3.19)

$$D'(s) = \frac{(s-s_0)^{L+1}}{\pi}\int_{s_{th}}^{\infty} ds' \frac{\nu(s')^L \rho(s')}{(s'-s)(s'-s_0)^{L+1}} + \sum_{m=0}^{L} a_m s^m + \sum_{i}^{M_L} \frac{R_i}{s-s_i} \tag{3.25}$$

where the last sum takes into account the possible presence of poles of D' (zeros of T') inside and along the integration contour, which is given by a circle in the infinity deformed to engulf the real axis along the right hand cut. Each term of this sum is referred to as a Castillejo-Dalitz-Dyson (CDD) pole after ref. [67]. Note that since $N' = 1$ from eq. (3.18) $T' = \dfrac{1}{D'}$.

Let us come back to QCD and split the subtraction constants a_m of eq. (3.25) in two pieces

$$a_m = a_m^L + a_m^{SL}(s_0) \tag{3.26}$$

The term a_m^L will go as N_c, because in the $N_c \to \infty$ limit, the meson-meson amplitudes go as N_c^{-1} [68]. Since the integral in eq. (3.25) is $\mathcal{O}(1)$ in this counting, the subleading term $a_m^{SL}(s_0)$ is of the same order and depends on the subtraction point s_0. This implies that eq. (3.25), when $N_c \to \infty$, will become

$$D'(s) \equiv D'^{\infty}(s) = \sum_{m=0}^{L} a_m^L s^m + \sum_{i}^{M_L^\infty} \frac{R_i^\infty}{s-s_i} \tag{3.27}$$

where R_i^∞ is the leading part of R_i and M_L^∞ counts the number of leading CDD poles.

Clearly eq. (3.27) represents tree level structures, contact and pole terms, which have nothing to do with any kind of potential scattering, which in large N_c QCD is suppressed.

In order to determine eq. (3.27) one can make use of χPT [5] and of the paper [11]. In this latter reference the way to include resonances with spin ≤ 1, consistently with chiral symmetry at lowest order in the chiral power counting, is shown. It is also seen that, when integrating out the resonance fields, the contributions of the exchange of these resonances essentially saturate the next to leading χPT Lagrangian. We will make use of this result in order to state that in the inverse of eq. (3.27) the contact terms come just from the lowest order χPT Lagrangian and the pole terms from the exchange of resonances in the s-channel in the way given by ref. [11] (consistently with our approximation of neglecting the left hand cut the exchange of resonances in crossed channels is not considered). In the latter statement it is assumed that the result of ref. [11] at $\mathcal{O}(p^4)$ is also applicable to higher orders. That is, local terms appearing in χPT and from eq. (3.27) of order higher than $\mathcal{O}(p^4)$ are also saturated from the exchange of resonances for $N_c >> 1$, where loops are suppressed.

In ref. [25] it is proved that eq. (3.27) can accommodate the tree level amplitudes coming from lowest order χPT [5] and the Lagrangian given in ref. [11] for the coupling of resonances (with spin$\leq$1) with the lightest pseudoscalars (π, K, η).

Thus, if we denote by T_2 the $\mathcal{O}(p^2)$ χPT amplitudes and by T^R the contribution from the s-channel exchange of resonances according to ref. [11], we can write:

$$T^\infty \equiv T_2 + T^R = \nu^L \left[D'^\infty\right]^{-1} \tag{3.28}$$

On the other hand, we define the function $g_L(s)$ by

$$g_L(s)\nu^L = -\sum_{m=0}^{L} a_m^{SL}(s_0)s^m - \frac{(s-s_0)^{L+1}}{\pi}\int_{s_{th}}^{\infty} ds' \frac{\nu(s')^L \rho(s')}{(s'-s)(s'-s_0)^{L+1}} \tag{3.29}$$

After these definitions, we can write our final formula for $T(s)$, in the case that unphysical cuts are not considered, as:

$$T(s) = \left[(T^\infty)^{-1} - g_L(s)\right]^{-1} \tag{3.30}$$

The physical meaning of eq. (3.30) is clear. The T^∞ amplitudes correspond to the tree level structures present before unitarization. The unitarization is then accomplished through the function $g_L(s)$.

From the former comments the generalization of eq. (3.30) to coupled channels should be obvious. In this case, $T^\infty(s)$ is a matrix determined by the tree level partial wave amplitudes given by the lowest order χPT Lagrangian [5] and the exchange of resonances [11]. For instance, $[T^\infty(s)]_{11} = (T_2)_{11} + T^R_{11}$, $[T^\infty_L(s)]_{12} = (T_2)_{12} + T^R_{12}$ and so on. Once we have $T^\infty(s)$ its inverse is the one which enters in eq. (3.30). Because $N'(s)$ is proportional to the identity, $g_L(s)$ will be a diagonal matrix, accounting for the right hand cut, as in the elastic case. In this way, unitarity, which in coupled channels reads (above the thresholds of the channels i and j)

$$[\mathrm{Im}\, T^{-1}]_{ij} = \rho_{ii}(s)\delta_{ij} = -\mathrm{Im}\, g_L(s)_{ii}\delta_{ij} \tag{3.31}$$

is fulfilled. The matrix element $g_L(s)_{ii}$ obeys eq. (3.29) with the right masses corresponding to the channel i and its own subtraction constants $a_i^{SL}(s_0)$.

In ref. [25] the coupling constants and resonance masses contained in $\mathrm{T}^\infty_L(s)$ are fitted to the experiment. The same happens with the a_i^{SL} although, as we will discuss below, they are related by $SU(3)$ considerations.

In Appendix A of ref. [25] the already mentioned coupled channel version of eq. (3.30) is deduced directly from the N/D method in coupled channels [69].

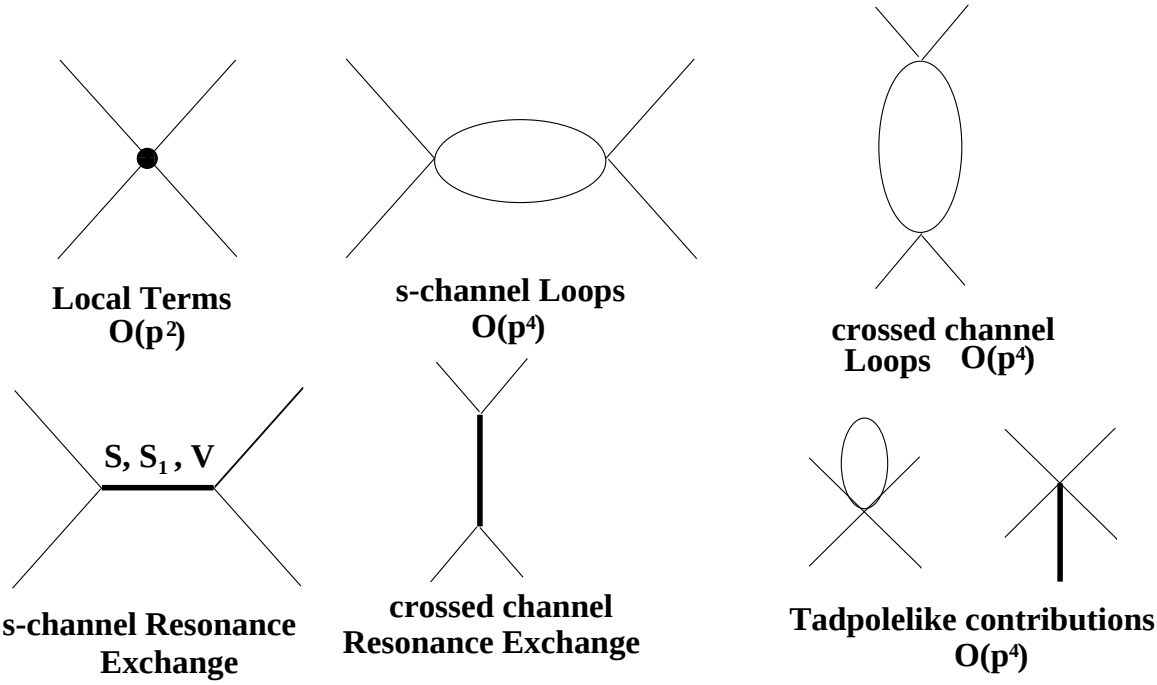

Figure 3.14: Diagrams contained in eq. (3.32), from χPT up to $\mathcal{O}(p^4)$ and from the exchange of resonances [11]. Wave function renormalization is not depicted.

The unphysical cuts at one loop at $\mathcal{O}(p^4)$

In a full calculation for a meson-meson partial wave amplitude combining χPT at $\mathcal{O}(p^4)$ and the exchange of resonances as done in ref. [56] one has to include the diagrams depicted in Fig. 3.14. The lowest order χPT amplitudes, T_2, plus the exchange of resonances in the s-channel, T^R, were already taken into account in the previous section. The sum of both contributions was denoted by T^∞. One also generates through the $g_L(s)$ function the loops in the s-channel responsible for unitarity. Thus, in matrix notation at $\mathcal{O}(p^4)$ we have from eq. (3.30): $T_2 \cdot g_L(s) \cdot T_2$. Note that the difference between the loops in the s-channel calculated in χPT at $\mathcal{O}(p^4)$ and the ones we have obtained can be at most of a polynomial of second order in s. We denote the rest of contributions coming from the exchange of resonances and loops in the crossed channels, tadpole-like contributions and the previous difference between our loops in the s-channel and the ones from χPT by T_{Left}, since they only have unphysical cuts. Then, in the present notation, a partial wave amplitude calculated as in ref. [56] can be written as:

$$T^\infty + T_{Left} + T_2 \cdot g_L(s) \cdot T_2 \tag{3.32}$$

An N/D representation of the former amplitude can be done as follows. This representation contains the unphysical cuts up to the order considered in eq. (3.32), that is, up to one loop calculated at $\mathcal{O}(p^4)$. In matrix formalism:

$$\begin{aligned} N &= T^\infty + T_{Left} \\ D &= I - N \cdot g_L \\ T &= D^{-1} \cdot N \end{aligned} \tag{3.33}$$

Making a chiral expansion of the former result, one has:

$$T = N + N \cdot g \cdot N + \mathcal{O}(p^6\hbar, \hbar^2) = T_0^\infty + T_{Left} + T_2 \cdot g_L \cdot T_2 + \mathcal{O}(p^6\hbar, \hbar^2) \tag{3.34}$$

reproducing eq. (3.32). In the former equation, $\mathcal{O}(p^6\hbar,\hbar^2)$ indicates that the result is valid up to one loop calculated at $\mathcal{O}(p^4)$. One can also check that, up to the same order in the unphysical cuts, the N and D functions satisfy eqs. (3.19) and (3.20):

$$\begin{aligned}
\text{Im } D &= N\cdot \text{Im } g_L = N\cdot\rho(s) && s>s_{th} \\
\text{Im } D &= \mathcal{O}(p^6\hbar,\hbar^2) && s \text{ in unphysical cuts} \\
\text{Im } N &= D\cdot \text{Im } T = \text{Im } T_{Left}+\mathcal{O}(p^6\hbar,\hbar^2) && s \text{ in unphysical cuts}
\end{aligned} \tag{3.35}$$

One can reabsorb T_0^∞ in D just by multiplying N and D at the same time by $(T_0^\infty)^{-1}$. In this way, neither their ratio nor their cut structure are modified since T_0^∞ is just a matrix of real rational functions. Then one has

$$\begin{aligned}
N &= I+(T^\infty)^{-1}\cdot T_{Left} \\
D &= (T^\infty)^{-1}-(I+(T^\infty)^{-1}\cdot T_{Left})\cdot g_L(s)
\end{aligned} \tag{3.36}$$

In any case eq. (3.33) can also be written as:

$$T=\left[(T^\infty+T_{Left})^{-1}-g_L(s)\right]^{-1} \tag{3.37}$$

setting T_{Left} to zero we recover once again the limit case of eq. (3.30), where no unphysical cuts are included.

The former equation has being used in ref. [70] to describe the coupled channel scattering of $K\pi$ and $K\eta'$ in order to obtain the scalar $K\pi$ form factor. It has also being used in ref. [71] to describe the strong WW scattering for a heavy Higgs boson. The main conclusion of this work is that for a general scenario with heavy particles with a mass much larger than $4\pi v\approx 3$ TeV, a isoscalar-scalar WW resonance would appear with a mass $\lesssim$1 TeV. As a consequence, this resonance, which would not be responsible for the spontaneous breaking of the electroweak symmetry $SU(2)_L\times U(1)_Y$, could be confused with a true Higgs particle with a mass around 1 TeV at LHC.

From eq. (3.37) one can also reobtain the IAM with coupled channels, eq. (3.9). In order to do this, let us expand the inverted matrix in eq. (3.37) analogously as in eq. (3.8):

$$\begin{aligned}
(T^\infty+T_{Left})^{-1}-g_L(s) &= (T_2+\mathcal{T}_4+...)^{-1}-g_L(s) \\
&= T_2^{-1}\cdot(1+\mathcal{T}_4\cdot T_2^{-1}+...)^{-1}-g_L(s) \\
&= T_2^{-1}\cdot(1-\mathcal{T}_4\cdot T_2^{-1}+...)-g_L(s) \\
&= T_2^{-1}\cdot(T_2-\mathcal{T}_4-T_2\cdot g_L(s)\cdot T_2+...)\cdot T_2^{-1} \\
&\approx T_2^{-1}\cdot(T_2-T_4)\cdot T_2^{-1}
\end{aligned} \tag{3.38}$$

In the previous equation $\mathcal{T}_4$ is the $\mathcal{O}(p^4)$ contribution of $T^\infty+T_{Left}$. Inverting the former result and assuming the saturation of the L_i coefficients by the exchange of resonances [11], one recovers eq. (3.9).

3.2.2 Results I: The vector sector

In ref. [25] the $\pi\pi$ and $K\pi$ scattering with I=L=1 and I=1/2, L=1, respectively, were studied. As we will see below, one reproduces the well known features associated with the vectors: VMD and the KSFR relation [72] for the couplings of these resonances to the pseudoscalars.

For the special case of the P-waves, since the zero at threshold is a simple one, instead of eq. (3.25), we consider the slightly modified formula:

$$\mathrm{D}(s) = \sum_i \frac{\gamma_i}{s - s_i} + a - \frac{s - s_0}{\pi} \int_{s_{th}}^{\infty} ds' \frac{\rho(s')}{(s' - s)(s' - s_0)} \tag{3.39}$$

where the threshold zero has passed to poles in the denominator function, D. This equation is derived analogously to eq. (3.25) but working directly with T rather than with T'. Another advantage of using eq. (3.39) instead of eq. (3.25) is that the comparison with the scalar sector will be more straightforward, because the dispersive integral will be the same.

The integral in eq. (3.39) will be evaluated making use of dimensional regularization. It can be identified up to a constant with eq. (3.12). This identification is a consequence of the fact that both the integral in eq. (3.39) and the one in eq. (3.12) have the same cut and the same imaginary part along this cut, as it can be easily checked. Thus, one has:

$$\begin{aligned} g_0(s) &= -a^{SL}(s_0) - \frac{s - s_0}{\pi} \int_{s_{th}}^{\infty} ds' \frac{\rho(s')}{(s' - s)(s' - s_0)} \\ &= \frac{1}{(4\pi)^2} \Big[\tilde{a}^{SL}(\mu) + \ln \frac{m_2^2}{\mu^2} - \frac{m_1^2 - m_2^2 + s}{2s} \ln \frac{m_2^2}{m_1^2} - \frac{\lambda^{1/2}(s, m_1^2, m_2^2)}{2s} \cdot \\ &\quad \cdot \ln \Big(\frac{m_1^2 + m_2^2 - s + \lambda^{1/2}(s, m_1^2, m_2^2)}{m_1^2 + m_2^2 - s - \lambda^{1/2}(s, m_1^2, m_2^2)} \Big) \Big] \end{aligned} \tag{3.40}$$

for $s \geq s_{th}$. For $s < s_{th}$ or s complex one has the analytic continuation of eq. (3.40). The function $\lambda^{1/2}(s, m_1^2, m_2^2)$ is given by $\sqrt{(s - (m_1 + m_2)^2)(s - (m_1 - m_2)^2)}$. The regularization scale μ, appearing in the last equality of eq. (3.40), plays a similar role than the arbitrary subtraction point s_0 present in the first one. In fact, both of them are arbitrary although the resulting $g_0(s)$ function is well defined because any change in μ or s_0 is reabsorbed in $\tilde{a}^{SL}(\mu)$ or $a^{SL}(s_0)$, respectively. The $\tilde{a}^{SL}(\mu)$ 'constant' will change under a variation of the scale μ to another one μ' as

$$\tilde{a}^{SL}(\mu') = \tilde{a}^{SL}(\mu) + \ln \frac{\mu'^2}{\mu^2} \tag{3.41}$$

in order to have $g_0(s)$ invariant under changes of the regularization scale. We will take $\mu = M_\rho = 770$ MeV [73]. The function $g_0(s)$ is also symmetric under the exchange $m_1 \leftrightarrow m_2$ and for the equal mass limit it reduces to

$$g_0(s) = \frac{1}{(4\pi)^2} \Big[\tilde{a}^{SL}(\mu) + \ln \frac{m_1^2}{\mu^2} + \sigma(s) \ln \frac{\sigma(s) + 1}{\sigma(s) - 1} \Big] \tag{3.42}$$

with

$$\sigma(s) = \sqrt{1 - \frac{4m_1^2}{s}} \tag{3.43}$$

Let us consider first the case of the P-wave $\pi\pi$ scattering [25]. Taking into account the zero at threshold, from eq. (3.39) we have:

$$\mathrm{T}^{\pi\pi}(s) = \Big[\frac{\gamma_1^{\pi\pi}}{s - 4m_\pi^2} + \tilde{a}_{\pi\pi}^L - g_0^{\pi\pi}(s) + \sum_{i=2} \frac{\gamma_i}{s - s_i} \Big]^{-1} \tag{3.44}$$

On the other hand, from χPT and the exchange of the ρ [11], one has:

$$\mathrm{T}^{\pi\pi\,\infty}(s) = -\frac{2}{3} \frac{p_{\pi\pi}^2}{f^2} + g_v^2 \frac{2}{3} \frac{p_{\pi\pi}^2}{f^2} \frac{s}{s - M_\rho^2} \tag{3.45}$$

with $p^2_{\pi\pi}$ the three-momentum squared of the pions in the c.m., $f = 87.3$ MeV the pion decay constant in the chiral limit [5]. The deviation of g_v^2 with respect to unity measures the variation of the value of the ρ coupling to two pions with respect to the KSFR relation [72], $g_v^2 = 1$. In ref. [74] this KSFR relation is justified making use of large N_c QCD (neglecting loop contributions) and an unsubtracted dispersion relation for the pion electromagnetic form factor (a QCD inspired high-energy behavior).

Comparing eqs. (3.44) and (3.45), one needs only one additional CDD pole apart from the one at threshold and we obtain

$$\begin{aligned} \tilde{a}^L &= 0 \\ \gamma_1^{\pi\pi} &= \frac{6f^2(4m_\pi^2 - M_\rho^2)}{(M_\rho^2 - 4m_\pi^2(1-g_v^2))} \\ \gamma_2^{\pi\pi} &= \frac{6f^2}{g_v^2 - 1}\,\frac{g_v^2 M_\rho^2}{M_\rho^2 - (1-g_v^2)4m_\pi^2} \\ s_2 &= \frac{M_\rho^2}{g_v^2 - 1} \end{aligned} \tag{3.46}$$

The former equation is an example of the matching between both representations: the one given by the N/D method [65], eq. (3.39), and the one derived from chiral symmetry [5,11]. In the following, we will not consider more this matching and we will take directly T^∞ as given by the lowest order χPT amplitudes [5] and the exchange of resonances in the s-channel [11], as discussed above.

For the P-wave $I = 1/2$ $K\pi$ elastic amplitude the tree level amplitude, $T^{K\pi\,\infty}$, is the same than for pions but multiplying it by 3/4 and substituting $p_{\pi\pi}$ by $p_{K\pi}$ and M_ρ by M_{K^*}, the mass of the $K^*(890)$ resonance.

The subleading constant $\tilde{a}^{SL}$ present in $g_0(s)$, eq. (3.40), should be the same for the $\pi\pi$ and $K\pi$ states because the dependence of the loop in eq. (3.12) on the masses of the intermediate particles is given by eq. (3.40). This point can be used in the opposite sense. That is, if it is not possible to obtain a reasonable good fit after setting $\tilde{a}^{SL}$ to be the same in both channels, some kind of SU(3) breaking is missing.

Making use of the minimization program MINUIT, in ref. [25] a simultaneous fit to the elastic $\pi\pi$ and $K\bar{K}$ phase shifts from threshold up to $\sqrt{s} \lesssim 1.2$ GeV was given. As a result one has:

$$\begin{aligned} g_v^2 &= 0.879 \pm 0.016 \\ \tilde{a}^{SL} &= 0.341 \pm 0.042 \end{aligned} \tag{3.47}$$

the errors are just statistical and are obtained by increasing in one unit the χ^2 per degree of freedom, $\chi^2_{d.o.f.}$. The $\chi^2_{d.o.f.}$ obtained is around 0.8.

The fact that g_v deviates from 1 just by a 6% states clearly that the KSFR result is phenomenologically successful.

3.2.3 Results II: The scalar sector

We know consider the S-wave I=0,1 and 1/2 amplitudes [25]. For the partial wave amplitudes with L=0 and I=0 and 1, coupled channels are fundamental in order to get an appropriate description of the physics involved up to $\sqrt{s} \leq 1.3$ GeV. This is an important difference with respect to the former vector channels, essentially elastic in the considered energy region. Up to $\sqrt{s} = 1.3$ GeV the most important channels are:

$$\begin{array}{ll} \text{I=0} & \pi\pi(1),\ K\bar{K}(2),\ \eta\eta(3) \\ \text{I=1} & \pi\eta(1),\ K\bar{K}(2) \\ \text{I=1/2} & K\pi(1),\ K\eta(2) \end{array} \tag{3.48}$$

where the number between brackets indicates the index associated to the corresponding channel when using a matrix notation.

For the I=0 S-wave, the 4π state becomes increasingly important at energies above $1.2 - 1.3$ GeV, so that, in this channel, one is at the limit of applicability of only two meson states when $\sqrt{s}$ is close to 1.4 GeV. In the I=1/2 channel, the threshold of the important $K\eta'$ state is also close to 1.4 GeV. Thus, one cannot go higher in energies in a realistic description of the scalar sector without including the $K\eta'$ and 4π states.

In order to fix T^∞ one needs to include explicit resonance fields. From ref. [73], two sets of resonances appear in the $L = 0$ partial wave amplitudes. A first one, with a mass around 1 GeV, contains the I=0 $f_0(400 - 1200)$ and $f_0(980)$ and the I=1 $a_0(980)$. A second set appears with a mass around 1.4 GeV as the I=0 $f_0(1370)$ and the $f_0(1500)$, the I=1 $a_0(1450)$ or the I=1/2 $K_0^*(1430)$. As a consequence, we first include the exchange of two scalar nonets, with masses around 1 and 1.4 GeV. In ref. [25] the expressions for the T_{ij}^∞ partial waves are collected. Once again, the minimization program MINUIT was used in order to fit the SU(3) related experimental data represented in Figs. 3.15–3.19. It happens that the couplings of the octet around 1 GeV and the singlet around 1.4 GeV are compatible with zero, giving rise to very narrow peaks that are not seen in experiment. In fact, one obtains an equally good fit by including one singlet around 1 GeV and an octet around 1.4 GeV. The values of the parameters given by the fit are [25]:

$$\begin{array}{ll} \text{Nonet (MeV)} & \\ c_d = 19.1^{+2.4}_{-2.1} & a^{SL} = -.75 \pm 0.2 \\ c_m = 15 \pm 30 & \mathcal{N} = (9.4 \pm 4.5)\, 10^{-5}\ \text{MeV}^{-2} \\ M_8 = 1390 \pm 20 & \\ \tilde{c}_d = 20.9^{+1.6}_{-1.0} & \chi^2_{d.o.f.} = 1.07 \\ \tilde{c}_m = 10.6^{+4.5}_{-3.5} & 188\ \text{points} \\ M_1 = 1021^{+40}_{-20} & \end{array} \tag{3.49}$$

Resonances

We consider now the resonance content of the former fit. The octet around 1.4 GeV gives rise to eight resonances which appear with masses very close to the physical ones, $f_0(1500)$, $a_0(1450)$ and $K_0^*(1430)$ [73]. However, a detailed study of the former resonances is not given because one has not included channels which become increasingly important for energies above $\gtrsim$ 1.3 GeV as 4π in I=0 or $K\eta'$ for I=1/2. This makes that the widths obtained from the pole position of the former resonances are systematically smaller than the experimental ones [73]. Thus, a more detailed study, which included all the relevant channels for energies above 1.3 GeV, should be done in order to obtain a better determination of the parameters for this octet around 1.4 GeV.

On the other hand, from Figs. 3.15 and 3.18, one can easily see two resonances with masses around 1 GeV, the well known $f_0(980)$ and $a_0(980)$ resonances. The first one is related to the singlet bare state with $M_1 = 1020$ MeV, but for the second there are no bare resonances to associate with, because the tree level resonance was included with a mass around 1.4 GeV and has evolved to the physical $a_0(1450)$. The situation is even more complex, because we also find in the amplitudes other poles corresponding to the $f_0(400 - 1200) \equiv \sigma$ and to the $K_0^* \equiv \kappa$. In Table 3.5 the pole positions of the resonances

in the second sheet[1] are given and also the modulus of the residues corresponding to the resonance R and channel i, ζ_i^R, given by

$$|\zeta_i^R \zeta_j^R| = \lim_{s \to s_R} |(s - s_R) \mathrm{T}_{ij}| \tag{3.50}$$

where s_R is the complex pole for the resonance R.

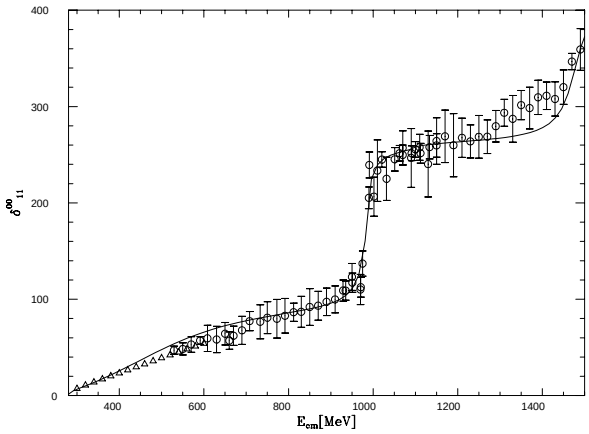

Figure 3.15: Elastic isoscalar $\pi\pi$ phase shifts, δ_{11}^{00}. The circles correspond to the average of [45–48] and [30, 38], as discussed in *section 3.1.1.* We have also included the triangle points form [35] to have some data close to threshold, although these points have not been included in the fit because they are given without errors.

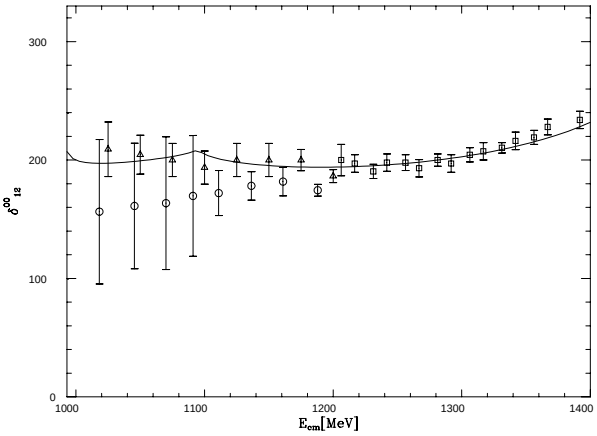

Figure 3.16: S-wave $K\bar{K} \to \pi\pi$ isoscalar phase shifts, δ_{12}^{00}. The triangles points are from [36], circles correspond to the average of ref. [75, 76] and squares to the one of ref. [36, 75, 76].

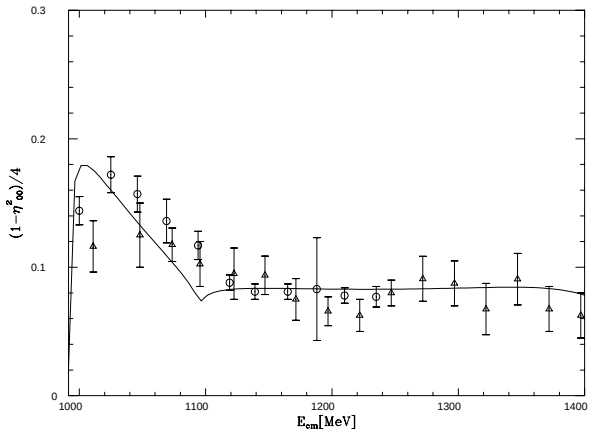

Figure 3.17: $\frac{1-\eta_{00}^2}{4}$ with η_{00} the I=L=0 S-wave inelasticity. Circles [36], triangles [75].

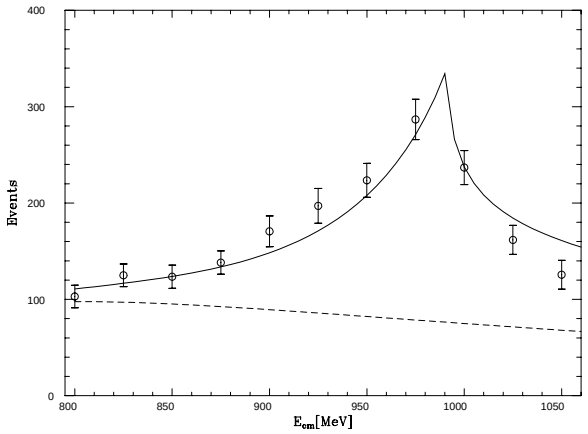

Figure 3.18: Distribution of events around the $a_0(980)$ mass corresponding to the central production $\pi\pi\eta$ in 300 GeV pp collisions [77]. The abscissa represents the $\pi\eta$ invariant mass, E_{cm}. The dashed line represents the background introduced in the same reference.

[1] I sheet: Im p_1 >0, Im p_2 >0, Im p_3 >0; II sheet: Im p_1 <0, Im p_2 >0, Im p_3 >0

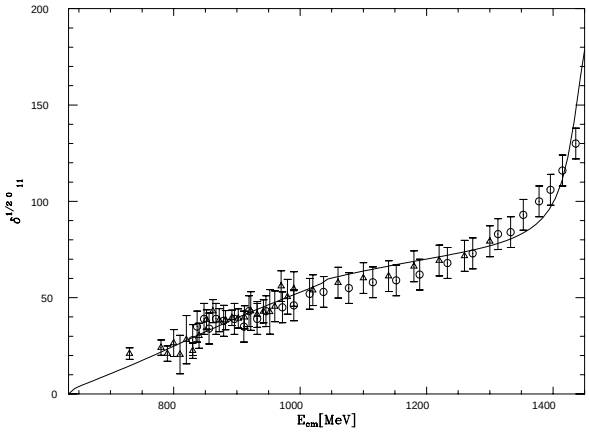

Figure 3.19: S-wave I=1/2 $K\pi$ elastic phase shifts, $\delta_{11}^{1/2\,0}$. The triangles correspond to the average, as described in $\delta_{11}^{1/2\,0}$ subsection, of ref. [48, 51, 52]. Circles correspond to [54].

Table 3.5: Pole position and residues for the full amplitude.

$\sqrt{s}_\sigma = 445 - i\,221$ MeV	$\sqrt{s}_{f_0} = 987 - i\,14$ MeV
$\zeta^\sigma_{\pi\pi} = 4.26$ GeV	$\zeta^{f_0}_{K\bar{K}} = 3.63$ GeV
$\frac{\zeta^\sigma_{K\bar{K}}}{\zeta^\sigma_{\pi\pi}} = 0.254$	$\frac{\zeta^{f_0}_{\pi\pi}}{\zeta^{f_0}_{K\bar{K}}} = 0.51$
$\frac{\zeta^\sigma_{\eta\eta}}{\zeta^\sigma_{\pi\pi}} = 0.036$	$\frac{\zeta^{f_0}_{\eta\eta}}{\zeta^{f_0}_{K\bar{K}}} = 1.11$
$\sqrt{s}_{a_0} = 1053.13 - i\,24$ MeV	$\sqrt{s}_\kappa = 779 - i\,330$ MeV
$\zeta^{a_0}_{K\bar{K}} = 5.48$ GeV	$\zeta^\kappa_{K\pi} = 4.99$ GeV
$\frac{\zeta^{a_0}_{\pi\eta}}{\zeta^{a_0}_{K\bar{K}}} = 0.70$	$\frac{\zeta^\kappa_{K\eta}}{\zeta^\kappa_{K\pi}} = 0.62$

While for the $f_0(980)$ one has a preexisting tree level resonance with a mass of 1020 MeV, for the other resonances present in Table 3.5 the situation is rather different. In fact, if one removes the tree level nonet contribution from T^∞, the $a_0(980)$, σ and κ poles still appear as can be seen in Table 3.6. For the $f_0(980)$, in such a situation, one has not a pole but a very strong cusp effect in the opening of the $K\bar{K}$ threshold. In fact, by varying a little the value of a^{SL} one can regenerate also a pole for the $f_0(980)$ from this strong cusp effect. In Table 3.6 we have not given an absolute value for the coupling of the $f_0(980)$ to the $K\bar{K}$ channel because one has not a pole for the given value of a^{SL}. However, the ratios between the different amplitudes are stable around the cusp position. As a result, the physical $f_0(980)$ will have two contributions: one from the bare singlet state with $M_1 = 1020$ MeV and the other one coming from meson-meson scattering, particularly $K\bar{K}$

Table 3.6: Pole position and residues when the bare resonant contributions are removed

$\sqrt{s}_{\sigma} = 434 - i\,244$ MeV	$\sqrt{s}_{f_0} =$ cusp effect
$\zeta^{\sigma}_{\pi\pi} = 4.21$ GeV	$\zeta^{f_0}_{K\bar{K}} = ...$
$\frac{\zeta^{\sigma}_{K\bar{K}}}{\zeta^{\sigma}_{\pi\pi}} = 0.301$	$\frac{\zeta^{f_0}_{\pi\pi}}{\zeta^{f_0}_{K\bar{K}}} = 0.38$
$\frac{\zeta^{\sigma}_{\eta\eta}}{\zeta^{\sigma}_{\pi\pi}} = 0.033$	$\frac{\zeta^{f_0}_{\eta\eta}}{\zeta^{f_0}_{K\bar{K}}} = 1.04$
$\sqrt{s}_{a_0} = 1081.95 - i\,13.3$ MeV	$\sqrt{s}_{\kappa} = 770 - i\,341$ MeV
$\zeta^{a_0}_{K\bar{K}} = 5.98$ GeV	$\zeta^{\kappa}_{K\pi} = 4.87$ GeV
$\frac{\zeta^{a_0}_{\pi\eta}}{\zeta^{a_0}_{K\bar{K}}} = 0.74$	$\frac{\zeta^{\kappa}_{K\eta}}{\zeta^{\kappa}_{K\pi}} = 0.61$

scattering, generated by the lowest order χPT Lagrangian.

When the resonant tree level contributions are removed from T^{∞}, only the lowest order, $\mathcal{O}(p^2)$, χPT contributions remain. Thus, except for the contribution to the $f_0(980)$ coming from the bare singlet at 1 GeV, the poles present in Table 3.6 originate from a 'pure potential' scattering, following the nomenclature given in ref. [78]. In this way, the source of the dynamics is the lowest order χPT amplitudes. The constant a^{SL} can be interpreted from the need to give a 'range' to this potential so that the loop integrals converge. In ref. [25] it is also shown that these meson-meson states in the SU(3) limit, equaling the masses of the pseudoscalars, appear as a degenerate octet plus a singlet.

Finally, in ref. [25] an estimation of the unphysical cut contributions was done from ref. [56] up to $\sqrt{s} \lesssim 800$ MeV for the resonance $L = 0$ partial waves. As shown in Table 3.7 the influence is rather small in the physical region.

Table 3.7: Influence of the unphysical cuts for the I=L=0 $\pi\pi$ and I=1/2, L=0 $K\pi$ partial waves [25]. The three first columns refer to $\pi\pi$ and the last three to $K\pi$. T_{Left} was already introduced at the end of the former section, eq. (3.32).

$\sqrt{s}$ MeV	$\frac{T_{Left}}{\lvert T_{11}\rvert}$ %	$\frac{T_{Left}}{T^{\infty}_{11}}$ %	$\sqrt{s}$ MeV	$\frac{T_{Left}}{\lvert T_{11}\rvert}$ %	$\frac{T_{Left}}{T^{\infty}_{11}}$ %
276	3.7	4.8	634	7.1	8.7
376.	3.5	5.1	684	3.7	4.7
476	4.1	5.7	734	0.3	0.4
576	5.7	6.	784	-2.5	-3.3
676	8.1	6.1	834	-5.7	-7.2
776	11.2	5.6			

3.3 Bethe-Salpeter equation for S-wave meson-meson and meson-baryon

In this sections we report about the use of the Bethe-Salpeter equation for the study of the S-wave meson-meson scattering [23] and for the S-wave meson-baryon system with strangeness(S)=-1 [79]. In both cases the potential is the lowest order χPT amplitude. The use of the Bethe-Salpeter equation together with χPT was first considered in ref. [80] in the meson-baryon sector.

One of the advantages of the approach in refs. [23, 79] is that the Bethe-Salpeter equation, which is an integral equation, is reduced to an algebraic one. This is accomplished through an analysis of the renormalization process embodied in a Bethe-Salpeter scattering equation.

3.3.1 Bethe-Salpeter equation for S-wave meson-meson scattering

To see how the former simplification occurs let us consider eq. (3.30). In that section, T^{∞} was defined to be the sum of the lowest order χPT amplitudes plus the s-channel resonance exchanges. If we consider only the contribution from the lowest order χPT we will have from that equation:

$$T = \left[T_2^{-1} - g_0(s)\right]^{-1} = \left[1 - T_2 \cdot g_0(s)\right]^{-1} \cdot T_2 \tag{3.51}$$

We can rewrite the previous equation in a form that will remind us of the Bethe-Salpeter equation:

$$T = T_2 + T_2 \cdot g_0(s) \cdot T \tag{3.52}$$

with $g_0(s)$ given in eq. (3.12). The above equation would correspond to a Bethe-Salpeter equation with a potential given by the corresponding lowest order χPT partial wave, T_2. However, while a true Bethe-Salpeter equation is an integral equation the former one is algebraic. Note that one should have instead of $T_2 \cdot g_0(s) \cdot T$ in eq. (3.52) the integral:

$$(T_2 g_0 T)_{\alpha\beta} = \sum_j \int \frac{d^4q}{(2\pi)^4} T_2(k,p;q)_{\alpha j} \frac{i}{\left(q^2 - m_{1j}^2\right)\left((P-q)^2 - m_{2j}^2\right)} T(q;k',p')_{j\beta} \tag{3.53}$$

where P is the total momentum, k and p represent the initial momenta of the ingoing mesons and k' and p' the final momenta of the outgoing ones. Only when T_2 and T are factorized on shell outside the integral in eq. (3.53) one recovers eq. (3.52). This is exactly what happens as stated by eq. (3.51). However, when considering this equation one has to recall also eq. (3.25) in order to realize that all the parameters that appear in T_2 have to be the physical or renormalized ones corresponding to the final positions and residues of the CDD poles or to the substraction constant that result from eq. (3.51).

The final result present in ref. [23] is obtained when approximating the 'physical values' of the parameters in T_2 by the ones dictated by the lowest order χPT results. That is, the constant f is translated to f_π and for the bare masses one takes the physical ones. Both in the IAM or in the N/D method with unphysical cuts, the parameters appearing in T_2 are renormalized according to χPT at $\mathcal{O}(p^4)$.

The argumentation given in ref. [23] for factorizing on shell the potential and the physical amplitude in eq. (3.53) is discussed below and will be considered in further detail

when discussing the Bethe-Salpeter equation for the meson-baryon scattering in the next subsection [79]. Briefly, in the former reference the potential was splitted in two parts:

$$T_2 = V_{on-shell} + V_{off-shell} \tag{3.54}$$

The $V_{on-shell}(p_i)$ part, with $p_i^2 = m_i^2$, factorizes out of the integral in eq. (3.53) since it only depends of the Mandelstam variable s. For $V_{off-shell}$ it was realized that since it only involves terms proportional to $p_i^2 - m_i^2$, they cancel one of the mesons propagators in the loop and give rise to tadpole-like contributions which can be reabsorbed in the final values of the parameters present in T_2. So that, at the end, one only needs $V_{on-shell}$ and hence, eq. (3.52) follows. This result has been recently derived from an alternative point of view in ref. [66].

In ref. [23] the $g_0(s)$ function was calculated making use of a cut off regularization. The cut off[2], Λ, was fixed to reproduce the experimental points, or in other words, to give the right value for the substraction constant a_0^{SL} in eq. (3.29). On the other hand, making use of the IAM one also recovers eq. (3.51) when putting $T_4^P = 0$ in eq. (3.11). In Fig. 3.20 we show the results of ref. [23] compared with data. The agreement is rather good and surprising. On the other hand, poles corresponding to the resonances $f_0(980)$, $a_0(980)$ and $\sigma(500)$ were found and their masses, partial and total decay widths were also analyzed.

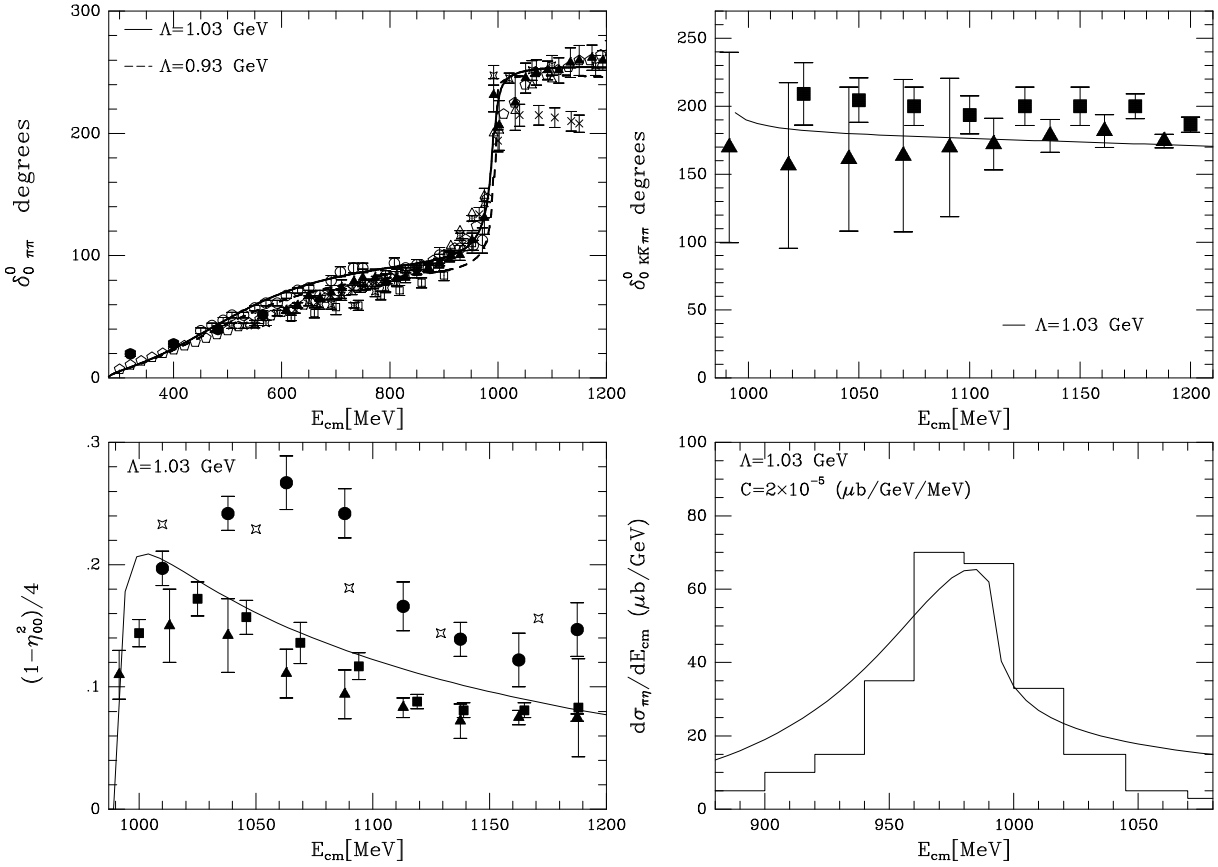

Figure 3.20: Results from ref. [23]. References to experimental data are also given in this paper.

Hence, we see that for the scalar sector with I=0,1 the unitarization of the lowest order χPT amplitudes plays a very important role and also that the resonances which appear there with masses $\leq$1 GeV will have a large meson-meson component in their nature. The same results are expected to hold in the I=1/2 S-wave amplitude by $SU(3)$ symmetry as

[2]The relation between Λ and the three momentum cut off q_{max}, introduced in *section 3.1.2*, is such that $\Lambda = \sqrt{m_K^2 + q_{max}^2}$.

we have seen in *section 3.2.3*. In the P-waves, where the resonances that appear there are of preexisting nature, one cannot reproduce the substraction constant a^L present in eq. (3.27) by a reasonable cut off and the method fails. In ref. [25] it is argued that a cut off around 300 GeV would be needed to reproduce the ρ which is a senseless result.

On the other hand, whereas in *section 3.2.3*, ref. [25], one needs seven free parameters, a nonet of resonances with 6 parameters and a subleading constant, for describing the scalar sector, in this section, ref. [23], there is only one free constant, a cut off, for the $I = 0$ and 1 S-waves. This is due to: 1) in ref. [25] the fit is pushed up to $\sqrt{s} \approx 1.4$ GeV, while in ref. [23] the fit is up to $\sqrt{s} = 1.2$ GeV. In fact, the effect of this octet around 1.4 GeV is soft enough below 1.2 GeV to be reabsorbed in the cut off (or subleading constant). In this way, below 1.2 GeV, one would have needed only 4 parameters in the approach of ref. [25]. 2) In this latter reference the $\eta\eta$ channel is included and in order to reproduce the $\frac{1-\eta_{00}^2}{4}$ data one has had to include the singlet resonance around 1 GeV. The $\eta\eta$ channel was not considered, however, in ref. [23]. Should one have taken the available data for η_{00}, which are measured with much worse precision than $\frac{1-\eta_{00}^2}{4}$, the effect of the $\eta\eta$ channel would have been masked by the large errors in η_{00}.

3.3.2 Bethe-Salpeter equation for S-wave meson-baryon scattering

The effective chiral Lagrangian techniques, which successfully describe meson-meson scattering at low energies [1–3, 5], have also proved to be an excellent tool to study low energy properties of meson-baryon systems when the interaction is weak, as is the case of the S-wave πN [2, 3, 81–85] and K^+N interactions [86, 87], where the leading term in the chiral expansion $\mathcal{O}(p)$ is the dominant one close to threshold. The perturbative scheme breaks down –even at low energies– in the vicinity of a resonance. This is the case of the $\bar{K}N$ system in the $S = -1$ sector with an isospin zero S-wave resonance, the $\Lambda(1405)$. Originally treated as a bound $\bar{K}N$ state [88], this resonance was later interpreted as a conventional three-quark system [89, 90]. Analysis in terms of the cloudy-bag model reinforced the idea of the $\Lambda(1405)$ being a $\bar{K}N$ bound state [91] and, in the framework of the bound-state soliton model, it corresponds to a bound state of a kaon in the background potential of the soliton [92]. The fact that the $\Lambda(1405)$ resonance is located 27 MeV below the K^-p threshold makes it difficult to reproduce the scattering observables whithin the standard chiral Lagrangian techniques, unless the resonance is explicitly introduced as an elementary field [93] or one resorts to nonperturbative techniques similar to those reviewed in previous sections for meson-meson scattering.

A nonperturbative scheme to study the $S = -1$ meson-baryon sector, yet using the input of the chiral Lagrangians, was employed in [80]. A potential model was constructed such that, in Born approximation, it had the same S-wave scattering length as the chiral Lagrangian up to order p^2. This potential, which includes also finite range factors to regularize the integrals, was inserted in a set of coupled-channel Lippmann Schwinger integral equations. The channels included were those opened around the K^-p threshold, namely $K^-p, \bar{K}^0n, \pi^0\Lambda, \pi^+\Sigma^-, \pi^0\Sigma^0$ and $\pi^-\Sigma^+$. By fiting five parameters, corresponding to, so far, unknown parameters of the second order chiral Lagrangian plus the range parameters of the potential, the $\Lambda(1405)$ resonance was generated as a quasibound meson-baryon state and the cross sections of the $K^-p \to K^-p, \bar{K}^0n, \pi^0\Lambda, \pi^+\Sigma^-, \pi^0\Sigma^0, \pi^-\Sigma^+$ reactions at low energies, plus the threshold branching ratios

$$\gamma \;=\; \frac{\Gamma(K^-p \to \pi^+\Sigma^-)}{\Gamma(K^-p \to \pi^-\Sigma^+)}$$

$$R_c = \frac{\Gamma(K^- p \to \text{charged channels})}{\Gamma(K^- p \to \text{all channels})} \qquad (3.55)$$
$$R_n = \frac{\Gamma(K^- p \to \pi^0 \Lambda)}{\Gamma(K^- p \to \text{neutral channels})}$$

were well reproduced. Although the cross sections and position of the resonance could also be reproduced with only the lowest order Lagrangian and one potential range parameter, the impossibility of obtaining a good result for the double charge exchange ratio γ was the reason for the need of including the S-wave terms of the next-to-leading order Lagrangian. However, a recent work [79], which shares many points with [80], showed that all the strangeness $S = -1$ meson-baryon scattering observables near threshold were reproduced with the lowest order Lagrangian and one cut off. The main reason was the inclusion of the $\eta\Lambda$ channel, neglected in ref. [80]. The chiral scheme employed in ref. [79], and summarized below, includes all meson-baryon states that can be generated from the octet of pseudoscalar mesons and the octet of ground-state baryons, thus including in addition the $\eta\Lambda, \eta\Sigma^0$ and the $K^+\Xi^-, K^0\Xi^0$ channels, adding up to a total of 10. It should be noted that if one sets equal baryon masses and equal meson masses in the scheme, one should get degenerate SU(3) multiplet states. This is only possible if all states of the 0^- meson and $\frac{1}{2}^+$ baryon octets are included in the scheme and one should start from such a situation to have control on the SU(3) breaking due to unequal masses.

At lowest order in momentum the interaction Lagrangian comes from the Γ_μ term in the covariant derivative of eqs. (2.35) and (2.36)

$$\mathcal{L}_1^{(B)} = \langle \bar{B} i\gamma^\mu \frac{1}{4f^2}[(\Phi\partial_\mu\Phi - \partial_\mu\Phi\Phi)B - B(\Phi\partial_\mu\Phi - \partial_\mu\Phi\Phi)]\rangle \qquad (3.56)$$

which leads to a common structure for the meson-baryon amplitudes of the type

$$V_{ij} = -\frac{C_{ij}}{4f^2}\bar{u}(-\vec{k}')\gamma^\mu(k_\mu + k'_\mu)u(-\vec{k}) \qquad (3.57)$$

for the different channels, where $u, \bar{u}$ are the Dirac spinors and k, k' the momenta of the incoming and outgoing mesons in the center of mass of the meson-baryon system. The particular values for the $\bar{K}N$ system of the SU(3) coefficients C_{ij}, which connect the meson-baryon channels j and i, can be found in ref. [79]. At low energies the spatial components can be neglected and the amplitudes reduce to

$$V_{ij} = -C_{ij}\frac{1}{4f^2}(k^0 + k'^0) \ . \qquad (3.58)$$

This amplitude is inserted in a coupled channel Bethe-Salpeter equation

$$T_{ij} = V_{ij} + \overline{V_{il}\, G_l\, T_{lj}} \qquad (3.59)$$

with

$$\overline{V_{il}\, G_l\, T_{lj}} = i\int \frac{d^4q}{(2\pi)^4}\, \frac{M_l}{E_l(-\vec{q})}\, \frac{V_{il}(k,q)\, T_{lj}(q,k')}{k^0 + p^0 - q^0 - E_l(-\vec{q}) + i\epsilon}\, \frac{1}{q^2 - m_l^2 + i\epsilon} \ , \qquad (3.60)$$

where only the positive energy component of the fermion propagator has been kept. The Bethe-Salpeter equation sums up automatically the series of diagrams of Fig. 3.21. The loop integral in eq. (3.60) is logarithmically divergent and can be regularized by a cut off $q_{\max}$. The quantities M_l and E_l in eq. (3.60) correspond to the mass and energy of the intermediate baryon, while m_l is the mass of the intermediate meson and $k^0 + p^0 \equiv \sqrt{s}$ is the total energy in the center of mass frame.

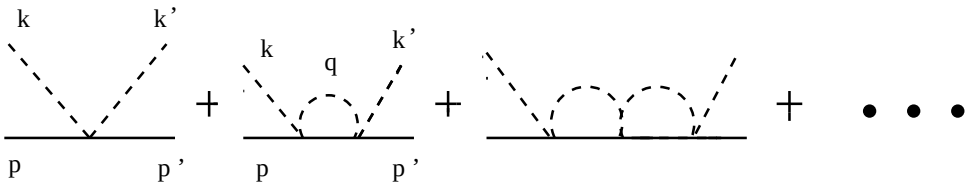

Figure 3.21: Bethe-Salpeter series for meson-baryon scattering

The same arguments given in the previous section for the meson-meson sector allow one to retain only the on shell part of the amplitudes appearing in eq. (3.60), while the rest goes into renormalization of couplings and masses. Take, as an example, the one loop diagram of Fig. 3.21 with equal masses in the external and intermediate states for simplicity. We have

$$\begin{aligned} V_{\rm off}^2 &= C(k^0+q^0)^2 = C(2k^0+q^0-k^0)^2 \\ &= C(2k^0)^2 + 2C(2k^0)(q^0-k^0) + C(q^0-k^0)^2 \end{aligned} \tag{3.61}$$

with C a proportionality constant. The first term in the last expression is the on shell contribution $V_{\rm on}^2$, with $V_{\rm on} \equiv C2k^0$. Neglecting $p^0 - E(-\vec{q})$ in eq. (3.60), a typical approximation in the heavy baryon formalism, the one loop integral for the second term of eq. (3.61) becomes

$$\begin{aligned} & 2iV_{\rm on} \int \frac{d^3q}{(2\pi)^3} \int \frac{dq^0}{2\pi} \frac{M}{E(-\vec{q})} \frac{q^0-k^0}{k^0-q^0} \frac{1}{q^{02}-\omega(\vec{q})^2+i\epsilon} \\ = \; & -2V_{\rm on} \int \frac{d^3q}{(2\pi)^3} \frac{M}{E(-\vec{q})} \frac{1}{2\omega(\vec{q})} \sim V_{\rm on}\, q_{\rm max}^2 \end{aligned} \tag{3.62}$$

with $\omega(\vec{q})^2 = \vec{q}^{\,2} + m^2$. This term, proportional to $V_{\rm on}$, has the same structure as the tree level term in the Bethe-Salpeter series and it can be reabsorbed in the lowest order Lagrangian by a suitable renormalization of the parameter f. Similarly, one of the two $(q^0 - k^0)$ factors in the last term of eq. (3.61) cancels the baryon propagator in eq. (3.60) while the remaining factor gives rise to another term proportional to k^0 (and hence $V_{\rm on}$) and a term proportional to q^0, which vanishes for parity reasons.

These arguments can be extended to coupled channels and higher order loops with the conclusion that V_{il} and T_{lj} factorize with their on shell values out of the integral in eq. (3.60), reducing the problem to one of solving a set of algebraic equations, written in matrix form as

$$T = V + V\,G\,T \tag{3.63}$$

with G a diagonal matrix given by

$$\begin{aligned} G_l(\sqrt{s}) &= i \int \frac{d^4q}{(2\pi)^4} \frac{M_l}{E_l(-\vec{q})} \frac{1}{\sqrt{s}-q^0-E_l(-\vec{q})+i\epsilon} \frac{1}{q^2-m_l^2+i\epsilon} \\ &= \int_{|\vec{q}|<q_{\rm max}} \frac{d^3q}{(2\pi)^3} \frac{1}{2\omega_l(\vec{q})} \frac{M_l}{E_l(-\vec{q})} \frac{1}{\sqrt{s}-\omega_l(\vec{q})-E_l(-\vec{q})+i\epsilon}\,. \end{aligned} \tag{3.64}$$

The value of the cut off in ref. [79], $q_{\rm max} = 630$ MeV, was chosen to reproduce the K^-p threshold branching ratios [94,95] , while the weak decay constant, $f = 1.15 f_\pi$, was taken in between the pion and kaon ones to optimize the position of the $\Lambda(1405)$ resonance [96–98]. The branching ratios as well as the predictions of the scattering lengths for K^-p and K^-n scattering are summarized in Table 3.8, where results omitting the η channels are also

shown. While the η channels have a moderate effect on the isospin $I = 1$ K^-n scattering length, a_{K^-n}, they have a tremendous influence on the K^-p scattering observables, especially on the ratio γ which changes by a factor of about 2. As was shown in ref. [79], it is the $I = 0$ $\eta\Lambda$ channel the one that was providing most of the changes. The K^-p scattering length is essentially in agreement with the most recent results from Kaonic hydrogen X rays [99], in qualitative agreement with the scattering lengths determined from scattering data in [100], with an estimated error of 15%, and in remarkable agreement with the result from a combined dispersion relation and M-matrix analysis [100].

Table 3.8: K^-p threshold ratios and K^-N scattering lengths

	All channels	No $\eta\Lambda$,$\eta\Sigma^0$	EXP
γ	2.32	1.04	2.36±0.04 [94, 95]
R_c	0.627	0.637	0.664±0.011 [94, 95]
R_n	0.213	0.158	0.189±0.015 [94, 95]
a_{K^-p} (fm)	−1.00+i0.94	−0.68+i1.64	(−0.78±0.18)+i(0.49±0.37) [99] −0.67+i0.64 [100] −0.98 (from Re(a)) [100]
a_{K^-n} (fm)	0.53+i0.62	0.47+i0.53	0.37+i 0.60 [100] 0.54 (from Re(a)) [100]

Finally, the K^-p cross sections for some selected channels ($K^-p \to K^-\pi$, $\bar{K}^0n$, $\pi^+\Sigma^-$, $\pi^-\Sigma^+$) are compared with the low-energy scattering data [101–106] in Fig. 3.22. The results using the isospin basis (short-dashed line) are close to those using the basis of physical states (solid line) but the cusp associated to the opening of the $\bar{K}^0n$ channel appears in the wrong place due to the use of an average mass for all the members of an isospin multiplet. The effects of neglecting the η channels (long-dashed line) are much more significant. Close to threshold, the $\pi^-\Sigma^+$ cross section is reduced by almost a factor of 3 and the $\pi^+\Sigma^-$ cross section is reduced by a factor 1.3 when the η channels are included. This enhances the ratio γ by a factor 2.2 and makes the agreement with the experimental value possible using only the lowest order chiral Lagrangian. It is also remarkable that the $\pi^+\Sigma^-$ cross section, which is zero at lowest order with the chiral Lagrangians, turns out to be about three times bigger that the analogous, allowed one, $\pi^-\Sigma^+$. The multiple scattering with coupled channels is responsible for this.

The predictions of this model for KN scattering in the strangeness $S = 1$ sector at low energies are quite satisfactory. As shown in ref. [79], the phase shifts in the isospin channel $I = 1$ are about 15% smaller than experiment [107]. This result is qualitatively similar to the one obtained in [80], where it was also shown that allowing for a K^+p shorter range parameter (larger cut off) the agreement with data improves. The predicted KN scattering lengths for isospin $I = 0$ and $I = 1$ are $a(S = 1, I = 0) = 2.4 \times 10^{-7}$ fm and $a(S = 1, I = 1) = -0.26$ fm, which compare favorably with present experimental data, 0.02 ± 0.04 fm ($I = 0$) and -0.32 ± 0.02 fm ($I = 1$) [108]. Note that the scattering length in $I = 0$ is zero at lowest order ($T = V$) and becomes finite, although negligibly small, as a consequence of the coupling to other channels when working in the particle basis.

We have seen that the use of only one cut off parameter and the input of the lowest-order Lagrangian reproduces the low energy data in the $S = -1$ sector as satisfactorily

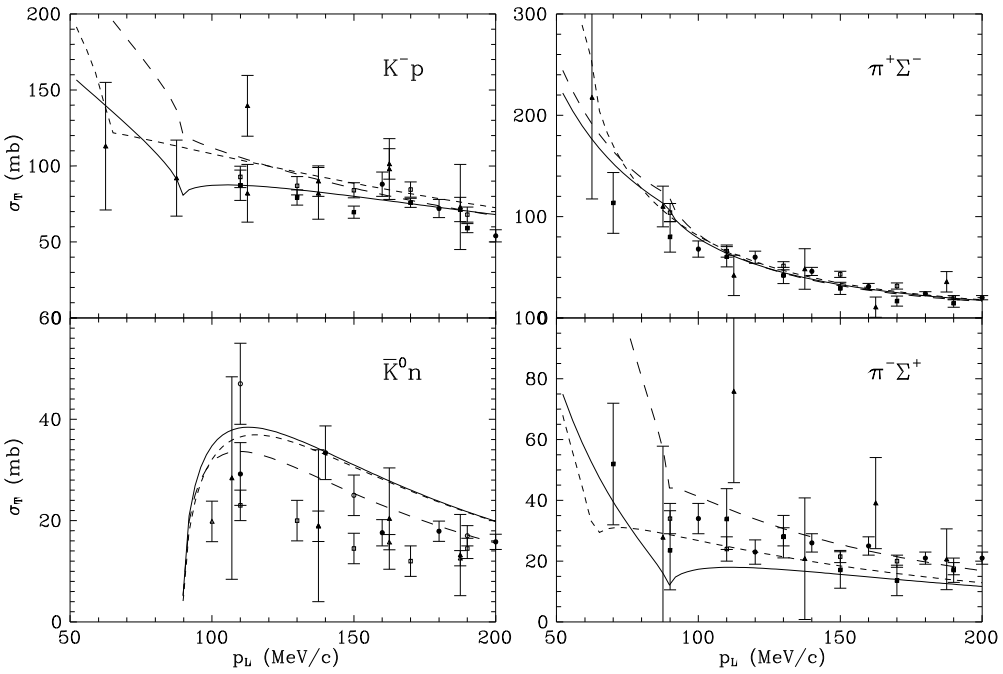

Figure 3.22: K^-p scattering cross sections as functions of the K^- momentum in the lab frame: with the full basis of physical states (solid line), omitting the η channels (long-dashed line) and with the isospin-basis (short-dashed line). The experimental data are taken from refs. [101–106]

as the model of ref. [80], where the η channels were omitted and the next-to-leading order terms of the chiral Lagrangian included. This is due to the fact that at low energies the η meson loops only contribute to the real part of the amplitudes and this can effectively be taken into account by means of parameters of the second-order Lagrangian. Nevertheless, the values of the $\mathcal{O}(p^2)$ countertems of the meson-baryon Lagrangian given in ref. [80] are affected by the resummation of the important contributions coming from the SU(3) channels with the η meson and, hence, their actual values can be very different.

The success in reproducing $\bar{K}N$ and KN low energy scattering observables with the lowest-order Lagrangian and one cut off [79] does not mean that this procedure can be generalized to all meson-baryon sectors. The richness of information available for meson-nucleon scattering requires the use of higher order Lagrangians, as it was the case in meson-meson scattering when including all the different channels [26, 41]. In fact, it has turned out to be impossible to dynamically reproduce the S-wave $N^*(1535)$ resonance and the low energy scattering data in the $S = 0$ sector with the lowest order Lagrangian and only one cut off. However, the extension of the model of ref. [80] to pion induced reactions in the $S = 0$ sector ($\pi^-p \to \eta\Lambda, K^0\Lambda, K^+\Sigma^-, \pi^+p \to K^+\Sigma^+$) produces the $N^*(1535)$ resonance as a quasibound $K\Sigma - K\Lambda$ state [109], using the same parameters of their next-to-leading order Lagrangian fitted to the low energy $\bar{K}N$ ($S = -1$) data. Simultaneously, the η and K photoproduction processes in the $S = 0$ channels were also studied ($\gamma p \to \eta p, K^+\Lambda, K^+\Sigma^0, K^0\Sigma^+$) and with a few more parameters a global reproduction of the strong and electromagnetic cross section was obtained [110]. The method is being extended to higher partial waves, to gain access to higher energies, other resonances and polarization

observables [111].

Recently, the unitarization of the Heavy Baryon χPT amplitudes at $\mathcal{O}(p^3)$ [82, 83] has regained interest. In ref. [112], this is done making use of the IAM method, giving rise to a reasonable account of the scattering data up to around 1.2 GeV, including the region of the $\Delta(1232)$ resonance in the P_{33} partial wave. In ref. [113] it is argued that a new rearrangement of the Heavy Baryon χPT series, in terms of which the IAM is once again applied, leads to much better results than making use of the more straightforward version of the IAM used in [112]. This seems to be the case for the P_{33} partial wave, although a convincing argumentation for this rearragement is lacking in ref. [113], particularly when considering other partial waves [3]. On the other hand, in ref. [114] the unitarization of the elastic πN scattering is accomplished using an adapted version of the method described in *section 3.2.1* for the meson-baryon sector, in a fully relativistic way. Explicit resonance fields are included in ref. [114] and a matching with the $\mathcal{O}(p^3)$ Heavy Baryon χPT πN amplitudes [82, 83] is given. The data are reproduced up to 1.3 GeV, where new channels would have to be introduced.

The field is at a stage where rapid progress is being done and a clearer and broader picture of the role of chiral dynamics in meson-baryon scattering can be expected in the near future.

[3] With respect to this point, J.A.O. acknowleges very fruitful and enlightening discussions with José Ramón Peláez.

Chapter 4

Final state interactions in meson pairs

In this chapter we present how to use the previous meson-meson strong amplitudes to calculate processes with mesons in the final state. In many of them, the final state interactions between these mesons are crucial and give rise to corrections of even orders of magnitude in describing the physics involved.

4.1 The $\gamma\gamma \to$ meson-meson reaction

The $\gamma\gamma \to$ meson-meson reaction provides interesting information concerning the structure of hadrons, their spectroscopy and the meson-meson interactions, given the sensitivity of the reaction to the hadronic final state interactions (FSI) [115, 116]. In this sense, the study of these processes constitutes a very interesting test of consistency of the approaches [23, 25, 41] for the scalar sector.

In ref. [117], a unified theoretical description of the reactions $\gamma\gamma \to \pi^+\pi^-$, $\pi^0\pi^0$, K^+K^-, $K^0\bar{K}^0$, $\pi^0\eta$ up to about $\sqrt{s} = 1.4$ GeV was presented for the first time. The agreement with the experimental data was very good as can be seen in Fig. 4.4.

For calculating the above processes one needs to correct for FSI the tree level amplitudes coming from Born terms, Fig. 4.1, in the case of the charged channels, and also from the exchange of vector and axial resonances in the crossed channels [118], Fig. 4.2.

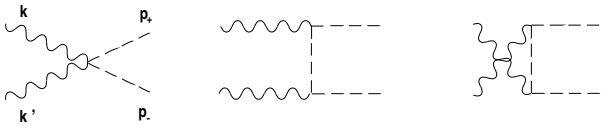

Figure 4.1: Born term amplitude for $\gamma\gamma \to M^+M^-$. k and k' are the momenta of the incoming photons and $p_+(p_-)$ the momentum of the positively(negatively) charged meson.

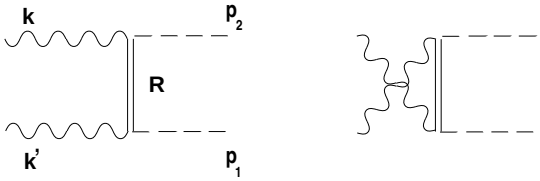

Figure 4.2: Tree level amplitude for $\gamma\gamma \to M_1M_2$ through the exchange of a resonance R(axial or vectorial) in the t,u channels.

4.1.1 FSI: S-wave

In ref. [117] the one loop corrections of the tree level amplitudes is first considered and then this result is extended to the string of loops represented in Fig. 4.3.

The one loop contribution generated from the Born terms with intermediate charged mesons can be directly taken from the χPT calculations [119, 120] of the $\gamma\gamma \to \pi^0\pi^0$ amplitude at $\mathcal{O}(p^4)$. The important point is that the $\mathcal{O}(p^2)$ χPT amplitude connecting the

charge particles with the $\pi^0\pi^0$ factorizes on shell outside the loop. One can schematically represent this situation by:

$$\sum_a L(s)_a \, T^{(2)}_{ab}(s) \tag{4.1}$$

where the subindex a represents the pair of intermediate charged mesons, b the final ones and $T^{(2)}$ the on shell $\mathcal{O}(p^2)$ amplitude.

The contribution of ref. [117] beyond this first loop is to include all meson loops (Fig. 4.3) generated by the coupled channel Bethe-Salpeter equations of *section 3.3.1*, ref. [23]. We also saw there that the on shell $\mathcal{O}(p^2)$ χPT amplitudes factorize outside the loop integrals. Thus, the immediate consequence of introducing these loops is to substitute the on shell $\mathcal{O}(p^2)$ $\pi\pi$ amplitude in eq. (4.1), by the on shell meson-meson amplitude, $T_{ab}(s)$, evaluated in ref. [23].

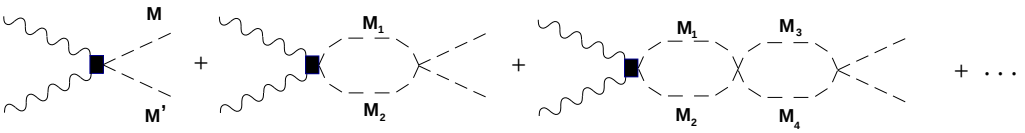

Figure 4.3: Diagrammatic series which gives rise to the FSI from a general $\gamma\gamma$ →M M' vertex, represented by the full square.

A similar procedure can be done to account for the FSI in the case of the tree level diagrams with the exchange of a resonance (vector or axial). As explained in ref. [117] one can justify the accuracy of factorizing the strong amplitude for the loops with crossed exchange of resonances, since this result is correct for $M_R^2 \to \infty$. Because we are dealing with real photons the intermediate axial or vector mesons are always off shell and the large mass limit is a sensible approximation. The errors were estimated to be below the level of 5% for M_R about 800 MeV.

4.1.2 D-wave contribution

For the $(2,2)$ component we take the results of ref. [121], obtained using dispersion relations

$$t^{(2,2)}_{BC} = \left[\frac{2}{3}\,\chi^{T=0}_{22}\, e^{i\delta_{20}} + \frac{1}{3}\,\chi^{T=2}_{22}\, e^{i\delta_{22}}\right] t^{(2,2)}_{B} \tag{4.2}$$

where the functions $\chi_{ij}(s)$ are just first order polynomials in the s variable.

For the $\gamma\gamma \to K^+K^-$ reaction the non resonant D-wave contribution is not needed because one is close to the $K\bar{K}$ threshold and furthermore the functions χ_{ij} are nearly zero close to the mass of the f_2 and a_2 resonances, which are also in the energy region we are considering.

The *resonance contribution* in the $D-$wave coming from the $f_2(1270)$ and $a_2(1320)$ resonances is parametrized in the standard way of a Breit-Wigner as done in ref. [122]. The parameters of these resonances are completely compatible with the ones coming from the Particle Data Group [73].

Once the FSI for the S- and D-waves have been taken into account, which completely dominate the $\gamma\gamma$ →meson-meson reactions up to the energies considered [117,121], one can compare with several experimental data.

4.1.3 Total and differential cross sections

The experimental data correspond to total and differential cross sections. As can be seen in Fig. 4.4, the agreement is very good in all the channels considered. It is worth mentioning that the results presented are not a fit, since the parameters of the axial, vector and tensor resonances were taken from the literature.

It is also worth remarking that in the figure corresponding to the $\gamma\gamma \to K^+K^-$ reaction, the Born term, indicated by the long-dashed line, reduces to the short-dashed line when taking into account the FSI. This implies a large reduction of this Born term thanks to which a good reproduction of the data is obtained, hence solving a long standing problem [116].

4.1.4 Partial decay widths to two photons of the $f_0(980)$ and $a_0(980)$

The same procedure as in *section 3.1.2* is followed in ref. [117] in order to calculate the partial decay widths of the $f_0(980)$ and $a_0(980)$ in terms of the strong [23] and photoproduction [117] amplitudes. From the amplitudes with isospin $I = 1$ and 0 [23], one considers the terms which involve the strong $M\bar{M} \to M\bar{M}$ amplitude. Then, one isolates the part of the $\gamma\gamma \to M\bar{M}$ process which proceeds via the resonances a_0 and f_0 respectively. In the vicinity of the resonance the amplitude proceeds as $M\bar{M} \to R \to M\bar{M}$. Hence, eliminating the $R \to M\bar{M}$ part of the amplitude plus the R propagator and removing the proper isospin Clebsch Gordan coefficients for the final states (1 for $\pi^0\eta$ and $-1/\sqrt{2}$ for K^+K^-), one obtains the coupling of the previous resonances to the $\gamma\gamma$ channel.

The results are:

$$\Gamma^{\gamma\gamma}_{a_0} = 0.78 \text{ KeV}\,; \quad \Gamma^{\gamma\gamma}_{a_0}\frac{\Gamma^{\eta\pi}_{a_0}}{\Gamma^{tot}_{a_0}} = 0.49 \text{ KeV}\,; \quad \Gamma^{\gamma\gamma}_{f_0} = 0.20 \text{ KeV} \tag{4.3}$$

The calculated width for the $f_0(980)$ is smaller than the average value of (0.56 ± 0.11) KeV reported in the PDG [73]. In doing this average the PDG refers to the work by Morgan and Pennington [121] where they quote a width of (0.63 ± 0.14) KeV. However, in a recent work by Boglione and Pennington they quote the much smaller width $(0.28^{+0.09}_{-0.13})$ KeV [123]. When taking into account the errors, the former result and the one from ref. [117] are compatible.

The value given above for the second magnitude in eq. (4.3) is larger than the value of $(0.28 \pm 0.04 \pm 0.1)$ KeV given in PDG. However, this value comes from references where a background is introduced in order to fit the data. In the analysis we have discussed in this section [117], no background is included and hence, in a natural way, the strength of the $a_0(980)$ to two photons is increased.

Conclusions

As important features of the approach of ref. [117], we can remark:

1) The resonance $f_0(980)$ shows up weakly in $\gamma\gamma \to \pi^0\pi^0$ and barely in $\gamma\gamma \to \pi^+\pi^-$.

2) In order to explain the angular distributions of the $\gamma\gamma \to \pi^+\pi^-$ reaction there is not need of the hypothetical $f_0(1100)$ broad resonance suggested in other works [121]. This also solves the puzzle of why it did not show up in the $\gamma\gamma \to \pi^0\pi^0$ channel. Furthermore, such resonance does not appear in the theoretical work of ref. [23], while the $f_0(980)$ showed up clearly as a pole of the T matrix in $I = 0$.

3) The resonance a_0 shows up clearly in the $\gamma\gamma \to \pi^0\eta$ channel and the experimental results are well reproduced without the need of an extra background from a hypothetical

$a_0(1100-1300)$ resonance suggested in ref. [116].

4) One can explain the *drastic reduction* of the Born term in the $\gamma\gamma \to K^+K^-$ reaction in terms of final state interaction of the K^+K^- system.

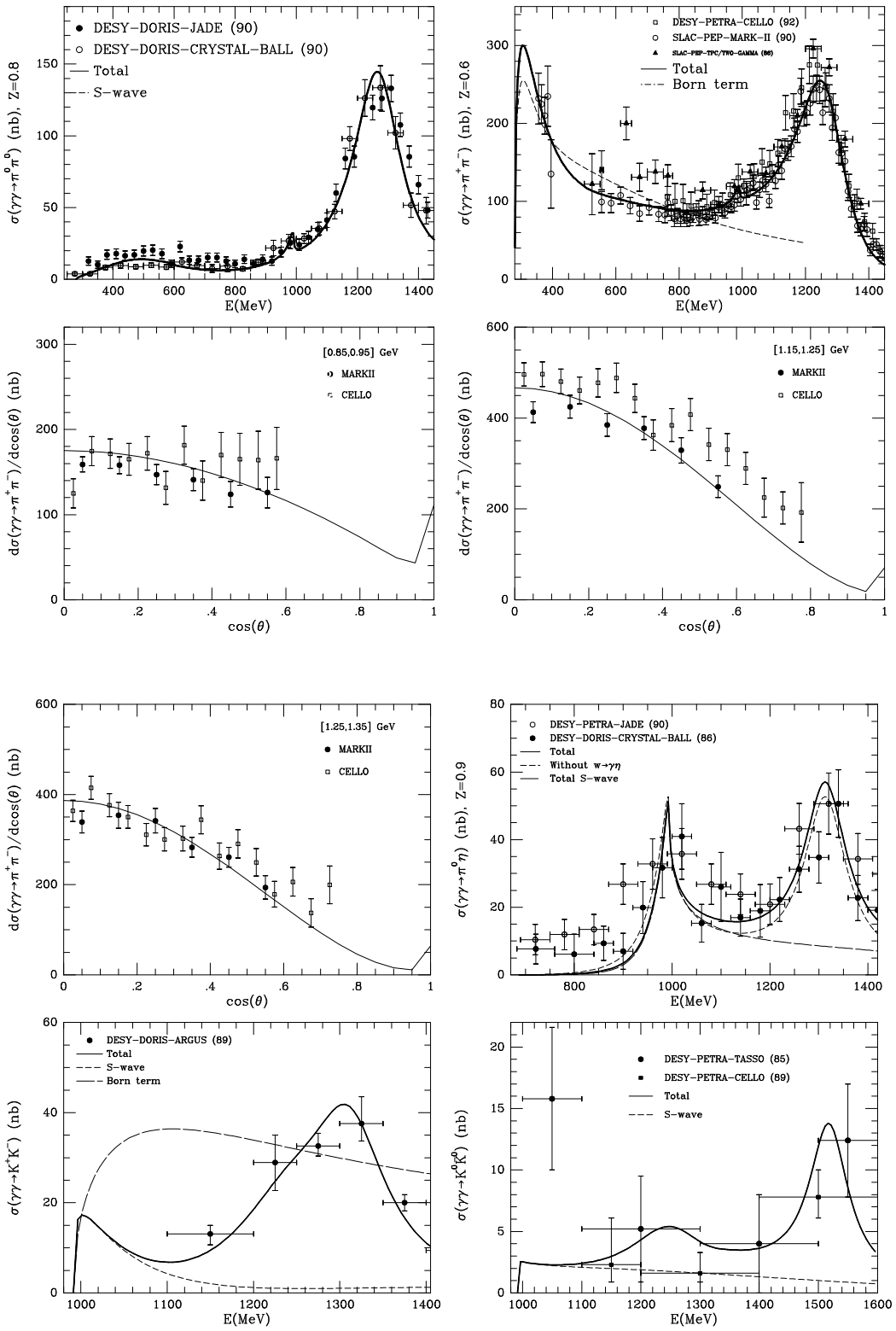

Figure 4.4: Total and differential cross sections for several photoproduction processes. The references to the experimental data are given in ref. [117].

4.2 The $\phi \to \gamma K^0 \bar{K}^0$, $\gamma\pi^0\pi^0$ and $\gamma\pi^0\eta$ decays

We first discuss the decay of the ϕ meson to $\gamma K^0 \bar{K}^0$ following ref. [124]. With the previous formalism fixed, we will consider the decay of the ϕ to $\gamma\pi^0\pi^0$ and $\gamma\pi^0\eta$ [125].

4.2.1 The $\phi \to \gamma K^0 \bar{K}^0$ decay

The study of the process $\phi \to \gamma K^0 \bar{K}^0$ is an interesting subject since it provides a background to the reaction $\phi \to K^0 \bar{K}^0$. This latter process has been proposed as a way to study CP violating decays to measure the small ratio ϵ'/ϵ [126], but, since this implies seeking for very small effects, a BR($\phi \to \gamma K^0 \bar{K}^0$)$\geq 10^{-6}$ will limit the scope of these perspectives. There are several calculations of this quantity [127–131]. In ref. [132] it is estimated for a *non resonant* decay process without including the f_0 and a_0 resonances. The issue was revisited in ref. [133].

The approach introduced in ref. [23] to treat the $I = 0, 1$ scalar meson-meson sector was the one used in ref. [124]. The formalism, reviewed in *section 3.3.1*, will allow us to consider simultaneously the influence of the $f_0(980)$ and the $a_0(980)$ resonances, as well as their mutual interference, in a way that takes into account the energy dependence of their widths and coupling constants to the $K\bar{K}$ system. Furthermore, other possible contributions, non resonant, are also considered. The final state interactions will be taken into account following the way of ref. [117] and discussed in the former section.

As in previous works [127–130], in ref. [124] the process $\phi \to \gamma K^0 \bar{K}^0$ is calculated through an intermediate K^+K^- loop which couples strongly to the ϕ and the scalar resonances, see Fig. 4.5.

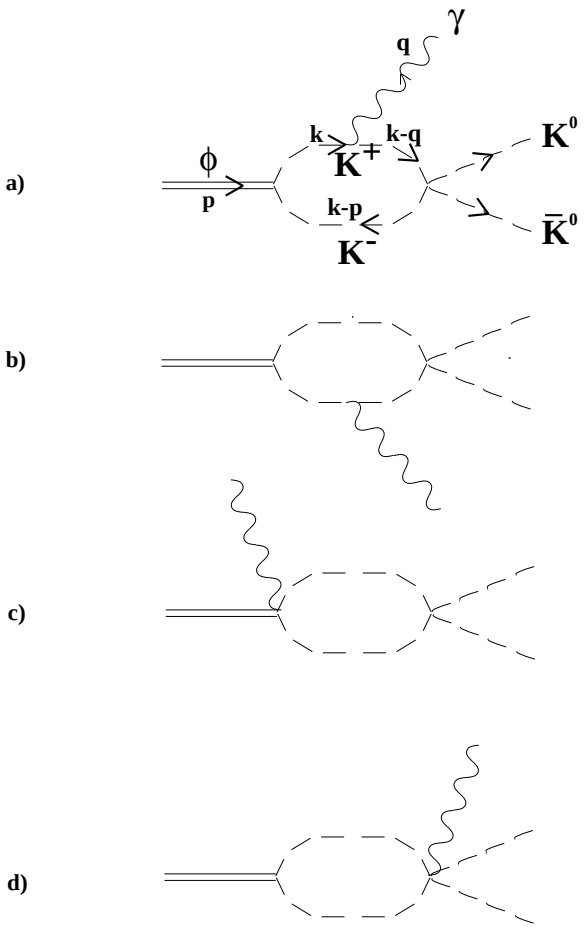

Figure 4.5: The loop radiation (a,b) and contact (c,d) contributions.

For calculating the contribution of these loop diagrams one uses the minimal coupling to make the interaction between the ϕ and the K^+K^- mesons gauge invariant, then we have

$$H_{int} = (eA_\mu + g_\phi \phi_\mu) i(\partial^\mu K^+ K^- - K^+ \partial^\mu K^-) - 2e g_\phi A^\mu \phi_\mu K^+ K^- \ , \tag{4.4}$$

where g_ϕ is the coupling constant between the ϕ and the K^+K^- system [1].

An essential ingredient to evaluate the loop in Fig. 4.5 is the strong amplitude connecting K^+K^- with $K^0\bar{K}^0$. As we said before, the amplitude calculated in ref. [23] is the one used in ref. [124] . This implies the sum of an infinite series of diagrams which is represented in Fig. 4.6 for the diagram of Fig. 4.5a, and the analogue sums corresponding to Figs. 4.5b,c,d. This way of taking into account the S-wave final state interactions is the same as shown above in Fig. 4.3 for the $\gamma\gamma \to$meson-meson reactions.

This series gives rise to the needed corrections due to final state interactions and in fact, from the vertex connecting the K^+K^- with the $K^0\bar{K}^0$, this series is the same one as that in ref. [23] which gives rise to the S-wave strong amplitude $K^+K^- \to K^0\bar{K}^0$, see eq. (3.52). In this approach the vertex between the loops correspond to the on shell lowest order χPT amplitude [5]. Note that an analogous series before the loop with the emission of the photon is absorbed in the infinite series of diagrams contained in the ϕ resonance propagator and its effective coupling.

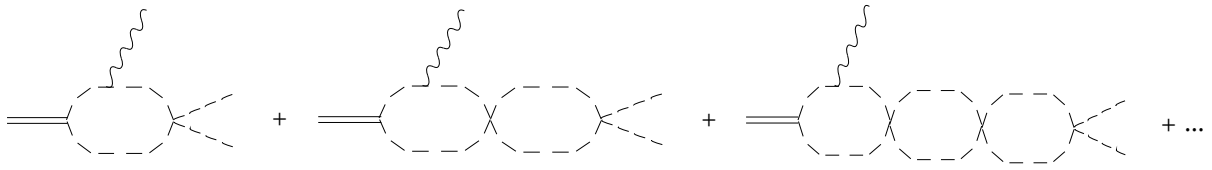

Figure 4.6: Diagrammatic series representing the FSI from a general loop of Fig. 4.5.

First of all, let us see that the strong amplitude connecting K^+K^- with $K^0\bar{K}^0$ calculated in the way shown in Fig. 4.6, ref. [23], must factorize out of the integral.

In order to see this, following ref. [124], consider the diagrams in Fig. 4.5 but with the $\mathcal{O}(p^2)$ χPT amplitude connecting the kaons. This amplitude is given by

$$< K^0\bar{K}^0|t|K^+K^- >= \frac{1}{2}\left[t_{I=0} - t_{I=1}\right] = -\frac{1}{4f^2}\left[s + \frac{4m_K^2 - \sum_i p_i^2}{3}\right] \ , \tag{4.5}$$

where f is the pion decay constant, $f \simeq 93$ MeV, I refers to the isospin channel of the amplitude and the subindex i runs from 1 to 4 and refers to any of the four kaons involved in the strong interaction. If the particle is on shell then $p_i^2 = m_K^2$. In the present case $p_{K^0}^2 = p_{\bar{K}^0}^2 = m_K^2$ so one has

$$-\frac{1}{4f^2}\left[s + \frac{(m_K^2 - p_{K^+}^2) + (m_K^2 - p_{K^-}^2)}{3}\right] \ . \tag{4.6}$$

The important point for the sequel is that the off shell part, which should be kept inside the loop integration, will not contribute.

First of all let us note that, due to gauge invariance, the physical amplitude for $\phi \to \gamma K^0\bar{K}^0$ has the form

$$M(\phi(p) \to \gamma(q) K^0\bar{K}^0) = [g^{\mu\nu}(p\cdot q) - p^\mu q^\nu]\epsilon_\mu^\gamma \epsilon_\nu^\phi H(p\cdot q, Q^2, q\cdot Q) \ , \tag{4.7}$$

[1] There is an extra contribution that does not come from minimal coupling and is given by the term proportional to F_V in eq. (2.24). However, this term only originates a correction to the coupling constant proportional to the momentum of the photon (see *section 4.2.2*) which, because we are very close to the threshold of the ϕ, is very tiny.

where ϵ_μ^γ and ϵ_ν^ϕ are the polarization vectors of the photon and the ϕ meson, $Q = p_{K^0} + p_{\bar{K^0}}$ and H is an arbitrary scalar function. In the calculation of this loop contribution the problem is the presence of divergences in the loops represented in Fig. 4.5. Following refs. [127–129] we will take into account the contribution of $p^\mu q^\nu$ of Figs. 4.5a,b, since Figs. 4.5c,d do not give such type of terms. Then, by gauge invariance, see formula (4.7), the coefficient for $(p\cdot q)g^{\mu\nu}$ is also fixed. In fact, as shown in ref [127–129, 133], the $p^\mu q^\nu$ contribution will be finite since the off shell part of the strong amplitudes does not contribute, as we argue below, and then one is in the same situation than in the latter references. On the other hand, depending on the renormalization scheme chosen, additional tadpole like terms can appear [134]. However, they do not contribute to the $p^\mu\, q^\nu$ structure and hence can be ignored.

If we take the diagrams of Figs. 4.5a,b, which give the same contribution, we find the following amplitude for the sum of both diagrams:

$$\begin{aligned} M' &= \epsilon_\mu^\gamma \epsilon_\nu^\phi \frac{2eg_\phi}{i}\int \frac{d^4k}{(2\pi)^4}\frac{(2k_\nu - p_\nu)(2k_\mu - q_\mu)}{(k^2 - m_K^2 + i\epsilon)((k-q)^2 - m_K^2 + i\epsilon)((k-p)^2 - m_K^2 + i\epsilon)} \\ &\times \frac{(-1)}{4f^2}\left[Q^2 + \frac{(m_K^2 - p_{K^+}^2) + (m_K^2 - p_{K^-}^2)}{3}\right] . \end{aligned} \tag{4.8}$$

The momentum for each particle in the loop is indicated in Fig. 4.5a and so one has $p_{K^+} = k - q$, $p_{K^-} = k - p$. Concentrating in the off shell part of the strong amplitude, one has the following integral

$$\begin{aligned} &\int \frac{d^4k}{(2\pi)^4}\frac{(2k_\nu - p_\nu)(2k_\mu - q_\mu)}{(k^2 - m_K^2 + i\epsilon)((k-q)^2 - m_K^2 + i\epsilon)((k-p)^2 - m_K^2 + i\epsilon)} \\ &\quad \times [(k-q)^2 - m_K^2 + (k-p)^2 - m_K^2] = \\ &\int \frac{d^4k}{(2\pi)^4}\frac{(2k_\nu - p_\nu)(2k_\mu - q_\mu)}{(k^2 - m_K^2 + i\epsilon)((k-p)^2 - m_K^2 + i\epsilon)} + \int \frac{d^4k}{(2\pi)^4}\frac{(2k_\nu - p_\nu)(2k_\mu - q_\mu)}{(k^2 - m_K^2 + i\epsilon)((k-q)^2 - m_K^2 + i\epsilon)} \end{aligned} \tag{4.9}$$

Taking into account that

$$\epsilon_\mu^\phi \cdot p^\mu = 0\ ;\ \epsilon_\nu^\gamma \cdot q^\nu = 0\ \ \text{(Feynman gauge)} \tag{4.10}$$

then one only has

$$\int \frac{d^4k}{(2\pi)^4}\frac{4k_\mu k_\nu}{(k^2 - m_K^2 + i\epsilon)((k-p)^2 - m_K^2 + i\epsilon)} + \int \frac{d^4k}{(2\pi)^4}\frac{4k_\mu k_\nu}{(k^2 - m_K^2 + i\epsilon)((k-q)^2 - m_K^2 + i\epsilon)} \tag{4.11}$$

The above integrals do not give contribution to $q^\mu p^\nu$ since in each integral there is only one of the two vectors q or p. In this way we see that the strong amplitude $\mathcal{O}(p^2)$ factorizes out on shell in (4.7). Note that the important point in the former argumentation is the form of the off shell part of the S-wave strong amplitude at $\mathcal{O}(p^2)$ and this is common to any other S-wave meson-meson amplitude at this order, as one can see in ref. [23].

Next we consider the sum of all the infinite series represented in Fig. 4.6. In ref. [124] this was accomplished by noting that at the one loop level the strong $\mathcal{O}(p^2)$ χPT amplitude factorizes on shell, as we have seen. Then, one can apply the same technique as for the $\gamma\gamma \to$meson-meson and substitute the $\mathcal{O}(p^2)$ amplitude by the full one calculated in ref. [23]. Then to all orders in the approach of ref. [23] one has the amplitude

$$t_S = \frac{1}{2}\left[t_{I=0} - t_{I=1}\right] . \tag{4.12}$$

Note that the amplitude obtained in ref. [23] contains also the resonances $f_0(980)$ and $a_0(980)$ which are generated dynamically. The final expression for the amplitude $\phi(p) \to$

$\gamma(q)K^0\bar{K^0}$, as given in ref. [124], is then

$$M = \epsilon_\mu^\gamma \epsilon_\nu^\phi \frac{2eg_\phi}{i} t_S \int \frac{d^4k}{(2\pi)^4} \frac{(2k_\nu - p_\nu)(2k_\mu - q_\mu)}{(k^2 - m_K^2 + i\epsilon)((k-q)^2 - m_K^2 + i\epsilon)((k-p)^2 - m_K^2 + i\epsilon)} \tag{4.13}$$

This integral has been evaluated in ref. [127] using dimensional regularization and confirmed in ref. [133], with the result

$$M = \frac{eg_\phi}{2\pi^2 i m_K^2} I(a,b) \left[(p\cdot q)(\epsilon_\gamma \cdot \epsilon_\phi) - (p\cdot \epsilon_\gamma)(q\cdot \epsilon_\phi)\right] t_S \ , \tag{4.14}$$

with $a = M_\phi^2/m_K^2$, $b = Q^2/m_K^2$ and

$$I(a,b) = \frac{1}{2(a-b)} - \frac{2}{(a-b)^2}\left[f\left(\frac{1}{b}\right) - f\left(\frac{1}{a}\right)\right] + \frac{a}{(a-b)^2}\left[g\left(\frac{1}{b}\right) - g\left(\frac{1}{a}\right)\right] \ , \tag{4.15}$$

where

$$\begin{aligned} f(x) &= \begin{cases} -\arcsin^2\left(\frac{1}{2\sqrt{x}}\right) & x > \frac{1}{4} \\ \frac{1}{4}\left[\ln\left(\frac{\eta_+}{\eta_-}\right) - i\pi\right]^2 & x < \frac{1}{4} \end{cases} \\ g(x) &= \begin{cases} (4x-1)^{\frac{1}{2}} \arcsin\left(\frac{1}{2\sqrt{x}}\right) & x > \frac{1}{4} \\ \frac{1}{2}(1-4x)^{\frac{1}{2}}\left[\ln\left(\frac{\eta_+}{\eta_-}\right) - i\pi\right] & x < \frac{1}{4} \end{cases} \\ \eta_\pm &= \frac{1}{2x}\left(1 \pm (1-4x)^{\frac{1}{2}}\right) \end{aligned} \tag{4.16}$$

After summing over the final polarizations of the photon, averaging over the ones of the ϕ and taking into account the phase space for three particles [73] one obtains

$$\Gamma(\phi \to \gamma K^0 \bar{K^0}) = \int \frac{dm_{12}^2 dQ^2}{(2\pi)^3 192 M_\phi^3} \left| eg_\phi \frac{I(a,b)}{2\pi^2 m_K^2} \right|^2 (M_\phi^2 - Q^2)^2 |t_S|^2 \tag{4.17}$$

where $m_{12}^2 = (q + p_{K^0})^2$. Taking $\dfrac{g_\phi^2}{4\pi} = 1.66$ from its width to K^+K^-, $M_\phi = 1019.41$ MeV, $\Gamma(\phi) = 4.43$ MeV, BR($\phi \to K^0\bar{K^0}$) $= 0.34$ and using the mass of the K^0 for the phase space considerations, ref. [73], one gets

$$\begin{aligned} \Gamma(\phi \to \gamma K^0 \bar{K^0}) &= 2.22 \times 10^{-7}\,\text{MeV} \\ BR(\phi \to \gamma K^0 \bar{K^0}) &= 0.50 \times 10^{-7} \\ \frac{\Gamma(\phi \to \gamma K^0 \bar{K^0})}{\Gamma(\phi \to K^0 \bar{K^0})} &= 1.47 \times 10^{-7} \end{aligned} \tag{4.18}$$

The uncertainties coming from the range of the possible values for the cut off give a relative error around 20%. Taking only into account the $I = 0$ contribution

$$\begin{aligned} \Gamma(\phi \to \gamma K^0 \bar{K^0}) &= 8.43 \times 10^{-7}\,\text{MeV} \\ BR(\phi \to \gamma K^0 \bar{K^0}) &= 1.90 \times 10^{-7} \\ \frac{\Gamma(\phi \to \gamma K^0 \bar{K^0})}{\Gamma(\phi \to K^0 \bar{K^0})} &= 5.58 \times 10^{-7} \end{aligned} \tag{4.19}$$

and with only the $I = 1$

$$\begin{aligned} \Gamma(\phi \to \gamma K^0 \bar{K^0}) = & \quad 2.03 \times 10^{-7}\,\mathrm{MeV} \\ BR(\phi \to \gamma K^0 \bar{K^0}) = & \quad 4.58 \times 10^{-8} \\ \frac{\Gamma(\phi \to \gamma K^0 \bar{K^0})}{\Gamma(\phi \to K^0 \bar{K^0})} = & \quad 1.35 \times 10^{-7} \end{aligned} \tag{4.20}$$

We see that the process is dominated by the $I = 0$ contribution and that the interference between both isospin channels is destructive. From the former results one concludes that the $\phi \to \gamma K^0 \bar{K^0}$ background will *not* be too significant for the purpose of testing CP violating decays from the $\phi \to K^0 \bar{K^0}$ process at DAΦNE in the lines of what was expected in ref. [133]. All these calculations have been done in a way that both the resonant and non-resonant contributions are considered at the same time and taking into account also the different isospin channels.

4.2.2 The $\phi \to \pi^0\pi^0\gamma$ and $\pi^0\eta\gamma$ decays

Radiative ϕ decay into neutral mesons has been a subject of interest often advocated as a source of information on the nature of the scalar meson resonances. Calculations in the line of the former section have been done [134] using the amplitude for the $K\bar{K} \to \pi^0\pi^0$ amplitude from χPT. Other calculations have concentrated on the possibility of using the reactions to decide the nature of the f_0 resonance between several models like a $K\bar{K}$ molecule, a $q\bar{q}$ state or a $q\bar{q}q\bar{q}$ structure [130]. The laboratories of Frascati and Novosibirsk have been actively pursuing research on this topic and very recently some novel results have been reported by two Novosibirsk groups [135–138]. In ref. [125] calculations along the lines reported in the previous section have been conducted following however the tensor approach to the vector mesons of ref. [11] reported in *section 2.4*. This approach had been previously used for the $\rho \to \pi^+\pi^-\gamma$ decay in the absence of final state interaction in ref. [139]. The novelties with respect to the approach of the former section can be summarized in the basic couplings involved in Fig. 4.5 given by

$$\begin{aligned} t_{\phi K^+K^-} &= \frac{G_V M_\phi}{\sqrt{2} f^2}(p_\mu - p'_\mu)\epsilon^\mu(\phi) \\ t_{\phi\gamma K^+K^-} &= -\sqrt{2}e\frac{G_V M_\phi}{f^2}\epsilon_\nu(\phi)\epsilon^\nu(\gamma) \\ &\quad -\frac{\sqrt{2}e}{M_\phi f^2}\left(\frac{F_V}{2} - G_V\right) P_\mu \epsilon_\nu(\phi)[k^\mu \epsilon^\nu(\gamma) - k^\nu \epsilon^\mu(\gamma)] \end{aligned} \tag{4.21}$$

with p_μ, p'_μ the K^+, K^- momenta, P_μ, k_μ the ϕ and photon momenta and f the pion decay constant.

The couplings of eq. (4.21) are easily induced from the Lagrangian of eq. (2.24). The ϕ meson is introduced in the scheme by means of a singlet, ω_1, going from SU(3) to U(3) through the substitution $V_{\mu\nu} \to V_{\mu\nu} + I_3 \frac{\omega_{1,\mu\nu}}{\sqrt{3}}$, with I_3 the 3×3 diagonal matrix. Then, assuming ideal mixing for the ϕ and ω mesons

$$\begin{aligned} \sqrt{\frac{2}{3}}\omega_1 + \frac{1}{\sqrt{3}}\omega_8 &\equiv \omega \\ \frac{1}{\sqrt{3}}\omega_1 - \frac{2}{\sqrt{6}}\omega_8 &\equiv \phi \end{aligned} \tag{4.22}$$

one obtains the required vertices after substituting in eq. (2.24) $V_{\mu\nu}$ by $\tilde{V}_{\mu\nu}$, given by

$$\tilde{V}_{\mu\nu} \equiv \begin{pmatrix} \frac{1}{\sqrt{2}}\rho^0_{\mu\nu} + \frac{1}{\sqrt{2}}\omega_{\mu\nu} & \rho^+_{\mu\nu} & K^{*+}_{\mu\nu} \\ \rho^-_{\mu\nu} & -\frac{1}{\sqrt{2}}\rho^0_{\mu\nu} + \frac{1}{\sqrt{2}}\omega_{\mu\nu} & K^{*0}_{\mu\nu} \\ K^{*-}_{\mu\nu} & \bar{K}^{*0}_{\mu\nu} & \phi_{\mu\nu} \end{pmatrix} \tag{4.23}$$

As we can see, with respect to the approach of the former section the contact term contains an extra part, the term proportional to $\frac{F_V}{2} - G_V$, which is gauge invariant by itself. The first part of the contact term proportional to G_V is not gauge invariant and this requires the addition of the diagrams (a) and (b) of Fig. 4.5 to have a gauge invariant set, as discussed in the former section. This means that in addition to the terms discussed there one gets now an additional term proportional to $(\frac{F_V}{2} - G_V)k$, where k is the photon momentum in the ϕ rest frame. This term appears only with the structure of diagram (c). This has as a consequence that in the treatment of the final state interaction the first loop contains only the two meson propagator and hence is the same function $g(M_I)$ defined in eq. (3.12). This technical detail plus the use of the $K^+K^- \to \pi^0\pi^0$ and $\pi^0\eta$ amplitudes instead of the $K^+K^- \to K^0\bar{K}^0$ in the former section are the basic modifications needed in this work. The values $G_V = 55$ MeV and $F_V = 165$ MeV which are suited to the $\phi \to K^+K^-$ and $\phi \to e^+e^-$ decay widths respectively have been used in ref. [125].

In Fig. 4.7 we show the distribution dB/dM_I for $\phi \to \pi^0\pi^0\gamma$ which allows one to see the $\phi \to f_0\gamma$ contribution since the f_0 is the important scalar resonance appearing in the $K^+K^- \to \pi^+\pi^-$ amplitude [23]. The solid curve shows the results with $F_V G_V > 0$, the sign predicted by vector meson dominance [11]. The intermediate dotted line corresponds to taking $G_V = 67$ MeV and $F_V = 154$ MeV [140], which are the values of the parameters for ρ decay, usually assumed as standard values. The two curves give us an idea of the theoretical uncertainties. The upper dashed curve is obtained considering $F_V G_V < 0$. These results are compared in the figure with the recent ones of the Novosibirsk experiment [135]. We can see that the shape of the spectrum is relatively well reproduced considering statistical and systematic errors (the latter ones not shown in the figure). The results considering $F_V G_V < 0$ are in complete disagreement with the data.

The finite total branching ratio for the $\phi \to \pi^0\pi^0\gamma$ is 0.8×10^{-4} . This latter number is slightly smaller than the result given in ref. [135], $(1.14 \pm 0.10 \pm 0.12) \times 10^{-4}$, where the first error is statistical and the second one systematic. The result given in ref. [136] is $(1.08 \pm 0.17 \pm 0.09) \times 10^{-4}$, compatible with the prediction. If the values for F_V, G_V of the ρ decay are used one obtains 1.7×10^{-4} [140]. The branching ratio obtained for the case $\phi \to \pi^0\eta\gamma$ is 0.87×10^{-4}. The results obtained at Novosibirsk are [137] $(0.83 \pm 0.23) \times 10^{-4}$ and [136] $(0.90 \pm 0.24 \pm 0.10) \times 10^{-4}$. If the values of the ρ decay are used one obtains 1.6×10^{-4} [140]. The spectrum, not shown, is dominated by the a_0 contribution.

The results of this section for these radiative decays are a striking success of the chiral unitary approach reported here . The evidence given by Fig. 4.7 in favour of the sign $F_V G_V > 0$ is much stronger than the one given in ref. [139] from the tail of the $\rho \to \pi^+\pi^-\gamma$ distribution.

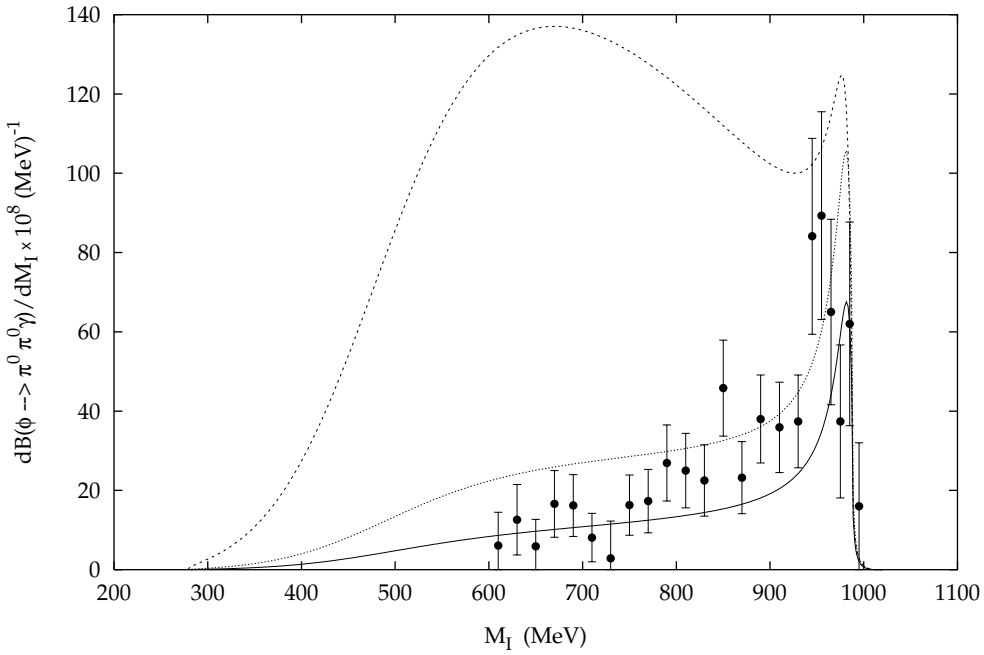

Figure 4.7: Distribution dB/dM_I for the decay $\phi \to \pi^0\pi^0\gamma$, with M_I the invariant mass of the $\pi^0\pi^0$ system. Solid line: our prediction, with $F_V G_V > 0$. Dashed line: result taking $F_V G_V < 0$. The intermediate dotted line corresponds to $G_V = 67$ MeV and $F_V = 154$ MeV [140], the values of the parameters for ρ decay. The data points are from ref. [135] and only statistical errors are shown. The systematic errors are similar to the statistical ones [135].

4.3 Vector and scalar pion form factors

The scalar and vector form factors of the pion are defined respectively as

$$\left\langle \pi^a(p')\pi^b(p)\,\mathrm{out}\left|\hat{m}(\bar{u}u+\bar{d}d)\right|0\right\rangle = \delta^{ab} m_\pi^2 \Gamma(s) \tag{4.24}$$

and

$$\left\langle \pi^i(p')\pi^l(p)\,\mathrm{out}\left|\bar{q}\gamma_\mu\left(\frac{\tau^k}{2}\right)q\right|0\right\rangle = i\,\epsilon^{ikl}(p'-p)_\mu\, F_V(s) \tag{4.25}$$

with $\hat{m} = (m_u + m_d)/2$ and ϵ^{ijk} the total antisymmetric tensor with three indices.

Assuming elastic unitarity (valid up to the $K\bar{K}$ threshold and neglecting multipion states) and making use of the Watson final state theorem [141] the phase of $\Gamma(s)$ and $F_V(s)$ is fixed to be the one of the corresponding partial wave strong amplitude:

$$\begin{aligned} \mathrm{Im}\,\Gamma(s+i\epsilon) &= \tan\delta_0^0\,\mathrm{Re}\Gamma(s) \\ \mathrm{Im}\,F_V(s+i\epsilon) &= \tan\delta_1^1\,\mathrm{Re}F_V(s) \end{aligned} \tag{4.26}$$

The solution of (4.26) is well known and corresponds to the Omnès type [142, 143]:

$$\begin{aligned} \Gamma(s) &= P_0(s)\,\Omega_0(s) \\ F_V(s) &= P_1(s)\,\Omega_1(s) \end{aligned} \tag{4.27}$$

with

$$\Omega_i(s) = \exp\left\{\frac{s^n}{\pi}\int_{4m_\pi^2}^{\infty}\frac{ds'}{s'^n}\,\frac{\delta_i^i(s')}{s'-s-i\epsilon}\right\} \tag{4.28}$$

In (4.27) $P_0(s)$ and $P_1(s)$ are polynomials of degree fixed by the number of subtractions done in $\ln\{\Omega_0(s)\}$ and $\ln\{\Omega_1(s)\}$ minus one, and the zeros of F_V and Γ. For $n = 1$, $P_i(s) = 1$. This follows from the normalization requirement that $\Gamma(0) = F_V(0) = 1$ and the absence of zeros for those quantities.[2]

In ref. [28] the previous dispersion integrals, eq. (4.28), are evaluated making use of the phase shifts calculated in the same reference, see *section 3.1.1.* The resulting vector and scalar form factors are shown in Figs. 4.8 and 4.9 respectively. The Omnès solution assumes the phase of the form factor to be that of the scattering amplitude, and that is true exactly only until the first inelastic threshold. The first inelastic threshold is the 4π one. However, as it was already said, its influence, in a first approach, is negligible. The first important inelastic threshold is the $K\bar{K}$ one around 1 GeV. This is essential in $I = L = 0$ but negligible in $I = L = 1$. This inelastic threshold, as discussed above, has been included in the approach and it is mostly responsible for the appearance of the $f_0(980)$ resonance.

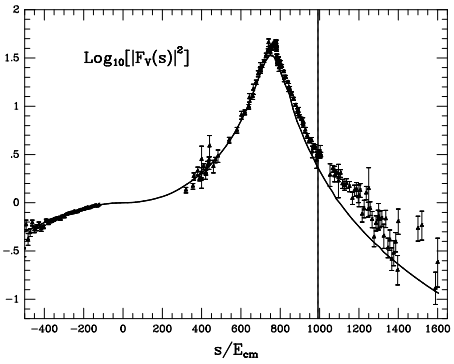

Figure 4.8: Vector pion form factor. The vertical line shows the opening of the $K\bar{K}$ threshold. Data from ref. [145].

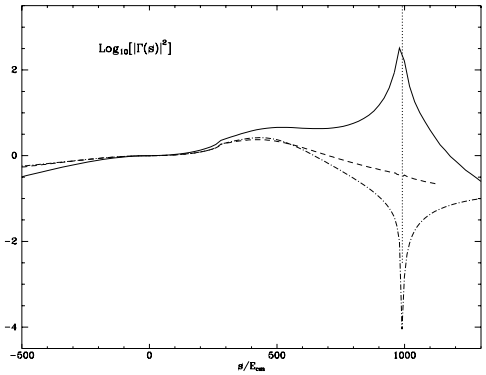

Figure 4.9: Scalar form factor. The dashed curve is the result unitarizing only with pions. The solid line is the full result with both pions and kaons in the intermediate state integrating up to infinity in eq. (4.28). The dotted-dashed line is the same as the solid one but integrating only up to the openning of the $K\bar{K}$ threshold. The vertical line shows the opening of this threshold

In the case of the $F_V(s)$ the agreement with existing data is quite satisfactory, with the dominant role played by the $\rho(770)$ resonance. On the other hand, taking into account possible uncertainties coming from orders higher than p^4 in χPT, the result obtained for the vector form factor is similar to the one obtained in ref. [146] using another phase shift expression. For the $I = L = 0$ channel the most dramatic effect is the openning of the $K\bar{K}$ channel. In Fig. 4.9 the continuous line corresponds to the use of eq. (4.27) integrating up to infinity in the Omnès formula (4.28). On the other hand, the dashed-dotted line corresponds to integrating only up to the openning of the $K\bar{K}$ threshold. The differences between both options are tremendous making evident that a coupled channel approach is necessary in order to describe properly the scalar form factor for energies above 400–500 MeV. Finally, the dashed line represents the scalar form factor unitarizing only with pions to obtain the $\delta_{00,\pi\pi}$ phase shift, in the line of the works [66, 147–149].

[2] In principle $\Gamma(0) \neq 1$. However, since this is the leading χPT result and we are at low energies, the difference with respect one is very small [144].

4.4 $\gamma p \to p$ meson-meson

An interesting example of final state interaction of two mesons appears in the photoproduction of pairs of mesons in the γp reaction when the pair is produced with an invariant mass close to the mass of one resonance. An example of it is given in ref. [150] where the photoproduction of scalar meson is studied. The process is depicted in Fig. 4.10 where the leading tree level process appears in diagram (a) and is a contact term induced from minimal coupling from the meson-baryon Lagrangian of eq. (3.56). This term is given by

$$V^{\gamma}_{\pi(K)} = -C_{\pi(K)} \frac{e}{2f^2} \bar{u}(p') \gamma^{\mu} u(p) \epsilon_{\mu} \ , \tag{4.29}$$

where C_{π} =1 and C_K=2 stand for the case of the production of a $\pi^+\pi^-$ or a K^+K^- pair respectively.

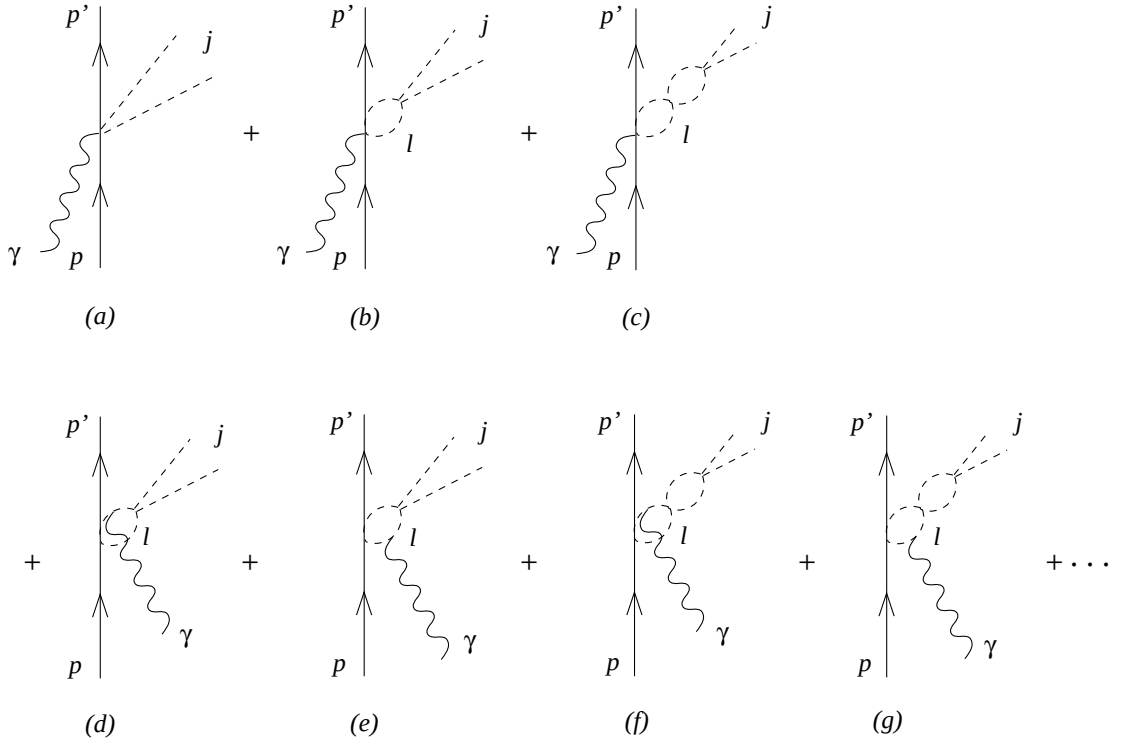

Figure 4.10: Tree level and iterated terms from the contact term and from mesonic Bremsstrahlung.

The final state interaction of the mesons is accounted for by means of the rest of the diagrams in the figure and, similarly to the case of the ϕ radiative decay, the photon lines must also be coupled to the lines in the loops to guarantee gauge invariance. Missing in the figure are the tree level diagrams of Bremmsstrahlung where the photon is coupled to any of the external meson lines in diagram (a). This is justified in the case of meson production close to threshold (for this purpose a photon beam of energy 1.7 GeV is suggested in ref. [150]) or in the case of production of neutral meson pairs like $\pi^0\pi^0$ or $\pi^0\eta$. At higher energies there can be more involved production mechanisms [151–153] and also at lower energies there are background terms which are important particularly for the case of $\pi^+\pi^-$ production [154,155]. Yet the resonant production should show up as a bump on top of the background and allow one to study the resonances in a different setup, and in addition study the production of the resonances in nuclei which we will address below. The technique to include final state interaction here follows closely the steps described in the study of the $\gamma\gamma \to$ meson-meson reaction in ref. [117] and of the ϕ radiative decay in ref. [125], which have been reported above. There is only one difference since the square of the momentum

transferred by the nucleon (which plays here the role of the ϕ mass squared in the ϕ decay) can be here negative. In this case one has to extrapolate analytically the $I(a,b)$ function of eq. (4.15) and detailed expressions are given in ref. [150].

The results obtained for the invariant mass distribution of the two mesons are given in Fig. 4.11 for different pairs of mesons in the final state. The figure shows clear peaks for the production of the f_0 and a_0 resonances in the $\pi^+\pi^-$, $\pi^0\pi^0$ and $\pi^0\eta$ production respectively. In these cases the ratio of the resonance signal to background is found to be optimal for the $\pi^0\pi^0$ and $\pi^0\eta$ cases. The figure also shows the cross section for K^+K^- production close to threshold which is appreciably renormalized by final state interaction with respect to the Born contribution. The $K^0\bar{K}^0$ production is found to be very small.

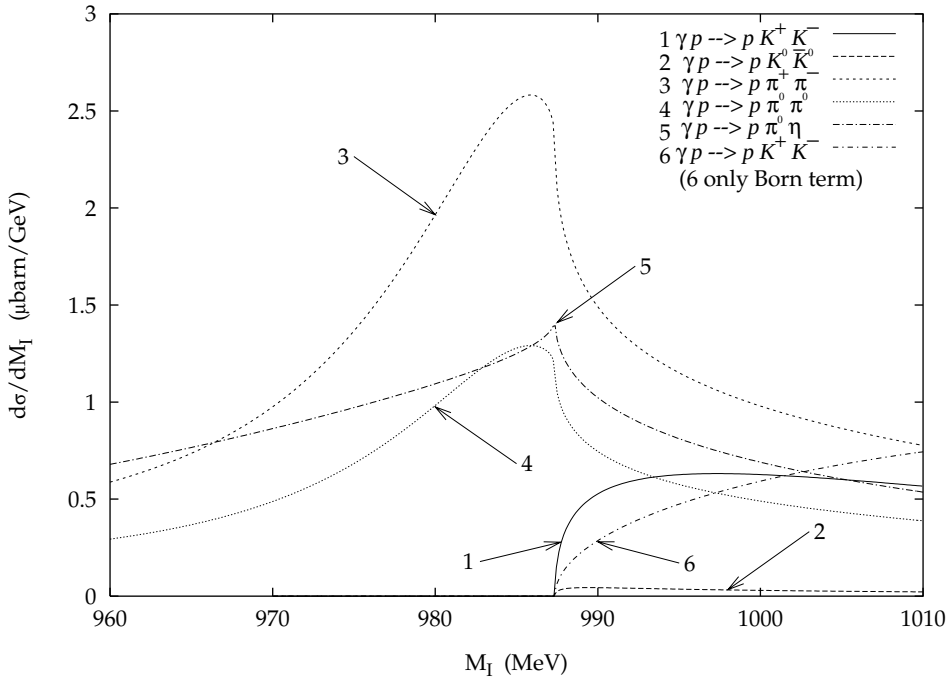

Figure 4.11: Results for the cross section on protons as a function of the invariant mass of the meson-meson system.

It is interesting to note that the signal for the $\pi\pi$ production around the f_0 resonance shows up with a peak. This is a novelty with respect to the case in $\pi\pi$ scattering where the f_0 shows up with a minimum in the cross section. The different structure of the loop function in the first loop in the figures with respect to the $g(s)$ function of the plain two meson propagator is responsible for this different interference pattern with the background from the σ pole contribution. This was also the case in the radiative ϕ decay where the f_0 resonance also appeared as a peak in the invariant mass distribution.

4.4.1 Scalar meson production in nuclei

It is also relevant to see that the previous reaction can be suited for the observation of the resonance modification in nuclei. The f_0 and a_0 couple strongly to $K\bar{K}$ but they are narrow because there is little phase space for the decay into that state. However, the kaons are apprecibly renormalized in nuclei and hence one expects that these resonances will also be appreciably modified inside a nuclear medium.

The interaction of K, $\bar{K}$ with nuclei is a subject that has attracted much attention [156–169]. Interesting developments have been done recently in K^-N scattering using the chiral Lagrangians [79, 80], which have allowed to tackle the problem of the K, $\bar{K}$ nucleus

interaction with some novel results [170–173]. The issue is not yet settled since there are still important discrepancies between the different results.

The first thing which we observe is that if one looks for a proton in the final state, one can also have the $\gamma n \to p\pi^-\eta(K^-K^0)$ reactions and approximately one would expect a cross section

$$\left.\frac{d\sigma}{dM_I}\right|_A \simeq Z\frac{d\sigma}{dM_I}(p) + N\frac{d\sigma}{dM_I}(n)\,. \tag{4.30}$$

The latter cross section can proceed through the meson channels K^-K^0 and $\pi^-\eta$, both in $I = 1$. These cross sections are found in ref. [150] to be one order of magnitude smaller than those on the proton target. Hence, in nuclei we should expect a cross section roughly Z times the one of the proton, unless the properties of the resonances a_0 and f_0 are drastically modified in the medium, which is, however, what one expects. As noted above, the relatively small width of the f_0 resonance is due to the small coupling to the $\pi\pi$ channel. The coupling of a_0 to $\pi^0\eta$ is comparatively much larger. These resonances, however, couple very strongly to the $K\bar{K}$ system but the decay is largely inhibited because the $K\bar{K}$ threshold is above the resonance mass. Only the fact that the f_0 and a_0 resonances have already a width for $\pi\pi$ and $\pi\eta$ decay, respectively, allows the $K\bar{K}$ decay through the tail of the resonance distribution. If the K^- develops a large width on its own this enlarges considerably the phase space for $K\bar{K}$ decay and the a_0, f_0 width should become considerably larger.

Given the interest that the modifications of meson resonances in nuclei, like the σ [174, 175], ρ [176, 177], etc., is raising, the study of the modifications of the f_0 and a_0 is bound to offer us some insight into the nature of these resonances, that has been so much debated, and into the chiral unitary approach to these resonances which we are discussing in this work. Preliminary results using the $K, \bar{K}$ self-energies in the medium discussed in *section 6.2* are already available [178] and indicate a large increase of the f_0 width in the medium.

Chapter 5

Initial and final state interaction in meson-baryon reactions

In *section 3.3.2* we studied the meson-baryon interaction around the region of the $\Lambda(1405)$ and $N^*(1535)$ resonances. We saw there how the unitarization in coupled channels was essential to reproduce the scattering data. In this chapter we show some examples of physical reactions where the meson-baryon interaction appears in the initial or final states. We shall show how the proper consideration of the initial state interactions along the lines discussed in *section 3.3.2* brings a natural solution to one problematic reaction, the K^-p radiative capture, where the ratio of Λ to Σ^0 production is abnormally low. The coupled channel unitary techniques will be also applied to study reactions in which the resonances appearing in the meson-baryon interactions are now generated in the final state. In addition we shall also devise how the techniques can be used to evaluate static properties of those resonances.

5.1 K^- proton radiative capture: $K^-p \to \gamma\Lambda, \gamma\Sigma^0$

The near threshold $K^-p \to \gamma Y$ reaction with $Y = \Lambda, \Sigma^0$ has long attracted a lot of interest, mainly because of the possibility of using this reaction to resolve the debates [179–185] over the structure of the $\Lambda(1405)$ resonance. Most of the earlier theoretical investigations [186] neglected the initial strong K^-p interactions. It was first demonstrated by Siegel and Saghai [187] that the initial K^-p interactions can drastically change the predicted capture rates and thus can significantly alter the interpretation of the data. With the phenomenological separable potentials, they, however, needed an about $30-50\%$ deviation of the coupling constants from the SU(3) values to obtain an accurate description of the data.

This unsatisfactory situation was revised in ref. [188], where it was investigated whether the data could be well described by treating the initial K^-p interactions within the unitary coupled-channel chiral approach of refs. [79,80], which has been discussed in detail in *section 3.3.2*. In the present section we report on the results obtained in ref. [188] and we will show that, indeed, a satisfactory agreement with the experiment can be obtained without the need of SU(3) breaking.

A detailed derivation of the $K^-p \to \gamma Y$ reaction can be found in ref. [188], where standard electromagnetig vertices are used and the initial state strong K^-p interaction is described through the coupled-channel Bethe-Salpeter equation. The resulting amplitude in the center of mass frame $P = (\sqrt{s}, \vec{0})$ reads

$$T_{\gamma Y,K^-p}(q,k') = Q_{\gamma Y,K^-p}(q,k') + [QGT]_{\gamma Y,K^-p}(q,k') + \Delta_{\gamma Y,K^-p}(q,k') \ , \qquad (5.1)$$

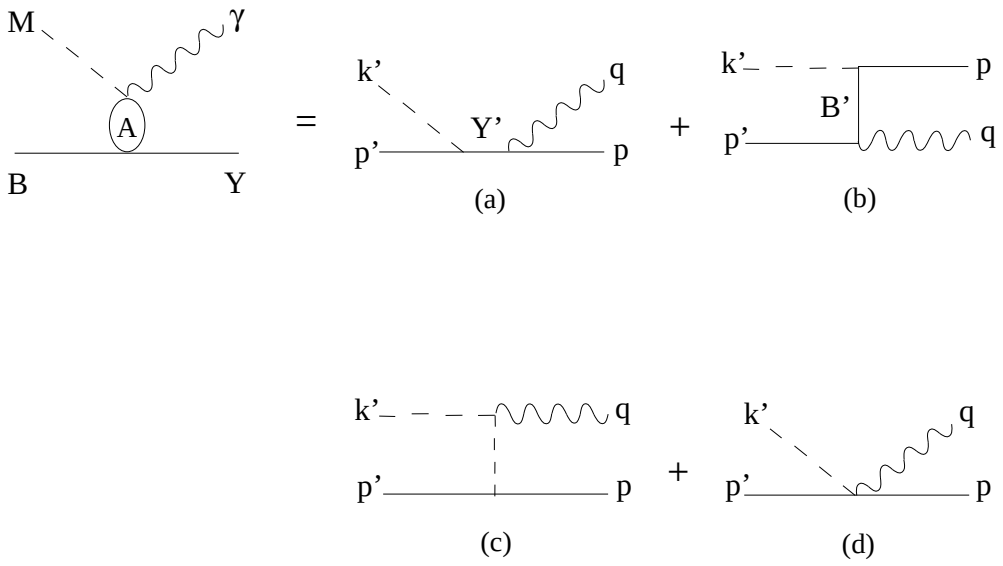

Figure 5.1: Elementary amplitudes for the reaction $K^- p \to \gamma Y$

where the first term

$$Q_{\gamma Y,MB}(q,k') = ie_M[\vec{\sigma}\ \vec{\epsilon}]\frac{C_{Y,MB}}{2f}\left(1 - \frac{\omega_M(k')}{2q} + \frac{\mu_M^2}{4qk'}\ln\frac{\omega_M(k')+k'}{\omega_M(k')-k'}\right)\ , \tag{5.2}$$

with $MB \equiv K^- p$, collects the Born terms for the elementary $K^- p \to \gamma Y$ reaction displayed in Fig. 5.1. Note that the above expression contains only the contact (Fig. 5.1d) and the meson exchange (Fig. 5.1c) terms. In the heavy-baryon approximation one can show that the baryon pole term (Fig. 5.1a) contributes only to the meson-baryon P-wave states, while some S-wave contributions from the baryon-exchange term (Fig. 5.1b) also vanish at threshold (K^- capture at rest). The charge and mass of the meson M are denoted, respectively, by e_M and μ_M. The SU(3) coupling constants $C_{Y,MB}$ for the $MB \leftrightarrow Y$ transition are given by

$$C_{Y,MB} = X_{Y,MB}(D+F) + Z_{Y,MB}(D-F)\ , \tag{5.3}$$

where the values of the X and Z coefficients are easily evaluated from the chiral Lagrangians and can be found in ref. [188]. The initial state strong interactions are present in the second term of Eq. (5.1)

$$\begin{aligned}[QGT]_{\gamma Y,K^-p}(q,k') &= \sum_{MB}\int\frac{d\vec{k}}{(2\pi)^3}\frac{M_B}{E_B(\vec{k})}\frac{1}{2\omega_M(\vec{k})}\frac{Q_{\gamma Y,MB}(q,k)}{\sqrt{s}-E_B(\vec{k})-\omega_M(\vec{k})+i\epsilon} \\ &\times\ T_{MB,K^-p}(\vec{k}_{MB},\vec{k}',\sqrt{s})\ ,\end{aligned} \tag{5.4}$$

where T_{MB,K^-p} is the amplitude for the strong $K^- p \to MB$ transition, as well as in the third term

$$\begin{aligned}\Delta_{\gamma Y,K^-p}(q,k') &= \sum_{MB}\int\frac{d\vec{k}}{(2\pi)^3}\frac{M_B}{E_B(\vec{k})}\frac{1}{2\omega_M(\vec{k}-\vec{q})}\frac{1}{\sqrt{s}-E_B(\vec{k})-q^0-\omega_M(\vec{k}-\vec{q})+i\epsilon} \\ &\times\ ie_M\frac{C_{Y,MB}}{2f}\frac{2[\vec{k}\vec{\epsilon}][\vec{\sigma}(\vec{k}-\vec{q})]}{(q^0+\omega_M(\vec{q}-\vec{k}))^2-\omega_M^2(\vec{k})}T_{MB,K^-p}(\vec{k}_{MB},\vec{k}',\sqrt{s})\ ,\end{aligned} \tag{5.5}$$

which is related to the exact treatment of the meson propagator. It corresponds to the contribution of the pole of the meson propagating between the emitted photon and the final

hyperon Y in Fig. 5.1c and in the loop diagrams generated by the initial state interactions. Note that, in the above expressions, the allowed intermediate states are the charged particle channels ($MB = K^-p, \pi^+\Sigma^-, \pi^-\Sigma^+$ and $K^+\Xi$). Moreover, the strong amplitude, T_{MB,K^-p}, appears with the on shell momentum k_{MB} and factors out of the integral because, as shown in the appendix of ref. [188], the off shell piece can be absorbed in the renormalization of the charge.

The results for the branching ratios, defined by

$$B_{K^-p\to\gamma Y} = \frac{\sigma_{K^-p\to\gamma Y}(\sqrt{s}_{\rm th})}{\sigma_{K^-p\to{\rm all}}(\sqrt{s}_{\rm th})}\,, \tag{5.6}$$

where $Y = \Lambda, \Sigma^0$ and $\sqrt{s}_{\rm th} \to \mu_{K^-} + M_p$, are compared to the experimental data [189] in Table 5.1.

Table 5.1: $K^-p \to \gamma\Lambda, \gamma\Sigma^0$ branching ratios defined in eq. (5.6) (in unit of 10^{-3})

Amplitude	$B_{K^-p\to\gamma\Lambda}$	$B_{K^-p\to\gamma\Sigma^0}$	$R = B_{K^-p\to\gamma\Lambda}/B_{K^-p\to\gamma\Sigma^0}$
Q	1.12	0.073	16.4
$Q + QGT$	1.31	0.95	1.38
$Q + QGT + \Delta$	1.58	1.33	1.19
$[Q + QGT + \Delta]_{\text{no } \eta}$	2.47	1.27	1.94
$[Q + QGT + \Delta]_{\text{with } \Lambda_\pi}$	1.10	1.05	1.04
EXP [189]	0.86 ± 0.16	1.44 ± 0.31	$0.4 - 0.9$

Neglecting initial meson-baryon interactions (first row in Table 5.1) gives a very weak branching ratio for $\gamma\Sigma^0$ production and the predicted ratio between the two production rates is an order of magnitude larger than the data. This is in agreement with the findings of Siegel and Saghai [187]. When the strong coupled-channel effects are included (third row in Table 5.1) the ratio is close to the experimental value. The predicted branching ratio for the $\gamma\Lambda$ production is about 50% larger than the experimental value, but it is within the experimental uncertainty for the $\gamma\Sigma^0$ production. As shown in ref. [188], the enhancement of the $\gamma\Sigma^0$ production is essentially coming from the coupling of the photon to intermediate $\pi^+\Sigma^-$ and $\pi^-\Sigma^+$ states. The exact treatment of the meson propagator in Fig. 5.1c leads to a contribution from a second meson pole, $\Delta_{\gamma Y,K^-p}$, which can change the $\gamma\Sigma^0$ branching ratio by about 40% and brings the predicted ratio closer to the experimental value. The influence of the η channels on the strong T_{MB,K^-p} amplitudes has, as for the case of the low energy K^-p scattering data [79], a significant effect here. Comparing the third and fourth rows in Table 5.1 one sees that the predicted branching ratio for $\gamma\Lambda$ production is increased by about 60% if the η channels are omitted in the calculation of the strong amplitudes. It is thus clear that including the η channels is also crucial in using this reaction to test the chiral SU(3) symmetry. We note that the η channels were omitted in the model of ref. [187] and, at the same time, the couplings had to be substantially changed with respect to their SU(3) values in order to obtain a good fit to the data. In retrospective one can say that the deviation of the coupling constants from their SU(3) value is in fact trying to restore the breaking that was induced by the omission of the η channels.

Finally, we note that the strong meson-baryon-baryon vertex in each of the photoproduction amplitudes should in principle have a form factor because hadrons are composite particles. The results obtained with a monopole form factor with a cut off of $\Lambda_\pi = 1$ GeV, a value which is commonly accepted, are shown in the fifth row of Table 5.1 and agree roughly with the data within experimental errors, which are of the order of 20%. If one compares with the central values of the experimental branching ratios, the results are on the upper edge of the $B_{K^-p\to\gamma\Lambda}$ ratio while those for $B_{K^-p\to\gamma\Sigma^0}$ are on the lower edge. Looked at it

in the context that the coupled channels and unitarization have reduced the ratio R by a factor 14, differences of the order of 10–20% are not so significative. Note that all coupling constants are consistent with the chiral SU(3) symmetry and the model depends on only the cut off parameter, which was fixed in the study of $S = -1$ meson-baryon reactions [79]. In this approach, neither the meson-baryon nor the photoproduction mechanisms involve the explicit consideration of excited hyperon states since the $\Lambda(1405)$ resonance, which plays a key role in these reactions, is generated dynamically, hence strengthening the interpretation of the $\Lambda(1405)$ as a quasi-bound meson-baryon system with $S = -1$, as already supported by the study of the strong interactions in [79, 80].

5.2 Photoproduction of the $\Lambda(1405)$ on protons and nuclei

As we saw in *section 3.3.2*, the $\Lambda(1405)$ resonance is produced dynamically by using the Bethe-Salpeter equation and the lowest order Lagrangian for meson-baryon interaction in S-wave suggesting that this resonance is like a quasibound meson-baryon state rather than a genuine $3q$ state. Further tests on the nature of the resonance can be done by studying different production processes. One of them was studied in ref. [190] by means of photoproduction on the proton, i.e.

$$\gamma p \to K^+ \Lambda(1405) \ . \tag{5.7}$$

The study of the reaction in nuclei is also of much interest since different studies predict sizeable changes of the resonance in nuclei [169–173] which would have also repercussions on the properties of $\bar{K}$ inside a nuclear medium. This is a hot topic since it relates to the possibility of having kaon condensation in stars and to the puzzle of the strong $\bar{K}$ attraction needed to explain the K^- atoms which seems to violate the low density theorem.

In ref. [190] a study was done along lines similar to those exposed in *section 4.3.1*, however, in this case a meson and a baryon combine through final state interaction to give the $\Lambda(1405)$. Diagrammatically the mechanism for the production is depicted in Fig. 5.2.

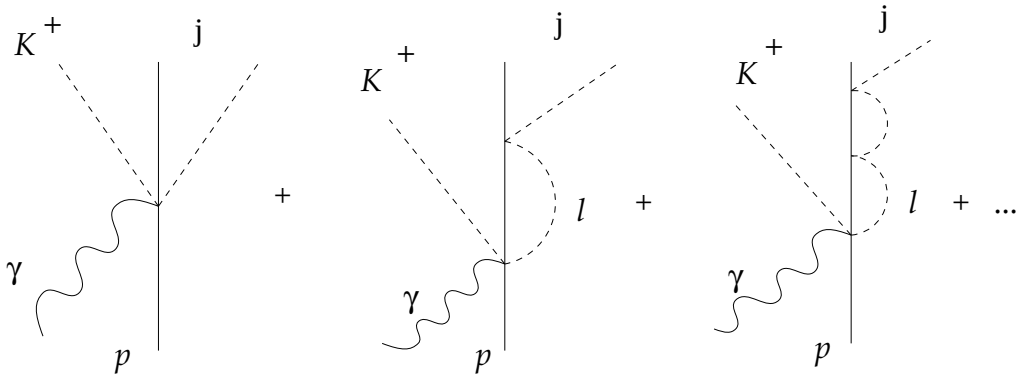

Figure 5.2: Diagrammatic representation of the meson-baryon final state interaction in the $\gamma p \to K^+ \Lambda(1405)$ process.

As we can see there, a K^+ is produced together with another meson and a baryon which combine through final state interaction with the coupled channels in the $S = -1$ sector and give rise to the $\Lambda(1405)$ resonance. Once again one needs the vertex with two mesons a photon and a baryon line which is obtained via minimal coupling from eq. (3.57) and is given by

$$V_{ij}^{(\gamma)} = C_{ij} \frac{e}{4f^2} (Q_i + Q_j)\, \overline{u}(p') \gamma^\mu u(p) \epsilon_\mu, \tag{5.8}$$

where Q_i, Q_j are the initial and final meson charges and ϵ_μ the photon polarization vector and C_{ij} the coefficients of eq. (3.57).

Once again Bremsstrahlung terms on the meson lines of the tree diagram are negligible if the reaction is done close to threshold. In ref. [190] the photon energy was chosen 1.7 GeV in the lab frame.

In Fig. 5.3 we show $d\sigma/dM_I$ for the different channels. While all coupled channels collaborate to the building up of the $\Lambda(1405)$ resonance, most of them open up at higher energies and the resonance shape is only visible in the $\pi^+\Sigma^-$, $\pi^-\Sigma^+$, $\pi^0\Sigma^0$ channels. The $\bar{K}N$ production occurs at energies slightly above the resonace and the $\pi^0\Lambda$, with isospin one, only provides a small background below the resonance.

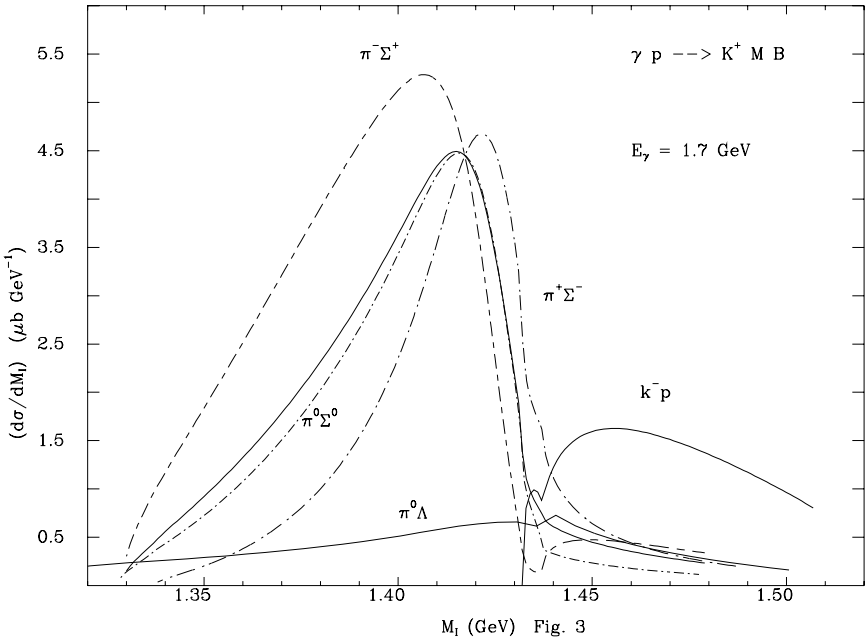

Figure 5.3: Mass distribution in the $\gamma p \to K^+MB$ reaction for the different channels. The dashed lines show the $\Sigma^+\pi^-$, $\Sigma^-\pi^+$ and $\Sigma^0\pi^0$ distributions. The solid line with the resonance shape is the sum of the three $\Sigma\pi$ channels divided by three. The distributions for $\pi^0\Lambda$ and K^-p production are also given, while that for $\bar{K}^0n$ production is small and not shown in the figure.

It is interesting to see the different shapes of the three $\pi\Sigma$ channels. This can be understood in terms of the isospin decomposition of the states

$$|\pi^+\Sigma^-\rangle = -\frac{1}{\sqrt{6}}|2,0\rangle - \frac{1}{\sqrt{2}}|1,0\rangle - \frac{1}{\sqrt{3}}|0,0\rangle \tag{5.9}$$

$$|\pi^-\Sigma^+\rangle = -\frac{1}{\sqrt{6}}|2,0\rangle + \frac{1}{\sqrt{2}}|1,0\rangle - \frac{1}{\sqrt{3}}|0,0\rangle \tag{5.10}$$

$$|\pi^0\Sigma^0\rangle = \sqrt{\frac{2}{3}}|2,0\rangle - \frac{1}{\sqrt{3}}|0,0\rangle \tag{5.11}$$

Disregarding the $I = 2$ contribution which is negligible, the cross sections for the three channels are proportional to the modulus squared of the amplitude and hence they go as:

$$\frac{1}{2}|T^{(1)}|^2 + \frac{1}{3}|T^{(0)}|^2 + \frac{2}{\sqrt{6}}\mathrm{Re}\,(T^{(0)}T^{(1)*})\,; \quad \pi^+\Sigma^- \tag{5.12}$$

$$\frac{1}{2}|T^{(1)}|^2 + \frac{1}{3}|T^{(0)}|^2 - \frac{2}{\sqrt{6}}\mathrm{Re}\,(T^{(0)}T^{(1)*})\,; \quad \pi^-\Sigma^+ \tag{5.13}$$

$$\frac{1}{3}|T^{(0)}|^2\,; \quad \pi^0\Sigma^0 \tag{5.14}$$

The crossed term $T^{(0)}T^{(1)*}$ is what makes these cross sections different. We can also see that

$$3\frac{d\sigma}{dM_I}(\pi^0\Sigma^0) \simeq \frac{d\sigma}{dM_I}(I=0) \tag{5.15}$$

$$\frac{d\sigma}{dM_I}(\pi^0\Sigma^0) + \frac{d\sigma}{dM_I}(\pi^+\Sigma^-) + \frac{d\sigma}{dM_I}(\pi^-\Sigma^+) \simeq \frac{d\sigma}{dM_I}(I=0) + \frac{d\sigma}{dM_I}(I=1) \tag{5.16}$$

This means that the real shape of the resonance must be seen in either the $\pi^0\Sigma^0$ channel or in the sum of the three $\pi\Sigma$ channels, provided the I = 1 cross section (not the crossed terms which are relatively large) is small as it is the case. Incidentally, eqs. (5.12),(5.13) also show that the difference between the $\pi^+\Sigma^-$ and $\pi^-\Sigma^+$ cross sections gives the crossed term and hence provides some information on the $I = 1$ amplitude.

In Fig. 5.4 the results are recombined in a practical way from the experimental point of view. They show the $I = 0$ contribution, the $\Sigma^0\pi^0$ contribution and the sum of all channels including the $\pi^0\Lambda$, and we see that they are all very similar and the total contribution is just the $\Lambda(1405)$ contribution plus a small background. In practical terms this result means that the detection of the K^+ alone (which sums the contribution of all channels) is sufficient to determine the shape and the strength of the $\Lambda(1405)$ resonance in this reaction.

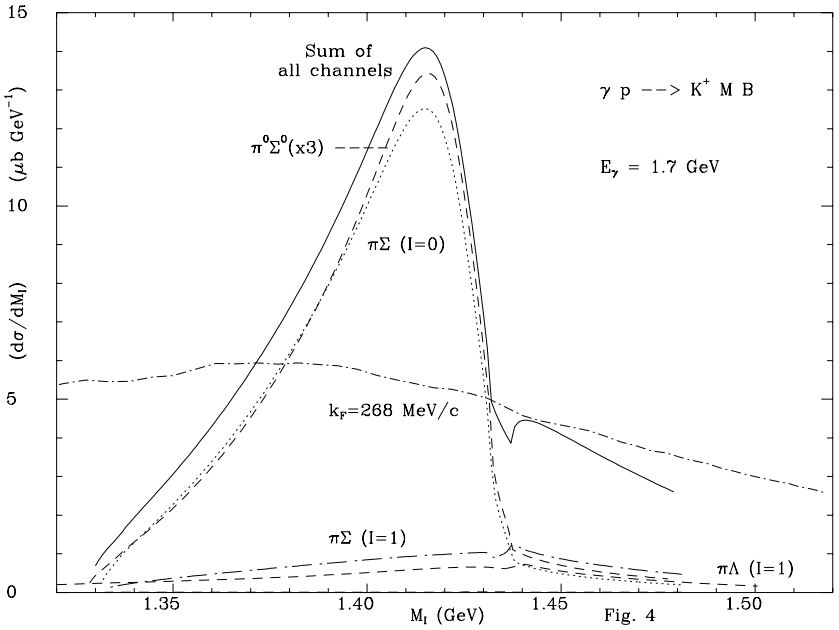

Figure 5.4: Mass distributions for the $\gamma p \to K^+MB$ reaction. Dashed line (resonant shape): $\Sigma^0\pi^0$ distribution multiplied by three. Dotted line (resonant shape): pure $I = 0$ contribution from the $\Sigma\pi$ channels. Solid line (resonant shape): Sum of the cross sections for all the channels. The $I = 1$ background contribution from the $\Sigma\pi$ and $\pi^0\Lambda$ channels is also shown. Short-dash-dotted line: Effects of the Fermi motion with $k_F = 268$ MeV/c ($\rho = \rho_0$) where the free space $\Lambda(1405)$ distribution is assumed in the calculation.

The study of the reaction in nuclei requires special care. Indeed, assume one uses the same set up as before with a nuclear target and measures the outgoing K^+. There the invariant mass will be given by

$$\begin{aligned} {M_I}^2(p) = (q+p-k)^2 \;\; &= \;\; M^2 + m_K^2 - 2q^0k^0 + 2\vec{q}\cdot\vec{k} + \\ &\quad 2p^0(q^0-k^0) - 2\vec{p}\cdot(\vec{q}-\vec{k}) \end{aligned} \tag{5.17}$$

with q, k, p the momenta of the photon, K^+ and initial proton respectively. Since $\vec{q}-\vec{k}$ has a large size, there will be a large spreading of invariant masses due to Fermi motion for a given set up of photon and K^+ momenta, unlike in the free proton case where ${M_I}^2$ is well determined[1]. The nuclear cross section normalized to the number of protons (the neutrons through K^-n and coupled channels only contribute to $I = 1$ with a small background) would be given by the convolution formula

$$\frac{1}{Z}\frac{d\sigma}{dM_I}\mid_A \simeq \frac{2}{\rho_p}\int \frac{d^3p}{(2\pi)^3}\frac{d\sigma}{dM_I(\vec{p})} \quad ; \qquad \rho_p = \frac{{k_F}^3}{3\pi^2} \tag{5.18}$$

where the integral over $\vec{p}$ ranges up to the Fermi momentum k_F.

In order to show the effects of the Fermi motion, values of $\vec{k}$ corresponding to forward K^+ in the CM (and hence largest value of $\vec{k}$ in the lab frame) are chosen in ref. [190]. These components would minimize the spreading of the ${M_I}^2(\vec{p})$ in eq. (5.17). Even then, the spreading of the invariant masses is so large that one looses any trace of the original resonance, as one can see in Fig. 5.4. The M_I in the x axis of the figure in this case is taken for reference from eq. (5.17) for a nucleon at rest. This result simply means that in order to see genuine dynamical effects one would have to look at the invariant mass of the resonance from its decay product, $\pi\Sigma$, tracing back this original invariant mass with appropiate final state interaction corrections.

One interesting thing here is that the $\Lambda(1405)$ resonance is produced with a large momentum in the nuclear lab frame. Because of that, Pauli blocking effects in the resonance decay, which are so important for the resonance at rest in the nucleus, become now irrelevant. Hence medium modifications of the resonance in the present situation should be attributed to other dynamical effects [172, 173].

Experiments on this reaction are now done at TJNAF and are being analysed. They are also scheduled to run with priority at LEPS of SPring8/RCNP. These experiments will allow to test current ideas on chiral symmetry for the elementary reaction. When used with nuclear targets they should provide us with much needed information on the in medium properties of the $\Lambda(1405)$ resonance and the K^- meson. This should help resolve questions like K^- condensation and the origin of the attraction seen in K^- atoms.

5.3 Radiative production of the $\Lambda(1405)$ resonance in K^- collisions on protons and nuclei

One of the problems which we encountered in the former section regarding the study of the properties of the $\Lambda(1405)$ resonance in nuclei is that the detection of the K^+ alone did not allow one to observe the shape of the resonance because the effect of Fermi motion of the nucleons in the nucleus produced a large spread of the invariant mass of the meson-baryon system building up the resonance. One had to reconstruct the invariant mass from the $\pi\Sigma$ decay products. In this section we report on an alternative reaction to produce the $\Lambda(1405)$ resonance which is dynamically quite different from the photoproduction process, hence offering extra tests of the chiral symmetry ideas in the baryon sector. Furthermore, it has an attractive feature since in this case an easy experimental set up is still sufficient to investigate the resonance properties in nuclei.

The reaction reported here is the $K^-p \to \Lambda(1405)\gamma$ at low K^- energies, which was studied in ref. [191].

Although the present reaction corresponds to a crossed channel of the $\gamma p \to K^+\Lambda(1405)$ reaction studied in ref. [190] and reported above, the two processes are rather different

[1] We are endebted to T. Nakano and J. K. Ahn for calling us the attention on this point

dynamically in their respective physical channels, with the dominant mechanisms in the photoproduction reaction being negligible in the present one, and others which could be proved negligible in the photoproduction one becoming now dominant. The set of diagrams considered in ref. [191] is depicted in Fig. 5.5. The first line simply shows the diagrams of the Bethe-Salpeter equation which are utilized to generate the meson-baryon scattering T-matrix with coupled channels. The channels considered here are the same 10 channels considered in *section 3.3.2*. The rest of the diagrams in Fig. 5.5 stand for the radiative production of the $\Lambda(1405)$.

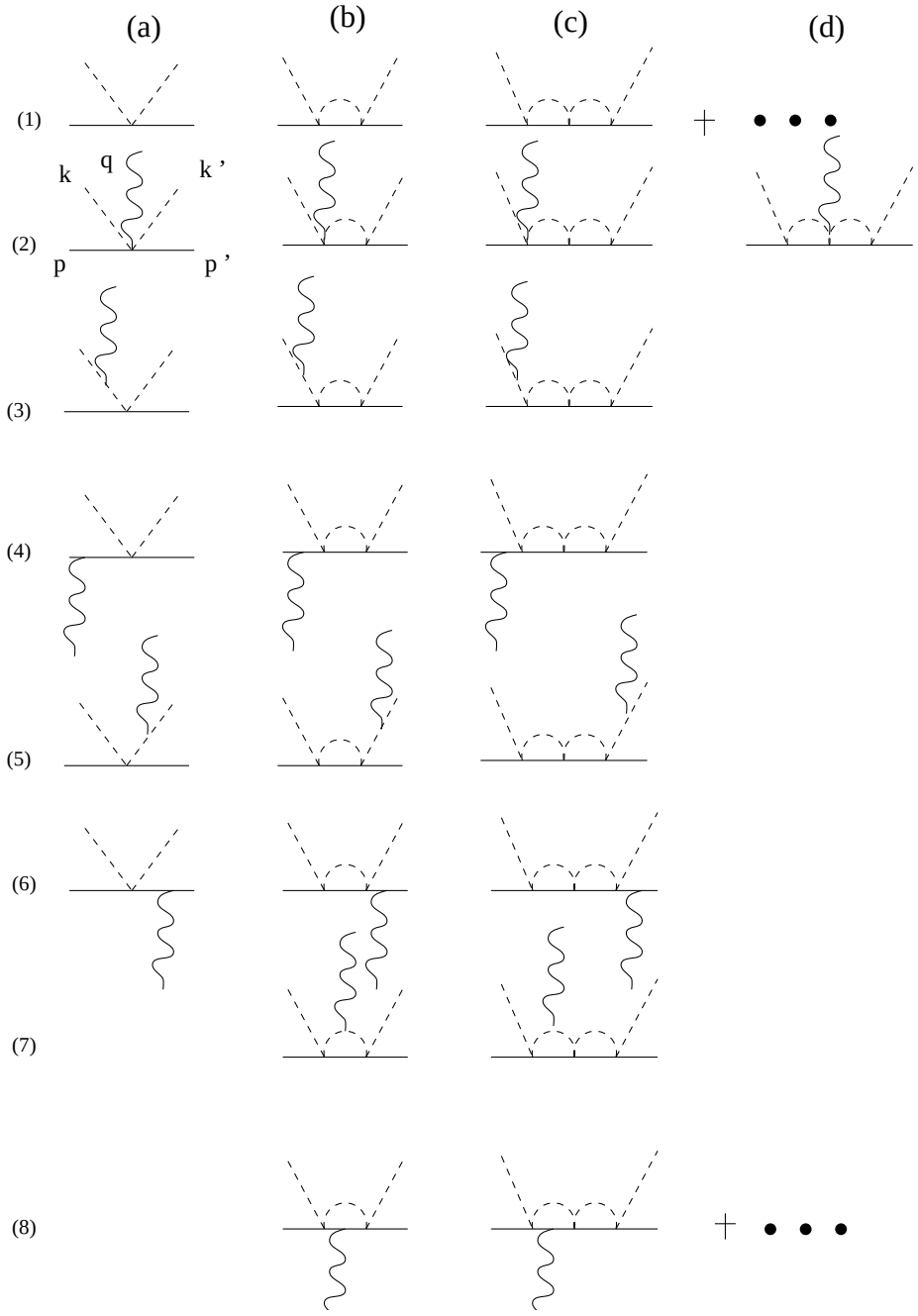

Figure 5.5: Feynman diagrams used in the model for the $K^- p \to \Lambda(1405)\gamma$ reaction.

Apart from the strong $MB \to M'B'$ vertices of eq. (3.57) we also need the coupling of the photon to the baryons, the mesons, plus the contact term of diagram (2.a) of Fig. 5.5 required by gauge invariance. These vertices are standard and after the nonrelativistic reduction of the γ matrices, are given in the Coulomb gauge, $\epsilon^0 = 0$, $\vec{\epsilon} \cdot \vec{q} = 0$, with $\vec{q}$ the photon momentum, by

$$a) - it_{M'M\gamma} = 2ieQ_M \vec{k}' \cdot \vec{\epsilon} \tag{5.19}$$

for the coupling of the photon to the mesons, with e electron charge, Q_M the charge of the meson, k' the momentum of the outgoing meson and ϵ_μ the photon polarization vector,

$$b) - it_{B'B\gamma} = ie(Q_B \frac{\vec{p}+\vec{p}'}{2M_B} - i\frac{\vec{\sigma}\times\vec{q}}{2M_B}\mu_B)\vec{\epsilon} \tag{5.20}$$

for the coupling of the photon to the baryons, with Q_B the charge of the baryon, $\vec{p}$, $\vec{p}'$ the incoming, outgoing baryon momenta and M_B, μ_B the mass and magnetic moment of the baryon, and

$$c) - it_{B'M'BM\gamma} = iC_{ij}(Q_i + Q_j)\{\frac{\vec{p}+\vec{p}'}{2\bar{M}} - i\frac{\vec{\sigma}\times(\vec{p}-\vec{p}')}{2\bar{M}}\}\vec{\epsilon} \tag{5.21}$$

for the contact term of diagram (2.a) of Fig. 5.5, with C_{ij} the coefficients of eq. (3.57), i, j standing for a MB state, Q_i, Q_j the charges of the mesons, $\bar{M}$ an average mass of the baryons and $\vec{p}$, $\vec{p}'$ the momenta of the incoming, outgoing baryons.

In ref. [191] one is concerned with K^- with momenta below 500 MeV/c in the lab frame. In this energy domain it is easy to see that the Bremsstrahlung diagrams from mesons and baryons (diagrams (3.a), (4.a), (5.a), (6.a)) are of the same order of magnitude and that the contact term (diagram (2.a)) is of order $q/2M$ of the corresponding meson Bremsstrahlung diagrams ((3.a) and (5.a)). With CM photon momenta q of the order of 150 MeV or below, the terms of row 2 represent corrections below the 8% level and are neglected. In addition, terms like in diagram (2.d), where the photon couples to internal vertices of the loops, vanish for parity reasons.

The diagrams in row 7 of Fig. 5.5 where the photon couples to mesons in the loops vanish due to the gauge condition $\vec{\epsilon}\cdot\vec{q} = 0$ and the same happens to the diagrams in row 8, where the photon couples with the dielectric part to the baryons inside the loops ($(\vec{p}+\vec{p}')$ term of eq. (5.21)). The magnetic coupling of the photons in row 8 survives.

Hence, the process is given, within the approximations mentioned, by the diagrams in rows 3, 4, 5, 6 plus the magnetic part in row 8. This situation is opposite to the one found in ref. [190] for $\Lambda(1405)$ photoproduction close to threshold, where the dominant terms came from the contact term and the Bremsstrahlung diagrams were negligible.

If one inspects the series of terms in rows 3 and 4 of Fig. 5.5 one can see that the strong part of the interaction to the right of the electromagnetic vertex involves the series of terms of the Bethe-Salpeter equation and generates the T-matrix from the initial MB state to the final $M'B'$ state after losing the energy of the photon, this is, with an argument M_I, where M_I is the invariant mass of the $M'B'$ state. Similarly, in the rows (5) (6) the strong T-matrix factorizes before the electromagnetic vertex with an argument $\sqrt{s}$, with s the Mandelstam variable for the initial K^-p system. In the diagrams of row (8) we have a loop with one meson and two baryons. The strong interaction to the left originates $T(\sqrt{s})$ and the one to the right $T(M_I)$. The loop function of row (8) contains two baryon propagators and for the small energies involved here can be obtained by differentiating the $G(\sqrt{s})$ function of a meson-baryon loop, eq. (3.64), with respect to $\sqrt{s}$, which duplicates the baryon propagator.

By choosing an appropiate pair (ϵ_1, ϵ_2) of orthogonal photon polarization vectors, also orthogonal to $\vec{q}$, and summing over final photon and baryon polarizations plus averaging over the initial proton polarizations, one obtains the cross section for the process given by (σ the cross section for each i, j transition)

$$\frac{d\sigma}{dM_I d\varphi} = \frac{1}{2\pi}\frac{d\sigma}{dM_I} + \frac{d\sigma_I}{dM_I d\varphi}\cos\varphi\,, \tag{5.22}$$

with φ the azimutal angle formed by the plane containing the $\vec{k}'$ and $\vec{q}$ vectors and the one containing the $\vec{k}$ and $\vec{q}$ vectors. The only dependence on the azimutal angle φ comes in the $\cos\varphi$ dependence which accompanies the interference cross section, σ_I, in eq. (5.22), which means that both $d\sigma/dM_I$ and $d\sigma_I/dM_I d\varphi$ do not depend on the angle φ. Explicit expressions for $d\sigma/dM_I$ and $d\sigma_I/dM_I d\varphi$ are given in ref. [191].

The results for $d\sigma/dM_I$ are shown in Fig. 5.6. There one can see the results for the cross sections in the $K^-p \to \pi^-\Sigma^+\gamma, \pi^+\Sigma^-\gamma, \pi^0\Sigma^0\gamma, \pi^0\Lambda\gamma$, $K^-p\gamma$ channels. The cross section for $K^-p \to \bar{K}^0 n\gamma$ is very small, around 0.1 mb GeV^{-1} in the range $1.44 - 1.52$ GeV, and is not plotted in the figure. The $\Lambda(1405)$ peak appears clearly in the $\pi\Sigma$ spectrum. It is interesting to notice the difference between the cross sections for the different $\pi\Sigma$ channels. The origin of this is the same one discussed in ref. [190] and reported in the former section due to the different isospin combinations of the three charged states and the crossed products of the $I = 1$, $I = 0$ amplitudes which appear in the cross section. The $\pi^0\Sigma^0$ has no $I = 1$ component and since the $I = 2$ component is negligible, the $\pi^0\Sigma^0$ distribution is very similar to the $I = 0$ $\Lambda(1405)$ distribution. The $I = 0$ contribution alone, coming from the excitation of the $\Lambda(1405)$, can be obtained using a combination of the three $\pi\Sigma$ amplitudes

$$(t_{K^-p\to\pi^-\Sigma^+} + t_{K^-p\to\pi^+\Sigma^-} + t_{K^-p\to\pi^0\Sigma^0})/\sqrt{3}\ . \tag{5.23}$$

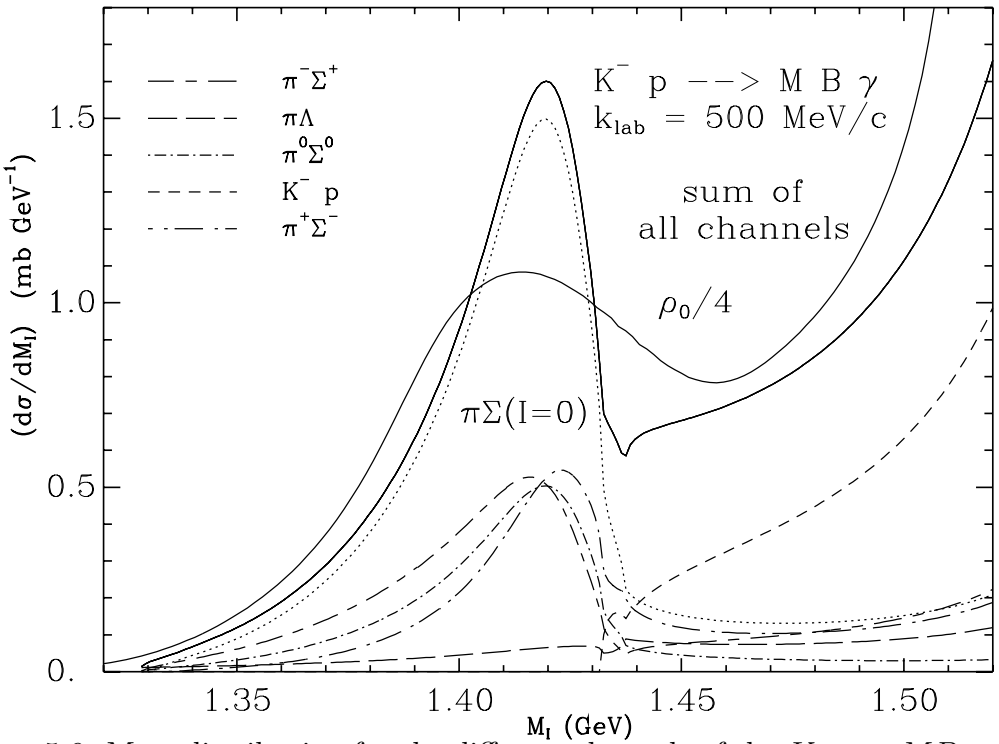

Figure 5.6: Mass distribution for the different channels of the $K^-p \to MB\gamma$ reaction. The solid line with the resonance shape is the sum of cross sections for all channels. Dotted line: pure $I = 0$ contribution from the $\Sigma\pi$ channels. The effects of the Fermi motion with $(\rho = \rho_0/4)$ is shown with solid line. The labels for the other lines are shown in the figure.

The results for the pure $I = 0$ excitation (dotted line) shown in Fig. 5.6 look very similar to the total strength around the $\Lambda(1405)$ peak. Below the K^-p threshold there is some strength for $I = 1$, $\pi^0\Lambda$ excitation, which is also very small. As a consequence of that, the sum of all channels in the $\Lambda(1405)$ region, which requires exclusively the detection of the photon, has approximately the $\Lambda(1405)$ shape and strength.

It is interesting to observe the fast rise of the cross section in the $K^-p \to K^-p\gamma$ channel, showing the Bremsstrahlung infrarred divergence at large M_I (small photon momentum).

The other channels also would show the infrarred divergence at higher energies, when the photon momentum goes to zero. The relative larger weight of the $K^- p \to K^- p\gamma$ reaction at these energies, with respect to the other ones, is a reflection of the fact that the $K^- p \to K^- p$ cross section at values of M_I or $\sqrt{s}$ of the order of 1500 MeV is much bigger than the other $K^- p \to M'B'$ cross sections.

There is a lower limit, which happens around 200 MeV/c for the K^- lab momentum, where the tails of the distribution, reflecting the Bremsstrahlung properties of the reaction, overlap with the peak of the resonance and hence the information on the $\Lambda(1405)$ is lost.

Let us now turn the attention to nuclei where we would consider the reaction $K^- A \to \Lambda(1405)\gamma(A-1)$. In this case if one detects only the photon one has a distribution of invariant masses due to Fermi motion since now $M_I^2 = (k + p_N - q)^2$ and p_N runs over all nucleon momenta of the occupied states. One can fold the results of $d\sigma/dM_I$ with the distribution of M_I coming from a Fermi sea of nucleons. The results in this case are shown in Fig. 5.6 for $\rho = \rho_0/4$, a likely effective density for this reaction, taking into account the distortion of the initial K^- through the nucleus. We can see a widening of the $\Lambda(1405)$ distribution, with the shape only moderately changed, such that other effects from genuine changes of the $\Lambda(1405)$ properties in the medium, predicted to be quite drastic [169–173], could in principle be visible. Certainly, the detailed measurement of the final meson-baryon in coincidence with the photon would allow a much better determination of the $\Lambda(1405)$ properties than just the photon detection, and ultimately these exclusive measurements should also be performed. But the fact that the simple detection of the photon can provide interesting information is a welcome feature from the experimental point of view.

The reactions discussed can be easily implemented at present facilities like KEK or Brookhaven. In Brookhaven some data from recent $K^- p$ experiment with detection of photons in the final state are in the process of analysis [192]. The present results should encourage the detailed analysis of the particular channels discussed here.

Chapter 6

Further nuclear applications

In *sections 5.2* and *5.3* we already discussed how the $\Lambda(1405)$ resonance could be generated in a nuclear environment and the additional information that this would bring on the nature of the resonance, plus the repercussions of these findings on the interaction of $\bar{K}$ with nuclei. In this chapter we will show some examples where the combination of the chiral unitary approach with the many body techniques proves to be a rather powerful tool to clarify issues which have remained so far controversial, particularly the problems of the $\pi\pi$ interaction in the nuclear medium and the interaction of K^- with nuclei.

6.1 The isoscalar $\pi\pi$ interaction in a nuclear medium

The $\pi\pi$ interaction in a nuclear medium in the $J = I = 0$ channel (σ channel) has stimulated much theoretical work lately. It was realized that the attractive P-wave interaction of the pions with the nucleus led to a shift of strength of the $\pi\pi$ system to low energies and eventually produced a bound state of the two pions around $2m_\pi - 10$ MeV [174]. This state would behave like a $\pi\pi$ Cooper pair in the medium, with repercussions in several observable magnitudes in nuclear reactions [174]. The possibility that such effects could have already been observed in some unexpected enhancement in the $(\pi, 2\pi)$ reaction in nuclei [193] was also noticed there. More recent experiments where the enhancement is seen in the $\pi^+\pi^-$ channel but not in the $\pi^+\pi^+$ channel [194] have added more attraction to that conjecture.

Yet, it was early realized that constraints of chiral symmetry in the amplitude at low energies might affect those conclusions [174]. In order to investigate the influence of chiral constraints in $\pi\pi$ scattering in the nuclear medium two different models [195,196] for the $\pi\pi$ interaction were used in ref. [197]. One of them [195] did not satisfy the chiral constraints, while another one [196] produced an amplitude behaving like m_π in the limit of small pion masses. The conclusion of ref. [197] was that, although in the chirally constrained model the building up of $\pi\pi$ strength at low energies was attenuated, it was still important within the approximations done in their calculations. Among these approximations there is the use of only Δh excitation with zero Δ width to build up the π nuclear interaction. Warnings were also given that results might depend on the off shell extrapolation of the $\pi\pi$ scattering matrix.

Further refinements were done in ref. [198], where the width of the Δ and coupling to $1p\,1h$ and $2p\,2h$ components were considered. The coupling of pions to the ph continuum led to a dramatic re-shaping of the $\pi\pi$ strength distribution, but the qualitative conclusions about the accumulated strength at low energies remained.

In ref. [175] the importance of the coupling to the ph components was reconfirmed and the use of more accurate models for the $\pi\pi$ interaction, as the Jülich model based on meson

exchange [199], did not change the conclusions on the enhanced $\pi\pi$ strength at low energies. However, the use of a linear and nonlinear models for the $\pi\pi$ interaction, satisfying the chiral constraints at small energies, led to quite different conclusions and showed practically no enhancement of the $\pi\pi$ strength at low energies. The same conclusions were reached using the Jülich model with a subtracted dispersion relation so as to satisfy the chiral constraints. The latter model employed the Blakenbecler-Sugar equation in which the 2π intermediate states were placed on shell. The conclusion of this paper was that the imposition of chiral constraints in the $\pi\pi$ amplitude prevented the pairing instabilities shown by the other models not satisfying those constraints.

In a further paper [200] the authors showed, however, that the imposition of the chiral constraints by themselves did not prevent the pairing instabilities and uncertainties remained related to the off shell extrapolation of the $\pi\pi$ amplitude and the possible ways to implement the minimal chiral constraints. The situation, as noted in ref. [200], is rather ambiguous, but the studies done have certainly put the finger in the questions that should be properly addressed: chiral symmetry, off shell extrapolations, unitarity, etc.

The chiral unitary methods discussed in *section 3* address automatically all these questions and seem most appropriate to tackle the problem discussed above. That task was undertaken in ref. [201] and we report here on their results. Since one is concerned about the S-wave $\pi\pi$ interaction, the Bethe-Salpeter approach is the most economical one to follow and this is what is done in ref. [201]. In the nuclear medium the pions will get renormalized and hence their propagators will differ from the free ones. In addition the point four meson vertices also get renormalized as we see below.

In order to illustrate the medium modifications in the $\pi\pi$ amplitude we show in Figs. 6.1, 6.2 and 6.3 the diagrams which are now involved at the level of just one loop. The pion is dressed by allowing it to excite ph and Δh components, as is usually done in pion nuclear physics [202].

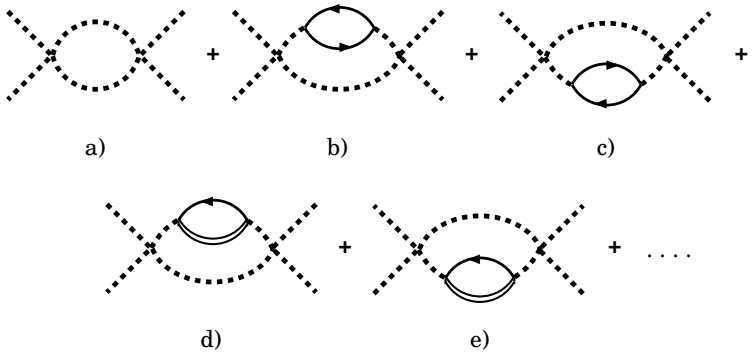

Figure 6.1: Terms appearing in the scattering matrix allowing the pions to excite ph and Δh components

The diagrams in Fig. 6.1 involve the usual ph and Δh excitation of the pion, which acquires a self-energy leading to a modification of the pion propagator, and the two pion loop function. In ref. [201] only the pions were renormalized but the kaons were also taken into account in the coupled channel Bethe-Salpeter equation. In Fig. 6.2 another sort of diagrams appears. These diagrams, which qualify as vertex corrections of the four meson vertex, come from the Lagrangian of Eq. (2.35), and involve a baryon line and three mesons. The need to consider this contact three meson term in connection with diagrams involving a pion pole, like one has in Fig. 6.1, was already known prior to the developments of χPT [203] and has been systematically used in studies of the $\pi N \to \pi\pi N$ reaction in refs. [204–208]. The advent of χPT has made it easier to extend these ideas to the strangeness sector [209] where the effective Lagrangians were not available. The

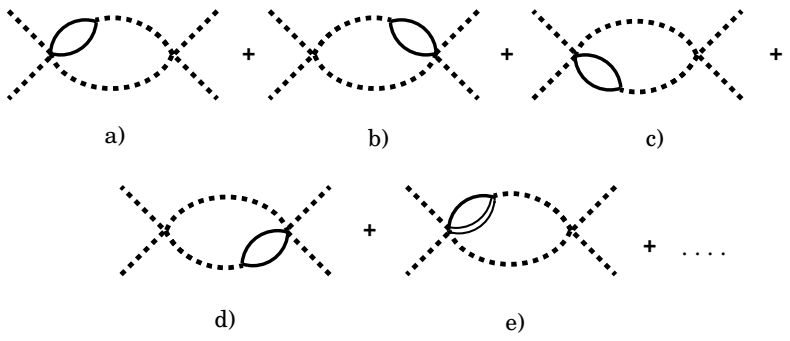

Figure 6.2: Terms of the $\pi\pi$ scattering series in the nuclear medium related to three meson baryon contact terms from the Lagrangian of eq. (2.7)

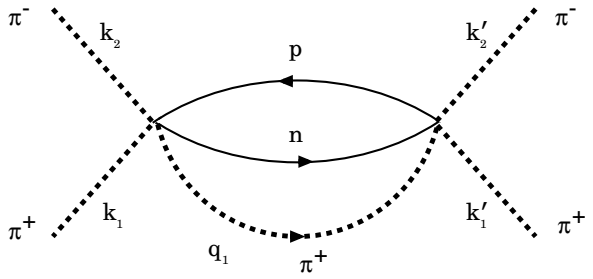

Figure 6.3: Diagram involving the three meson baryon contact terms of fig. 6.2 in each of the vertices

presence of the three meson contact term leads also to the term in Fig. 6.3 in a natural way. The interesting feature of these diagrams is that when one separates the four pion vertex appearing in Figs. 6.1, 6.2 into an on shell and an off shell part, as done in *section 3.3.1*, eq. (3.54), there is an exact cancellation between the off shell parts and the three meson contact terms of Figs. 6.2, 6.3, such that at the end only diagrams of the type of Fig. 6.1 must be evaluated and with all the four pion vertices evaluated on shell (i.e. taking p^2=m^2 for all the meson lines in the expression of the amplitude). This subtle cancellation, which also makes the work simpler technically, was first observed in ref. [210] when checking that the results cannot depend on the arbitrary coefficient that one has in chiral theories at the level of three pion fields in the expansion of the U function defined after eq. (2.5).

The interplay found here for the pion pole term and the three meson contact term has been investigated in other nuclear problems before, where also interesting cancellations were found. In ref. [209] it was shown that the real part of the kaon self-energy in the nuclear medium tied to the scattering of the kaons with the virtual pion nuclear cloud was zero, because of exact cancellations between the four meson terms and the contact three meson baryon terms. This solved a puzzle at the time where large uncertainties were tied to the off shell part of the $K\pi$ amplitude [163, 211]. The phenomenology also demanded that this real part be close to zero [211]. Similarly, in ref. [212] the pion self-energy tied to the interaction of the pions with the virtual pion cloud was found to be very small, with partial cancellations which became complete in the chiral limit.

The results obtained for the imaginary part of the $\pi\pi$ amplitude are shown in Fig. 6.4

for different values of the Fermi momentum. One can observe a depletion of the strength in the region of 600-900 MeV, but more interesting, in connection with the experiments reporting an enhancement of the invariant mass of the two pions close to threshold, is the strength found in the figure in that region.

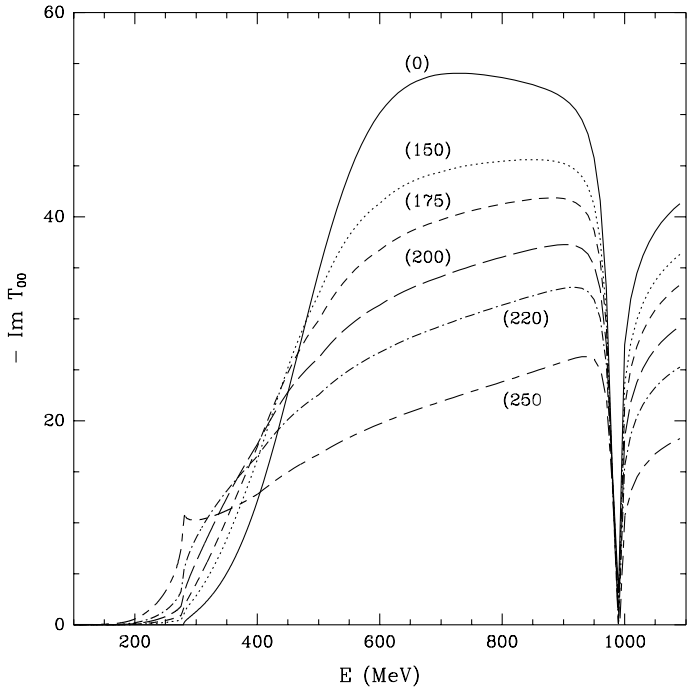

Figure 6.4: Im T_{22} for $\pi\pi \to \pi\pi$ scattering in $J = I = 0$ (T_{00} in the figure) in the nuclear medium for different values of k_F versus the CM energy of the pion pair. The labels correspond to the values of k_F in MeV.

The results shown in Fig. 6.4 are very similar to those of ref. [175] where minimal chiral constraints were imposed in their models which eliminated the peaks below threshold found in earlier works.

The situation is nevertheless still puzzling. Indeed, by using a model of ref. [200] for the $\pi\pi$ interaction in the medium and a model for the $(\pi, \pi\pi)$ reaction from ref. [205], a spectrum of invariant masses similar to the experimental one could be reproduced in ref. [213]. A more detailed work was carried in ref. [214] improving on the approximations done in ref. [213] and it was found that the enhancement of the invariant mass found was narrowly tied to the approximations done, and when more accurate calculations were done there was no much sign of an enhanced invariant mass in the two pion mass distribution. One of the reasons for the apparent lack of enhancement is that there are large cancellations of pieces of the amplitude for the case of $\pi^+\pi^-$ production which is not the case for $\pi^+\pi^+$ production. This latter process exhibits a peak at low invariant masses mostly due to phase space reasons. Should there be a renormalization of some terms in the nucleus which would alter the cancellation found in free space, then the results would look more like those of the $\pi^+\pi^+$ production and the experimental observation could be understood. Further work is necessary to understand better the process before we can see in this reaction a precursor of the chiral symmetry restoration, which is one of the appealing possibilities suggested so far [215].

6.2 The K^- nucleus interaction

The properties of the kaons and antikaons in the nuclear medium have been the object of numerous investigations since the possibility of the existence of a kaon condensed phase in dense nuclear matter was pointed out [216]. If the K^- meson develops sufficient attraction in dense matter it could be energetically more favorable, after a certain critical density, to neutralize the positive charge with antikaons rather than with electrons. A condensed kaon phase would then start to develop, changing drastically the properties of dense neutron star matter [217–223]. In fact, the enhancement of the K^- yield in Ni+Ni collisions measured recently by the KaoS collaboration at GSI [224] can be explained by assuming the K^- meson to feel a strong attraction in the medium [225–228], although alternative mechanisms, such as the production of antikaons via Σ hyperons, have also been suggested [229]. Kaonic atom data, a compilation of which is given in ref. [165], also favor an attractive K^- nucleus interaction.

The theoretical investigations that go beyond pure phenomenology [230] have mainly followed two different strategies. One line of approach is that of the mean field models, built within the framework of chiral Lagrangians [228, 231–233], based on the relativistic Walecka model extended to incorporate strangeness in the form of hyperons or kaons [234] or using explicitly quark degrees of freedom [235]. The other type of approach aims at obtaining the in-medium $\bar{K}N$ interaction microscopically by incorporating the medium modifications in a $\bar{K}N$ amplitude that reproduces the low energy scattering data and generates the $\Lambda(1405)$ resonance dynamically [167–173]. For instance, Pauli blocking on the intermediate nucleon states of the Lippmann-Schwinger or, alternatively, the Bethe-Salpeter equation makes the $\bar{K}N$ interaction density dependent and this, in turn, modifies the K^- properties from those in free space. These medium modifications were already included long time ago [167] in the context of Brueckner-type many body theory using a separable $\bar{K}N$ interaction to obtain the kaon-nucleus optical potential for kaonic atoms. The more recent theoretical works [169–173] take the $\bar{K}N$ interaction from the chiral Lagrangian. The blocking of intermediate states shifts the resonance to higher energy and this changes the $\bar{K}N$ interaction at threshold from being repulsive in free space to being attractive in the medium. A recent self-consistent calculation of the K^- self-energy [172] has shown that the position of the resonance remains unchanged, due to a compensation of the repulsive Pauli blocking effects with the attraction felt by the K^- meson, in qualitatively agreement with was was noted in ref. [168] using a constant mean field potential for the $\bar{K}$.

Additional medium effects have been considered in a recent work [173], including the self-energy of the pions in the $\pi\Lambda$, $\pi\Sigma$ intermediate states, which couple strongly to the $\bar{K}N$ state, as well as the dressing of the baryons (N, Λ, Σ) through density-dependent mean-field binding potentials. The starting point is the chiral model of ref. [79], described in *section 3.3.2*, which reproduces the $\bar{K}N$ low energy scattering observables. The medium effects on the $\bar{K}N$ interaction are incorporated replacing the free meson and baryon propagators in the meson-baryon loop of Eq. (3.64) by in-medium ones. For the nucleon, a mean-field propagator

$$A(\sqrt{s} - q^0, -\vec{q}, \rho) = \frac{1 - n(\vec{q}_{\rm lab})}{\sqrt{s} - q^0 - E_l(-\vec{q}) + i\epsilon} + \frac{n(\vec{q}_{\rm lab})}{\sqrt{s} - q^0 - E_l(-\vec{q}) - i\epsilon} \qquad (6.1)$$

is taken, where $n(\vec{q}_{\rm lab})$ is the occupation probability of a nucleon of momentum $\vec{q}_{\rm lab}$ in the lab frame. For the hyperons (Λ and Σ), the occupation probability is simply zero. The single particle energy, $E_l(-\vec{q})$, now contains a mean-field potential of the type $U_0\rho/\rho_0$, with $\rho_0 = 0.17$ fm^{-3} being the normal nuclear matter density. For the nucleon, a reasonable depth value is $U_0^N = -70$ MeV, as suggested by numerous calculations of the nucleon

potential in nuclear matter. For the Λ hyperon, it is reasonable to take $U_0^\Lambda = -30$ MeV, as implied by the extrapolation to very heavy systems of the experimental Λ single particle energies in Λ hypernuclei [236]. For the Σ hyperon, there is no conclusive information on the potential. Early phenomenological analyses [237] and calculations [238] found the Σ atom data to be compatible with $U_0^\Sigma \sim -30$ MeV, but more recent analysis do not exclude a repulsive potential in the nuclear interior [239]. In the work of ref. [173] the potential used is $U^\Sigma = -30\rho/\rho_0$ MeV, as commonly accepted for low densities, but the effects of using a repulsive depth of 30 MeV are also explored. The meson propagator for the $\bar{K}$ and π mesons is replaced by the dressed one

$$D_l(q^0,\vec{q},\rho) = \frac{1}{(q^0)^2 - \vec{q}^{\,2} - m_l^2 - \Pi_l(q^0,\vec{q},\rho)} = \int_0^\infty d\omega\, 2\omega\, \frac{S_l(\omega,\vec{q},\rho)}{(q^0)^2 - \omega^2 + i\epsilon}\ , \tag{6.2}$$

where $\Pi_l(q^0,\vec{q},\rho)$ is the meson self-energy. The second equality in Eq. (6.2) is the Lehmann representation of the meson propagator and $S_l(\omega,\vec{q},\rho) = -\mathrm{Im}D_l(\omega,\vec{q},\rho)/\pi$ is the meson spectral density which, in the case on undressed mesons, reduces to $\delta(\omega-\omega_l(\vec{q}))/2\omega_l(\vec{q})$. With these modifications the loop integral becomes

$$\begin{aligned} G_l(P^0,\vec{P},\rho) &= \int_{|\vec{q}|<q_{\max}} \frac{d^3q}{(2\pi)^3}\frac{M_l}{E_l(-\vec{q})}\int_0^\infty d\omega\, S_l(\omega,\vec{q},\rho) \\ &\times \left\{\frac{1-n(\vec{q}_{\rm lab})}{\sqrt{s}-\omega-E_l(-\vec{q})+i\epsilon} + \frac{n(\vec{q}_{\rm lab})}{\sqrt{s}+\omega-E_l(-\vec{q})-i\epsilon}\right\}\ , \end{aligned} \tag{6.3}$$

where $(P^0,\vec{P})$ is the total four-momentum in the lab frame and $s = (P^0)^2 - \vec{P}^2$.

The in-medium $\bar{K}N$ interaction, $T_{\rm eff}(P^0,\vec{P},\rho)$, is then obtained by solving the coupled-channel Bethe-Salpeter equation using the dressed meson-baryon loop of Eq. (6.3). The S-wave $\bar{K}$ self-energy ($\bar{K} = K^-$ or $\bar{K}^0$) is determined by summing the in-medium $\bar{K}N$ interaction over the nucleons in the Fermi sea

$$\Pi_{\bar{K}}^s(q^0,\vec{q},\rho) = 2\sum_{N=n,p}\int \frac{d^3p}{(2\pi)^3} n(\vec{p})\, T_{\rm eff}^{\bar{K}N}(q^0+E(\vec{p}),\vec{q}+\vec{p},\rho)\ . \tag{6.4}$$

Note that a self-consistent approach is required since one calculates the $\bar{K}$ self-energy from the effective interaction $T_{\rm eff}$ which uses $\bar{K}$ propagators which themselves include the self-energy being calculated. A P-wave contribution to the $\bar{K}$ self-energy coming from the coupling of the $\bar{K}$ meson to hyperon-hole excitations is also included and the expression can be found in ref. [173].

The pion self-energy is built from a model that contains the effect of one- and two-nucleon absorption and is conveniently modified to include the effect of nuclear short-range correlations (see ref. [240] for details). To assess the importance of dressing the pions we show in Fig. 6.5 the spectral density of the π meson in nuclear matter at density $\rho = \rho_0$ for several momenta. The strength is distributed over a wide range of energies and, as the pion momentum increases, the position of the peak is increasingly lowered from the corresponding one in free space as a consequence of the attractive pion-nuclear potential. Note that, to the left of the peaks, there appears the typical structure of the $1p1h$ excitations which give rise to $1p1h\Lambda$ and $1p1h\Sigma$ components in the effective $\bar{K}N$ interacion.

The spectral function of a K^- meson of zero momentum is shown in Fig. 6.6 for various densities: ρ_0, $\rho_0/2$ and $\rho_0/4$. The results in the upper panel include only Pauli blocking effects, i.e. the nucleons propagate as in Eq. (6.1) but the mesons behave as in free space. At $\rho_0/4$ one clearly sees two excitation modes. The left one corresponds to the K^- pole branch, appearing at an energy smaller than the kaon mass, m_K, due

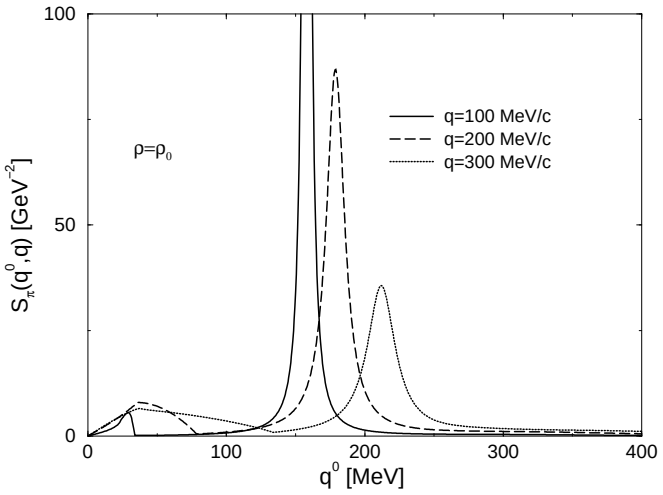

Figure 6.5: Pion spectral density at $\rho = \rho_0$ for several momenta

to the attractive medium effects. The peak on the right corresponds to the $\Lambda(1405)$-hole excitation mode, located above m_K because of the shifting of the $\Lambda(1405)$ resonance to energies above the $K^- p$ threshold. As density increases, the K^- feels an enhanced attraction while the $\Lambda(1405)$-hole peak moves to higher energies and loses strength, a reflection of the tendency of the $\Lambda(1405)$ to dissolve in the dense nuclear medium. These features were already observed in ref. [171]. The (self-consistent) incorporation of the $\bar{K}$ propagator in the Bethe-Salpeter equation softens the effective interaction, $T_{\rm eff}$, which becomes more spread out in energies. The resulting K^- spectral function (middle panel in Fig. 6.6) shows the displacement of the resonance to lower energies because, as noted by Lutz [172], the attraction felt by the $\bar{K}$ meson lowers the threshold for the $\bar{K}N$ states that had been increased by the Pauli blocking on the nucleons. This has a compensatory effect and the resonance moves backwards, slightly below its free space value. The K^- pole peak appears at similar or slightly smaller energies, but its width is larger, due to the strength of the intermediate $\bar{K}N$ states being distributed over a wider region of energies. Therefore the K^- pole and the $\Lambda(1405)$-hole branches merge into one another and can hardly be distinguished. Finally, when the pion is dressed according to the spectral function shown in Fig. 6.5 the effective interaction $T_{\rm eff}$ becomes even smoother. The resulting K^- spectral function is shown in the bottom panel in Fig. 6.6. As seen by the long-dashed line, even at very small densities one no longer distinguishes the $\Lambda(1405)$-hole peak from the K^- pole one. As density increases the attraction felt by the K^- is more moderate and the K^- pole peak appears at higher energies than in the other two approaches. However, more strength is found at very low energies, especially at ρ_0, due to the coupling of the K^- to the $1p1h$ and $2p2h$ components of the pionic strength. It is precisely the opening of the $\pi\Sigma$ channel, on top of the already opened $(1p1h)\Sigma$ and $(2p2h)\Sigma$ ones, the reason for the cusp structure which appears slightly above 400 MeV.

The isospin averaged in-medium scattering length, defined as

$$a_{\rm eff}(\rho) = -\frac{1}{4\pi}\frac{M}{m_K + M}\frac{\Pi_{\bar{K}}(m_K, \vec{q} = 0, \rho)}{\rho} \ , \tag{6.5}$$

is shown in Fig. 6.7 as a function of the nuclear density ρ. The change of $\mathrm{Re}\, a_{\rm eff}$ from negative to positive values indicates the transition from a repulsive interaction in free space to an attractive one in the medium. As shown by the dotted line, this transition happens at a density of about $\rho \sim 0.1\rho_0$ when only Pauli effects are considered, in agreement with what was found in ref. [170]. However, this transition occurs at even lower densities ($\rho \sim 0.04\rho_0$)

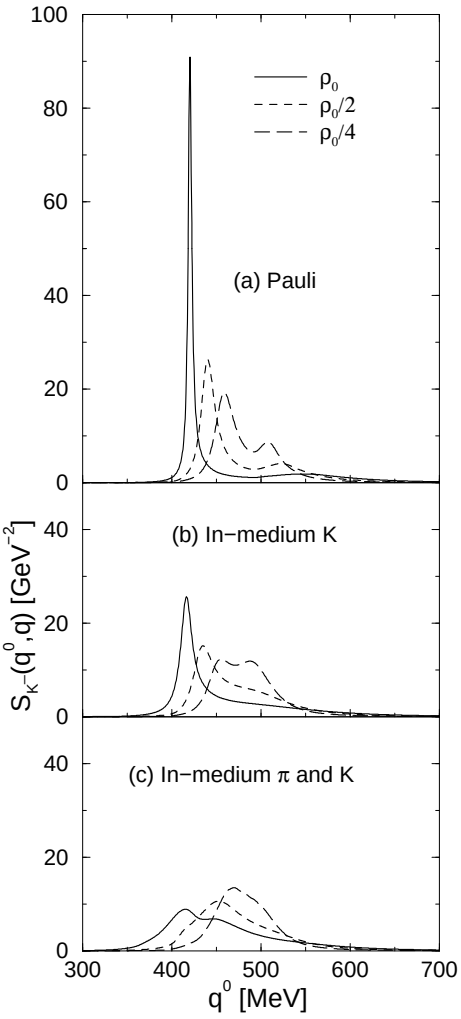

Figure 6.6: K^- spectral density for zero momentum

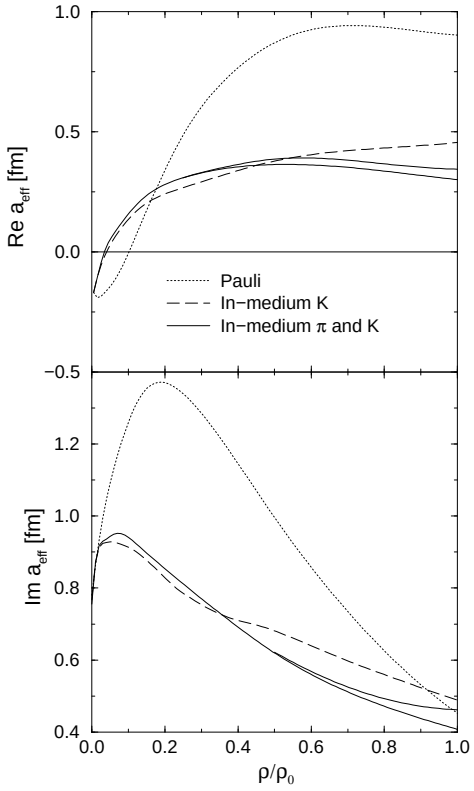

Figure 6.7: K^-N scattering length as a function of density

when one considers the self-energy of the mesons in the description, whether one dresses only the $\bar{K}$ meson (dashed line) or both the $\bar{K}$ and π mesons (solid line). The deviations from the approach including only Pauli blocking or those dressing the mesons are quite appreciable over a wide range of densities. The thin solid lines show the results obtained with a repulsive Σ potential of the type $U^\Sigma = U_0^\Sigma \rho/\rho_0$, with $U_0^\Sigma = 30$ MeV. The deviations from the thick solid line, obtained for an attractive potential depth of $U_0^\Sigma = -30$ MeV, are smaller than 10% and only show up at the higher densities.

The implications on kaonic atoms of the scattering length displayed in Fig. 6.7 or, equivalently, the K^- optical potential, $V_{\rm opt}(\rho) = \Pi_{\bar{K}}(m_K, \vec{q} = 0, \rho)/2m_K$, have been analyzed in the framework of a local density approximation, where the nuclear matter density ρ is replaced by the density profile $\rho(r)$ of the particular nucleus [241]. As can be seen from Fig. 6.8, both the energy shifts and widths of kaonic atom states agree well with the bulk of experimental data.

The model reported here gives a K^- nuclear potential depth of -44 MeV at $\rho = \rho_0$. This is about half the attraction of that obtained with other recent theories and approximation schemes [170, 171, 228, 233–235], which give rise to potential depths at the center of the nucleus in between -140 and -75 MeV, and also lies very far from the depth of around -200 MeV obtained from a best fit to K^- atomic data with a phenomenological potential that includes an additional non-linear density dependent term [165]. On the other hand,

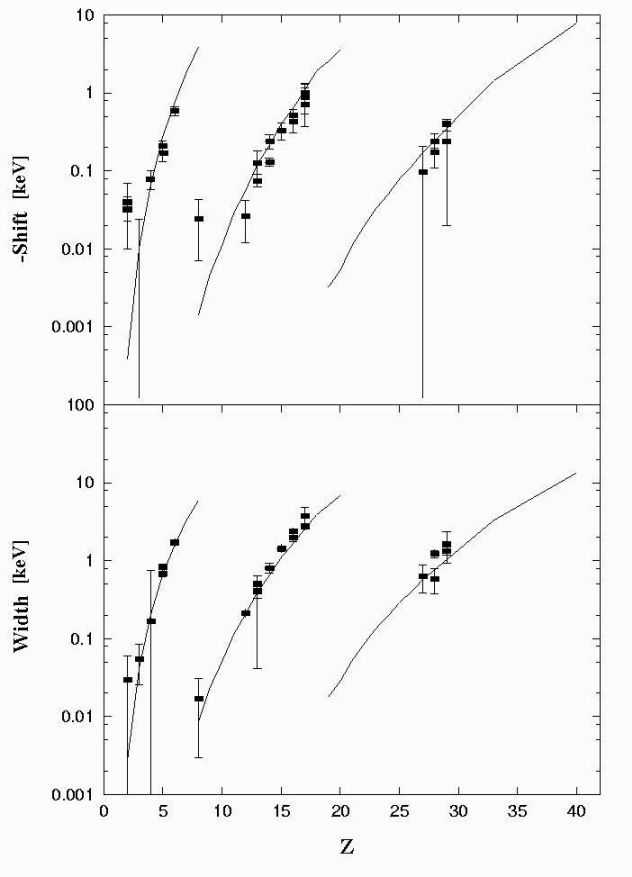

Figure 6.8: Energy shifts and widths of kaonic atom states as predicted by the model of ref. [241]. The experimental data are taken from the compilation given in ref. [166].

the early Brueckner-type calculations of ref. [167] also obtained a shallow K^--nucleus potential, of the order of -40 MeV at the center of ^{12}C, and predicted reasonably well the K^- atomic data available at that time and recent self-consistent calculations [229] find a moderate attraction of -32 MeV. Acceptable fits to kaonic atom data have also been obtained using charge densities and a phenomenological $T_{\rm eff}\rho$ type potential with a depth of the order of -50 MeV in the nuclear interior [242]. But, when matter densities are used instead, the fit gives a potential depth of -80 MeV [165]. A comparison of kaonic atom results obtained with various K^--nucleus potentials can be found in ref. [243]. A hybrid model, combining a relativistic mean field approach in the nuclear interior and a phenomenological density dependent potential at the surface that is fitted to K^- atomic data, also favors a strongly attractive K^- potential of depth -180 MeV [244].

In summary, although all models predict attraction for the K^--nucleus potential, there are still large discrepancies for the precise value of its depth, which has important implications for the occurrence of kaon condensation. It is then necessary to gather more data that could help in disentangling the properties of the $\bar{K}$ in the medium. Apart from the valuable information that can be extracted from the production of K^- in heavy-ion collisions, one could also measure deeply bound kaonic states, which have been predicted to be narrow [241,243,245] and could be measured in (K^-,γ) [241] or (K^-,p) reactions [246,247].

Chapter 7

Conclusions

After a short review of the basic concepts of chiral symmetry and of several chiral Lagrangians we have discussed various nonperturbative methods to deal with the meson-meson and meson-baryon interactions which allow one to extend the region of applicability of the theory to higher energies than in χPT, where the low lying mesonic and baryonic resonances appear. The common ground of all these methods was the exact implementation of unitarity in coupled channels. The constraints imposed by unitarity allow one to extract information contained in the chiral Lagrangians which is not accessible with the standard χPT expansion.

One of the procedures followed was the Inverse Amplitude Method, which relies upon the expansion of the inverse of the scattering matrix and gives rise to an expansion in powers of p^2 with a larger convergence radius than χPT. In that method one could extend the predictions for meson-meson interactions up to about 1.2 GeV, and all mesonic resonances up to this energy were well reproduced, as well as phase shifts and inelasticities.

A second method relied upon the use of the N/D method and the hypothesis of resonance saturation. In this case, the use of the information contained in the lowest order chiral Lagrangian, together with chiral loops and the explicit exchange of some resonances, which are genuine QCD states in the sense that they would remain in the large N_c limit, allow also a good description of the meson-meson data up to about 1.5 GeV. This second method is particularly rewarding for it allows one to dig into the nature of the mesonic resonances and separate those which are preexisting QCD resonances, in the limit of large N_c, from others which qualify as dynamical meson-meson resonances coming from the multiple scattering of the mesons. In this way, it was stablished that the low lying scalar resonances, the σ, κ, $a_0(980)$ and to large extent the $f_0(980)$, are generated dynamically from multiple scattering from the lowest order chiral Lagrangian. On the contrary, a singlet contribution to the $f_0(980)$ and a scalar octet around 1.35 GeV would be the lightest preexisting scalar states. This latter method also allows one to understand why in the case of the scalar sector a succesful reproduction of the data can be obtained simply by means of the lowest order chiral Lagrangian and the Bethe-Salpeter equation, together with a suitable cut off, or regularizing scale.

In the meson-baryon problem, applications were only done in the scalar sector taking advantage of the simplification of the Bethe-Salpeter equation, which was found to be a suitable approach much as in the case of the meson-meson scalar sector. In this case, low lying resonances like the $\Lambda(1405)$ or the $N(1535)$ were generated within that approach, and a good reproduction of the low energy scattering data was found, particularly in the case of the K^-N interaction and coupled channels.

Applications to problems of initial and final state interaction have also been shown. Since the energy region of applicability of the reported methods is much larger than the one of χPT, one could tackle many new problems formerly inaccessible with plain χPT

theory.

We have also shown how these chiral approaches to the meson-baryon and meson-meson interactions have repercussions in nuclear physics and provide a new perspective into problems which have been rather controversial up to now, like the $\pi\pi$ scattering in a nuclear medium or the K^- nucleus interaction. Several reactions which can bring new light into these problems have also been reviewed and the implementation of the experiments is already planned in some laboratories.

The methods exposed here open new possibilities to face a large number of problems, of which we have only given a few examples. Extension of the methods to higher energies by incorporating channels with more than two particles and application to other physical domains remain as challenges for the future.

Acknowledgements

This work has been partially supported by CICYT contracts PB95-1249, PB96-0753 (Spain) and by the Eurodaphne project, EEC-TMR contract FMRX-CT98-0169.

We would like to thank our colleagues H.C. Chiang, F. Guerrero, S. Hirenzaki, A. Hosaka, T.S.H. Lee, E. Marco, Ulf-G. Meissner, J.C. Nacher, M. Oka, Y. Okumura, A. Parreño, J.R. Peláez, A. Pich, H. Toki and M.J. Vicente Vacas for many stimulating discussions and for their collaboration in some of the works reported here.

Bibliography

[1] A. Pich, Rep. Prog. Phys. 58 (1995) 563.

[2] U. G. Meissner, Rep. Prog. Phys. 56 (1993) 903; V. Bernard, N. Kaiser and U. G. Meissner, Int. J. Mod. Phys. E4 (1995) 193.

[3] G. Ecker, Prog. Part. Nucl. Phys. 35 (1995) 1.

[4] J. Goldstone, Nuovo Cimento 19 (1961) 154.

[5] J. Gasser and H. Leutwyler, Ann. Phys. NY 158 (1984) 142; J. Gasser and H. Leutwyler, Nucl. Phys. B250 (1985) 465, 517, 539.

[6] M. Gell-Mann, Phys. Rev. 125 (1962) 1067.

[7] S. Okubo, Prog. Theor. Phys. 27 (1962) 949.

[8] J. Wess and B. Zumino, Phys. Rev. 163 (1967) 1727; J. Wess and B. Zumino, Phys. Lett. B37 (1971) 95.

[9] E. Witten, Ann. Phys. NY 128 (1980) 363; E. Witten, Nucl. Phys. B223 (1983) 422.

[10] A. Manohar and H. Georgi, Nucl. Phys. B234 (1984) 189.

[11] G. Ecker, J. Gasser, A. Pich and E. de Rafael, Nucl. Phys. B321 (1989) 311.

[12] M. L. Goldberger and S. B. Treiman, Phys. Rev. 110 (1958) 1178.

[13] N. M. Kroll and M. A. Ruderman, Phys. Rev. 93 (1954) 233.

[14] S. Weinberg, Physica A 96 (1979) 327.

[15] T. Applequist and C. Bernard, Phys. Rev. D22 (1980) 200; A. C. Longhitano, Nucl. Phys. B188 (1981) 118.

[16] H. Leutwyler, Phys. Rev. D49 (1994) 3033; H. Leutwyler, Helv. Phys. Acta 70 (1997) 275; S. C. Zhang, Science 275 (1997) 1089; C. P. Burgess and A. Lutken, Phys. Rev. B57 (1998) 8642.

[17] J. V. Steele, H. Yamagishi and I. Zahed, Nucl. Phys. A615 (1997) 305; M. R. Pennington and J. Portolés, Phys. Lett. B344 (1995) 399.

[18] A. C. Longhitano, Nucl. Phys. B188 (1981) 118; Phys. Rev. D22 (1980) 1166.

[19] T. N. Truong, Phys. Rev. Lett. 61 (1988) 2526; Phys. Rev. Lett. 67 (1991) 2260; A. Dobado, M. J. Herrero and T. N. Truong, Phys. Lett. B235 (1990) 134; A. Dobado and J. R. Peláez, Phys. Rev. D47 (1993) 4883; Phys. Rev. D56 (1997) 3057.

[20] A. Dobado, M. J. Herrero and T. N. Truong, Phys. Lett. B235 (1990) 129; A. Dobado, M. J. Herrero and J. Terrón, Z. Phys. C50 (1991) 205; Z. Phys. C50 (1991) 465; J. R. Peláez, Phys. Rev. D55 (1997) 4193.

[21] J. Weinstein and N. Isgur, Phys. Rev. Lett. 48 (1982) 659; J. Weinstein and N. Isgur, Phys. Rev. D27 (1983) 588; Phys. Rev. D41 (1990) 2236.

[22] G. Jansen, B. C. Pearce, K. Holinde and J. Speth, Phys. Rev. D52 (1995) 2690.

[23] J. A. Oller and E. Oset, Nucl. Phys. A620 (1997) 438; *erratum* Nucl. Phys. A652 (1999) 407.

[24] N. A. Tornqvist, Phys. Rev. Lett. 49 (1982) 624; M. Roos and N. A. Tornqvist, Phys. Rev. Lett. 76 (1996) 1575.

[25] J. A. Oller and E. Oset, Phys. Rev. D60 (1999) 074023.

[26] J. A. Oller, E. Oset and J. R. Peláez, Phys. Rev. Lett. 80 (1998) 3452.

[27] A. D. Martin and T. D. Spearman, Elementary Particle Theory, John Willey, 1970, p 187.

[28] F. Guerrero and J. A. Oller, Nucl. Phys. B537 (1999) 459.

[29] V. Bernard, N. Kaiser and U. G. Meissner, Nucl. Phys. B357 (1991) 129.

[30] R. Kaminski, L. Lesniak and K. Rybicki, Z. Phys. C74 (1997) 79.

[31] B. Hyams et al., Nucl. Phys. B64 (1973) 134.

[32] P. Estabrooks et al., AIP Conf. Proc. 13 (1973) 37.

[33] G. Grayer et al., Proc. 3rd Philadelphia Conf. on Experimental Meson Spectroscopy, Philadelphia, 1972 (AIP, NY, 1972), p 5.

[34] S. D. Protopopescu and M. Alson-Granjost, Phys. Rev. D7 (1973) 1279.

[35] C. D. Frogatt and J. L. Petersen, Nucl. Phys. B129 (1977) 113.

[36] D. Cohen et al., Phys. Rev. D22 (1980) 2595.

[37] A. D. Martin and E. N. Ozmuth, Nucl. Phys. B158 (1979) 520.

[38] W. Ochs, University of Munich thesis, 1974.

[39] L. Rosselet et al., Phys. Rev. D15 (1977) 574.

[40] A. Schenk, Nucl. Phys. B363 (1991) 97.

[41] J. A. Oller, E. Oset and J. R. Peláez, Phys. Rev. D59 (1999) 74001; *erratum* Phys. Rev. D60 (1999) 099906.

[42] N. Kaiser, Eur. Phys. J. A3 (1998) 307.

[43] G. Grayer et al., in Experimental Meson Spectroscopy, edited by A. H. Rosenfeld and K. W. Lai, AIP Conf. Proc. 8 (AIP, New York, 1972) p 117.

[44] G. Grayer et al., Paper No.768 Contributed to the 16th Int. Conf. on High Energy Physics, Batavia, 1972.

[45] G. Grayer et al., Nucl. Phys. B75 (1974) 189.

[46] W. Manner, Contribution to the 4th Int. Conf. on Experimental Meson Spectroscopy, Boston, Massachusetts, USA, April 1974 and CERN preprint.

[47] S. J. Lindenbaum and R. S. Longacre, Phys. Lett. B274 (1992) 492.

[48] P. Estabrooks et al., Nucl. Phys. B133 (1978) 490.

[49] D. Linglin et al., Nucl. Phys. B57 (1973) 64.

[50] Amsterdam, CERN, Nijmegen-Oxford Collaboration, J. B. Gay et al., Phys. Lett. B63 (1976) 220.

[51] R. Mercer et al., Nucl. Phys. B32 (1971) 381.

[52] H. H. Bingham et al., Nucl. Phys. B41 (1972) 1.

[53] S. L. Baker et al., Nucl. Phys. B99 (1975) 211.

[54] D. Aston et al., Nucl. Phys. B296 (1988) 493.

[55] J. A. Oller, E. Oset, J. R. Peláez, *The $\phi \to \pi^+\pi^-$ within a chiral unitary approach*, submitted to Phys. Rev. D, hep-ph/9911297.

[56] V. Bernard, N. Kaiser and U. G. Meissner, Nucl. Phys. B364 (1991) 283.

[57] F. Guerrero and A. Pich, Phys. Lett. B412 (1997) 382.

[58] M. F. L. Golterman and S. Peris, hep-ph/9908252.

[59] For general reviews about the issue: L. Montanet, Rep. Prog. Phys. 46 (1983) 337; F.E. Close, Rep. Prog. Phys. 51 (1988) 833; M. R. Pennington, Nucl. Phys. B21 (Proc. Suppl.) (1991) 37.

[60] D. Morgan, Phys. Lett. B51 (1974) 71.

[61] R. L. Jaffe, Phys. Rev. D15 (1977) 267; R. L. Jaffe, Phys. Rev. D15 (1977) 281.

[62] N. N. Achasov, S. A. Debyanin and G. N. Shestakov, Z. Phys. C22 (1984) 53; N. N. Achasov, S. A. Devyanin and G. N. Shestakov, Phys. Lett. B96 (1980) 168; N. N. Achasov, S. A. Devyanin and G. N. Shestakov, Phys. Scripta 27 (1983) 330.

[63] R. L. Jaffe, Phys. Lett. 41 (1975) 267; D. Robson, Nucl. Phys. B130 (1977) 328.

[64] T. Barnes, in Proceedings of the Fourth Workshop on Polarized Targets Materials and Techniques, Bad Honned, Germany, 1984, edited by W. Meyer (Bonn Univeristy, Bonn, 1984); J.F. Donoghue, in Hadron Spectroscopy-1985, Proceedings of the International Conference, College Park, Maryland, edited by S. Oneda, AIP Conf. Proc. No. 132 (AIP, New York, 1985), p 460; also, Close [59].

[65] G. F. Chew and S. Mandelstam, Phys. Rev. 119 (1960) 467.

[66] J. Nieves and E. Ruiz Arriola, Phys. Lett. B455 (1999) 30; hep-ph/9907469.

[67] L. Castillejo, R. H. Dalitz and F. J. Dyson, Phys. Rev. 101 (1956) 453.

[68] G. 't Hooft, Nucl. Phys. B72 (1974) 461; E. Witten, Nucl. Phys. B160 (1979) 57.

[69] J. D. Bjorken, Phys. Rev. Lett. 4 (1960) 473.

[70] M. Jamin, J. A. Oller and A. Pich, forthcoming.

[71] J. A. Oller, Phys. Lett. B, in print. hep-ph/9908493.

[72] K. Kawarabayashi and M. Suzuki, Phys. Rev. Lett. 16 (1996) 255; Rizuddin and Fayyazuddin, Phys. Rev. 147 (1966) 1071.

[73] C. Caso et al., The European Physical Journal C3 (1998) 1.

[74] G. Ecker, J. Gasser, H. Leutwyler, A. Pich and E. de Rafael, Phys. Lett. B223 (1989) 425.

[75] A. Etkin et al., Phys. Rev. D28 (1982) 1786.

[76] W. Wetzel et al., Nucl. Phys. B115 (1976) 208; V. A. Polychronakos et al., Phys. Rev. D19 (1979) 1317; G. Costa et al., Nucl. Phys. B175 (1980) 402.

[77] T. A. Armstrong et al., Z. Phys. C52 (1991) 389.

[78] G. F. Chew and S. C. Frautschi, Phys. Rev. 124 (1961) 264.

[79] E. Oset and A. Ramos, Nucl. Phys. A635 (1998) 99.

[80] N. Kaiser, P. B. Siegel and W. Weise, Nucl. Phys. A594 (1995) 325.

[81] V. Bernard, N. Kaiser and U.G. Meissner, Nucl. Phys. A615 (1997) 483.

[82] N. Fettes, U.G. Meissner and S. Steininger, Nucl. Phys. A640 (1998) 199.

[83] M. Mojzis, Eur. Phys. J C2 (1998) 181.

[84] A. Datta and S. Pakvasa, Phys. Rev. D56 (1997) 4322.

[85] P.J. Ellis and H.B. Tang, Phys. Rev C57 (1998) 3356.

[86] C. H. Lee, H. Jung, D. P. Min and M. Rho, Phys. Lett. B326 (1994) 14.

[87] G. E. Brown, C.-H. Lee, M. Rho and V. Thorsson, Nucl. Phys. A567 (1994) 937.

[88] R.H. Dalitz and S.F. Tuan, Phys. Rev. Lett. 5 (1959) 425; R.H. Dalitz and S.F. Tuan, Ann. Phys. (NY) 10 (1960) 307.

[89] N. Isgur and G. Karl, Phys. Rev. D18 (1978) 4187.

[90] M. Arima, S: Matsui and K. Shimizu, Phys. Rev. C49 (1994) 2831.

[91] E.A. Veit, B.K. Jennings, R.C. Barret and A.W. Thomas, Phys. Lett. B137 (1984) 415; E.A. Veit, B.K. Jennings, A.W. Thomas and R.C. Barret, Phys. Rev. D31 (1985) 1033.

[92] C.L. Schat, N.N. Scoccola and C. Gobbi, Nucl. Phys. A585 (1995) 627.

[93] C.-H. Lee, D. P. Min and M. Rho, Nucl. Phys. A602 (1996) 334.

[94] D. N. Tovee et al., Nucl. Phys. B33 (1971) 493.

[95] R. J. Nowak et al., Nucl. Phys. B139 (1978) 61.

[96] D. W. Thomas, A. Engler, H. E. Fisk and R. W. Kraemer, Nucl. Phys. B56 (1973) 15.

[97] R. J. Hemingway, Nucl. Phys. B253 (1985) 742.

[98] R.H. Dalitz and A. Deloff, J. Phys. G17 (1991) 289.

[99] M. Iwasaki et al., Phys. Rev. Lett. 78 (1997) 3067.

[100] A. D. Martin, Nucl. Phys. B179 (1981) 33.

[101] W.E. Humphrey and R.R. Ross, Phys. Rev. 127 (1962) 1305.

[102] M. Sakitt et al., Phys. Rev. 139 (1965) 719.

[103] J. K. Kim, Phys. Rev. Lett. 21 (1965) 29; J. K. Kim, Columbia University Report, Nevis 149 (1966).

[104] W. Kittel, G. Otter and I. Wacek, Phys. Lett. 21 (1966) 349.

[105] J. Ciborowski et al., J. Phys. G8 (1982) 13.

[106] D. Evans et al., J. Phys. G9 (1983) 885.

[107] B. R. Martin, Nucl. Phys. B94 (1975) 413.

[108] See C. Dover and G. Walker, Phys. Reports 89 (1982) 1 for a compilation of data.

[109] N. Kaiser, P.B. Siegel and W. Weise, Phys. Lett, B362 (1995) 23.

[110] N. Kaiser, T. Waas and W. Weise, Nucl. Phys. A612 (1997) 297.

[111] J. Caro Ramon, N. Kaiser, S. Wetzel and W. Weise, Nucl. Phys. A , in print. nucl-th/9912053.

[112] A. Gómez Nicola and J.R. Peláez, hep-ph/9912512.

[113] J. Nieves and E. Ruiz-Arriola, hep-ph/0001013.

[114] U.G. Meissner and J.A. Oller, Nucl. Phys. A, in print. nucl-th/9912026.

[115] M. R. Pennington, The Second DAPHNE Physics Handbook (1995) Vol. II, p 531.

[116] M. Feindt and J. Harjes, Nucl. Phys. B21 (Proc. Suppl.) (1991) 61.

[117] J. A. Oller and E. Oset, Nucl. Phys. A629 (1998) 739.

[118] P. Ko, Phys. Rev. D41 (1990) 1531; J. F. Donoghue and B. R. Holstein, Phys. Rev. D48 (1993) 137; J. F. Donoghue, B. R. Holstein and D. Wyler, Phys. Rev. D47 (1993) 2089.

[119] J. Bijnens and F. Cornet, Nucl. Phys. B296 (1988) 557.

[120] J. F. Donoghue, B. K. Holstein and Y. C. Lin, Phys. Rev. D37 (1988) 2423.

[121] D. Morgan and M. R. Pennington, Z. Phys. C37 (1988) 431.

[122] H. Albrecht et al., Z. Phys. C48 (1989) 183.

[123] M. Boglione and M. R. Pennington, Eur. Phys. J. C9 (1999) 11.

[124] J. A. Oller, Phys. Lett. B426 (1998) 7.

[125] E. Marco, S. Hirenzaki, E. Oset and H. Toki, Phys. Lett. B, in print, hep-ph/9903217.

[126] I. Dunietz, J. Hauser and J. L. Rosner, Phys. Rev. D35 (1987) 2166.

[127] J. Lucio and J. Pestiau, Phys. Rev. D42 (1990) 3253; J. Lucio and J. Pestiau, Phys. Rev. D43 (1991) 2447.

[128] S. Nussinov and T. N. Truong, Phys. Rev. Lett. 63 (1989) 1349.

[129] S. Nussinov and T. N. Truong, Phys. Rev. Lett. 63 (1989) 2003.

[130] N. N. Achasov and V. N. Ivachenko, Nucl. Phys. B315 (1989) 465.

[131] T. L. Yhuang, M. L. Yan, X. J. Wang, hep-ph/9907233.

[132] N. Paver and Riazuddin, Phys. Lett. B246 (1990) 240.

[133] F. E. Close, N. Isgur, S. Kumano, Nucl. Phys. B389 (1993) 513.

[134] A. Bramon, A. Grau and G. Pancheri, Phys. Lett. B289 (1992) 97.

[135] M.N. Achasov et al., Phys. Lett. B440 (1998) 442.

[136] R.R. Akhmetshin et al., Phys. Lett. B462 (1999) 380.

[137] M.N. Achasov et al., Phys. Lett. B438 (1998) 441.

[138] R.R. Akhmetshin et al., Phys. Lett.B462 (1999) 371.

[139] K. Huber and H. Neufeld, Phys. Lett. B357 (1995) 221.

[140] E. Oset, S. Hirenzaki, E. Marco, J.A. Oller, J.R. Peláez and H. Toki, Contribution to the Workshop on physics and detectors for DAPHNE, Frascati, November 1999.

[141] K. M. Watson, Phys. Rev. 95 (1955) 228.

[142] N. I. Muskhelishivili, Singular Integral Equations (Noordhoof, Groningen, 1953).

[143] R. Omnès, Nuovo Cimento 8 (1958) 316.

[144] J. Gasser and U. G. Meissner, Nucl. Phys. B357 (1991) 90.

[145] L. M. Barkov, Nucl. Phys. B256 (1985) 365.

[146] F. Guerrero, Phys. Rev. D57 (1998) 4136.

[147] See the Phys. Rev. Lett. papers by Truong in [19].

[148] L. Beldjoudi and T. N. Truong, hep-ph/9403348.

[149] T. Hannah, Phys. Rev. D55 (1997) 5613.

[150] E. Marco, E. Oset and H. Toki, Phys. Rev. C60 (1999) 015202.

[151] C. R. Ji, R. Kaminsky, L. Lesniak, A. Szczpaniak and R. Williams, Phys. Rev. C58 (1998) 1205.

[152] C.D. Fries et al., Nucl. Phys. B143 (1978) 408.

[153] A. I. Titov, Y. Oh, S. N. Yang and T. Mori, Phys. Rev. C58 (1998) 2429; A. I. Titov, T.S.H. Lee and H. Toki, nucl-th/9812074.

[154] J.A. Gómez Tejedor and E. Oset, Nucl. Phys. A571 (1994) 667; J.A. Gómez Tejedor and E. Oset, Nucl. Phys. A600 (1996) 413.

[155] K. Ochi, M. Hirata and T. Takaki, Phys. Rev. C56 (1997) 1472.

[156] W. Weise and L. Tauscher, Phys. Lett. B64 (1976) 424.

[157] S.R. Cotanch and F. Tabakin, Phys. Rev. C15 (1977) 1379.

[158] M. Thies, Phys. Lett. B70 (1977) 401; Nucl. Phys. A298 (1978) 344.

[159] A. Deloff, Phys. Rev. C21 (1980) 1516.

[160] A. S. Rosenthal and F. Tabakin, Phys. Rev. C22 (1980) 711.

[161] C. M. Chen and D. J. Ernst, Phys. Rev. C45 (1992) 2019.

[162] M. J. Jiang, D. J. Ernst and C. M. Chen, Phys. Rev. C51 (1995) 857.

[163] M. F. Jiang and D. S. Koltun, Phys. Rev. C46 (1992) 2462.

[164] M. Mizoguchi, S. Hirenzaki and H. Toki, Nucl. Phys. A567 (1994) 893.

[165] E. Friedman, A. Gal, C.J. Batty, Nucl. Phys. A579 (1994) 518.

[166] C. J. Batty, E. Friedman and A. Gal, Phys. Reports 287 (1997) 385.

[167] M. Alberg, E.M. Henley and L. Wilets, Ann. Phys. 96 (1976) 43.

[168] L.R. Staronski and S. Wycech, J. Phys. G: Nucl. Phys. 13 (1987) 1361.

[169] V. Koch, Phys. Lett. B337 (1994) 7.

[170] T. Waas, N. Kaiser and W. Weise, Phys. Lett. B365 (1996) 12.

[171] T. Waas and W. Weise, Nucl. Phys. A625 (1997) 287.

[172] M. Lutz, Phys. Lett. B426 (1998) 12; M. Lutz, nucl-th/9802033.

[173] A. Ramos and E. Oset, Nucl. Phys. A, in print, nucl-th/9906016.

[174] P. Schuck, W. Nörenberg and G. Chanfray, Z. Phys. A330 (1988) 119.

[175] Z. Aouissat, R. Rapp, G Chanfray, P Schuck and J. Wambach, Nucl. Phys. A581 (1995) 471.

[176] M. Soyeur, G.E. Brown and M. Rho, Nucl. Phys. A556 (1993) 355.

[177] M. Hermann, B.L. Friman and W. Nörenberg, Nucl. Phys. A560 (1993) 411.

[178] M.J. Vicente-Vacas and E. Oset, forthcoming.

[179] M. Jones, R.H. Dalitz and R.R. Horgan, Nucl. Phys. B129 (1977) 45.

[180] J.D. Darewych, R. Koniuk and N. Isgur, Phys. Rev. D32 (1985) 1765.

[181] E.A. Veit, B.K. Jennings, A.W. Thomas and R.C. Barrett, Phys. Rev. D31 (1985) 1033.

[182] Y.S. Zhong, Q.W. Thomas, B.K. Jennings and R.C. Barrett, Phys. Rev. D38 (1988) 837.

[183] E. Kaxiras, E.J. Moniz and M. Soyeur, Phys. Rev. D32 (1985) 695.

[184] G. He and R.H. Landau, Phys. Rev. C48 (1993) 3047.

[185] A. Arima, S. Matsui and K. Shimizu, Phys. Rev. C49 (1994) 2831.

[186] R.L. Workman and Harold W. Fearing, Phys. Rev. D37 (1988) 3117; J. Lowe, Nuovo Cimento, A102 (1989) 16, and other references therein.

[187] Peter B. Siegel and Bijan Saghai, Phys. Rev. C52 (1995) 392.

[188] T.-S.H. Lee, J.A. Oller, E. Oset and A. Ramos, Nucl. Phys. A643 (1998) 402.

[189] D.A. Whitehouse et al., Phys. Rev. Lett. 63 (1989) 1352.

[190] J.C. Nacher, E. Oset, H. Toki and A. Ramos, Phys. Lett. B455 (1999) 55.

[191] J.C. Nacher, E. Oset, H. Toki and A. Ramos, Phys. Lett. B461 (1999) 299.

[192] R. J. Peterson, private communication.

[193] N. Grion et al., Phys. Rev. Lett. 59 (1987) 1080.

[194] F. Bonutti et al., Phys. Rev. Lett. 77 (1996) 603.

[195] J.A. Johnstone and T.S. H. Lee, Phys. Rev. C34 (1986) 243.

[196] J. W. Durso, A. D. Jackson and B. J. Verwest, Nucl. Phys. A345 (1980) 471.

[197] G. Chanfray, Z. Aouissat, P. Schuck and W. Nörenberg, Phys. Lett. B256 (1991) 325.

[198] Z. Aouissat, G. Chanfray and P. Schuck, Mod. Phys. Lett. A8 (1993) 1379.

[199] D. Lohse, J.W. Durso, K. Holinde and J. Speth, Phys. Lett. B234 (1989) 235; Nucl. Phys. A516 (1990) 513.

[200] R. Rapp, J.W. Durso and J. Wambach, Nucl. Phys. A596 (1996) 436.

[201] H.C. Chiang, E. Oset and M.J. Vicente-Vacas, Nucl. Phys. A644 (1998) 77.

[202] T.E.O. Ericson and W. Weise , Pions and Nuclei, Clarendon Press, 1988.

[203] S. Weinberg, Phys. Rev. Lett. 17 (1966) 616; Phys. Lett. 18 (1967) 188.

[204] M.G. Olsson and L. Turner, Phys. Rev. Lett. 20 (1968) 1127.

[205] E. Oset and M.J. Vicente Vacas, Nucl. Phys. A446 (1985) 584.

[206] O. Jaekel, M. Dillig, C. A. Z. Vasconcelos, Nucl. Phys. A541 (1992) 673.

[207] V. Bernard, N. Kaiser and U.G. Meissner, Nucl. Phys. B457 (1995) 147; V. Bernard, N. Kaiser and U.G. Meissner, Nucl. Phys. A619 (1997) 261.

[208] T.S. Jensen and A.F. Miranda, Phys. Rev. C55 (1997) 1039; Nucl. Phys. A541 (1992)673.

[209] U.G. Meissner, E. Oset and A. Pich, Phys. Lett. B353 (1995) 161.

[210] G. Chanfray and D. Davesne, Nucl. Phys. A646 (1999) 125.

[211] C. García-Recio, J. Nieves and E. Oset, Phys. Rev. C51 (1995) 237.

[212] E. Oset, C. García-Recio and J. Nieves, Nucl. Phys. A584 (1995) 653.

[213] R. Rapp et al., Phys. Rev. C59 (1999) R1237.

[214] M.J. Vicente-Vacas and E. Oset, Phys. Rev. C60 (1999) 064621.

[215] T. Hatsuda, T. Kunihiro and H. Shimizu, Phys. Rev. Lett. 82 (1999) 2840; T. Kunihiro, hep-ph/9905262.

[216] D.B. Kaplan and A.E. Nelson, Phys. Lett. B175 (1986) 57.

[217] G.E. Brown, K. Kubodera, M. Rho and V. Thorsson, Phys. Lett. B291 (1992) 355.

[218] V. Thorsson, M. Prakash and J. Lattimer, Nucl. Phys. A572 (1994) 693.

[219] P.J. Ellis, R. Knorren and M. Prakash, Phys. Lett. B349 (1995) 11.

[220] H. Fuji, T. Maruyama, T. Muto and T. Tatsumi, Nucl. Phys. A597 (1996) 645.

[221] T. Tatsumi and M. Yasuhira, Phys. Lett. B441 (1998) 9; T. Tatsumi and M. Yasuhira, Nucl. Phys. A653 (1999) 133.

[222] G.Q. Li, C.-H. Lee and G.E. Brown, Phys. Rev. Lett. 79 (1997) 5214.

[223] N.K. Glendenning and J. Schaffner-Bielich, Phys. Rev. Lett. 81 (1998) 4564.

[224] R. Barth et al., Phys. Rev. Lett. 78 (1997) 4007; F. Laue et al., Phys. Rev. Lett. 82 (1999) 1640.

[225] W. Cassing, E.L. Bratkovskaya, U. Mosel, S. Teis and A. Sibirtsev, Nucl. Phys. A614 (1997) 415; E.L. Bratkovskaya, W. Cassing and U. Mosel, Nucl. Phys. A622 (1997) 593.

[226] G.Q. Li, C.N. Ko and X.S. Fang, Phys. Lett. B329 (1994) 149.

[227] G.Q. Li and C.N. Ko, Phys. Rev. C54 (1996) 2159.

[228] G.Q. Li, C.-H. Lee and G.E. Brown, Nucl. Phys. A625 (1997) 372.

[229] J. Schaffner-Bielich, V. Koch and M. Effenberg, Nucl. Phys. A, in print, nucl-th/9907095.

[230] A. Sibirtsev and W. Cassing, Nucl. Phys. A641 (1998) 476.

[231] C.-H. Lee, G.E. Brown and M. Rho, Phys. Lett. B335 (1994) 266; C.-H. Lee, G.E. Brown, D.P. Min and M. Rho, Nucl. Phys. A585 (1995) 401.

[232] C.-H. Lee, Phys. Reports 275 (1996) 255

[233] G. Mao, P. Papazoglou, S. Hofmann, S. Schramm, H. Stöcker and W. Greiner, Phys. Rev. C59 (1999) 3381.

[234] J. Schaffner and I.N. Mishustin, Phys. Rev. C53 (1996) 1416; J. Schaffner-Bielich, I.N. Mishustin and J. Bondorf, Nucl. Phys. A625 (1997) 325.

[235] K. Tsushima, K. Saito, A.W. Thomas and S.V. Wright, Phys. Lett. B429 (1998) 239.

[236] H. Bandō, T. Motoba and J. Žofka, Int. J. Mod. Phys. A5 (1990) 4021.

[237] C.J. Batty et al, Phys. Lett. 74B (1978) 27, C.J. Batty et al, Phys. Lett. 87B (1979) 324.

[238] E. Oset, P. Fernández de Córdoba, L.L. Salcedo and R. Brockmann, Phys. Reports 188 (1990) 79.

[239] C.J. Batty, E. Friedman and A. Gal, Phys. Lett. B335 (1994) 273.

[240] A. Ramos, E. Oset and L.L. Salcedo, Phys. Rev. C50 (1994) 2314.

[241] S. Hirenzaki, Y. Okumura, H. Toki, E. Oset and A. Ramos, Phys. Rev. C, in print and in proceedings of XV^{th} Particles and Nuclei International Conference, Eds. G. Fäldt, B. Höistad and S. Kullander, Nucl. Phys. A, in print.

[242] C.J. Batty, Nucl. Phys. A372 (1981) 418.

[243] A. Baca, C. García-Recio and J. Nieves, Nucl. Phys. A, in press, nucl-th/0001060.

[244] E. Friedman, A. Gal, J. Mareš and A. Cieplý, Phys. Rev. C60 (1999) 024314.

[245] E. Friedman and A. Gal, Phys. Lett. B459 (1999) 43.

[246] E. Friedman and A. Gal, Nucl. Phys. A658 (1999) 345.

[247] T. Kishimoto, Phys. Rev. Lett. 83 (1999) 4701.

This figure "kaonatom.png" is available in "png" format from:

http://arXiv.org/ps/hep-ph/0002193v1